ÉCOLE DE TECHNOLOGIE SUPÉRIEURE
UNIVERSITÉ DU QUÉBEC

THESIS PRESENTED TO
ÉCOLE DE TECHNOLOGIE SUPÉRIEURE

IN PARTIAL FULFILLMENT OF THE REQUIREMENTS FOR
THE DEGREE OF DOCTOR OF PHILOSOPHY
Ph.D.

BY
Minh AU

ANALYSIS AND MODELLING OF RADIO FREQUENCY INTERFERENCES INDUCED BY ELECTRIC ARC DISCHARGES IN HIGH VOLTAGE SUBSTATIONS

MONTREAL, 26 APRIL 2016

 Minh Au, 2016

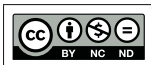

This Creative Commons license allows readers to download this work and share it with others as long as the author is credited. The content of this work cannot be modified in any way or used commercially.

THIS THESIS HAS BEEN EVALUATED

BY THE FOLLOWING BOARD OF EXAMINERS:

Pr. François Gagnon, Thesis Supervisor
Department of Electrical Engineering, École de technologie supérieure

Dr. Basile L. Agba, Co-supervisor
Institute of Research Hydro-Québec (IREQ)

Pr. Éric David, President of the Board of Examiners
Department of Mechanical Engineering, École de technologie supérieure

Pr. Jean-Marc Lina, Member of the jury
Department of Electrical Engineering, École de technologie supérieure

Pr. Tayeb A. Denidni, External Examiner
Institut National de la Recherche Scientifique, INRS-EMT

THIS THESIS WAS PRESENTED AND DEFENDED

IN THE PRESENCE OF A BOARD OF EXAMINERS AND THE PUBLIC

ON "DEFENSE DATE"

AT ÉCOLE DE TECHNOLOGIE SUPÉRIEURE

ACKNOWLEDGEMENTS

First, I would like to thank my supervisors, Pr. François Gagnon and Dr. Basile Agba. Their guidance, advice and support has helped me achieve my personal and research goals over these past five years. The long and winding road that leads to your area of expertise is always inspiring to me, and it will never disappear.

I thank MICTACS and Hydro-Québec for funding this project. I also thank Chantal Cyr for her constant support through all the administrative procedures. I am also indebted to Normand Gravel, Sylvain Morin, Jean Béland, Mélanie Lévesque and Calogero Guddemi for their technical support.

It would be difficult to name all the people who have contributed to this PhD. My special acknowledgements go to Brent Delaine, who helped me improve my English writing without whom this manuscript would still be a rough stone. I cannot forget Fanny Parzysz and Mouna Hajir who supported me regardless of the doubts and troubles I have gone through – but there is no doubt about your love. The happiness that shines through your smile is a warm gun.

Finally, I acknowledge colleagues, friends, and IREQ researchers: Mathieu, Ismail, Byron, Moshiur, Edena, Sara, Pascal, Pr. Georges Kaddoum, Sofiane, Alexandre, Phuong, Olfa, Marthe, Yamina...I wish you all the best. I would like to send my kind regards to all friends and my family in France. Cảm ơn mẹ được ở đây cho con.

ANALYSE ET MODÉLISATION DES SOURCES D'INTERFÉRENCES RF INDUITES PAR LES DÉCHARGES ÉLECTRIQUES DANS LES POSTES À HAUTE-TENSION

Minh AU

RÉSUMÉ

Dans le contexte général des réseaux électrique intelligent (smart grid), l'utilisation des systèmes de communication analogique et/ou numérique avancés dans les postes à haute-tension permet d'améliorer significativement, l'efficacité, la qualité et la sécurité du réseau électrique. En effet, le déploiement d'un réseau de capteurs intelligents permet l'émergence d'outils de diagnostique, de décision et de contrôle, plus performants, à la fois, rapides et automatisés sur les équipements majeurs des postes tel que les transformateurs de courant, de tension et de puissance, les disjoncteurs et sectionneurs. Les capteurs sans fil offrent un énorme potentiel dans ce domaine. Cependant, les environnements des postes sont sujet à de fortes perturbations électromagnétiques qui affectent ostensiblement les performances des communications sans fil. Ce projet de recherche consiste à identifier, analyser, caractériser et modéliser les interférences électromagnétiques dans les postes à haute-tension avec l'optique de déployer des réseaux de communication sans fil.

Dans une première partie, nous proposons un protocole de mesure radio fréquence afin d'identifier et de caractériser les sources d'interférences électromagnétiques sur une bande de fréquence allant de 800 MHz à 5 GHz dans les postes à haute-tension. Les sources majeures de perturbations sont les irradiations causées par les décharges partielles. Les signaux induits sont caractérisés par de fortes impulsions transitoires et les occurrences ont la particularité d'être cyclostationnaire. Ensuite, nous proposons une méthode de caractérisation permettant de mesurer les caractéristiques physiques des signaux émis par les décharges en termes de statistiques du premier- et du second-ordre.

Dans une seconde partie, nous étudions la modélisation des sources d'interférences électromagnétiques induites par les décharges partielles. Dans un premier temps, nous proposons un modèle complet et cohérent qui lie les caractéristiques physiques des équipements haute-tension au spectre radio fréquence des sources de bruit impulsif. En utilisant des métriques statistiques de validation, nous avons pu mesurer la qualité de l'ajustement permettant, ainsi, de valider le modèle en termes de statistiques du premier- et du second-ordre.

Enfin, nous proposons un modèle généralisé lorsque plusieurs sources de décharges partielles ont lieu dans l'espace et dans le temps. En se basant sur un champ d'interférences de Poisson dans l'espace et le temps, nous dégageons certaines propriétés statistiques intéressantes sur les moments, les cumulants et les principales distributions de probabilités. Ceux-ci peuvent, à leur tour, être utilisés dans les algorithmes de traitement du signal pour l'identification rapide des

décharges partielles, de la localisation, et des techniques d'atténuation du bruit impulsif pour les communications sans fil dans les postes.

Mots clés: Décharge partielles, Bruit impulsif, Caratérisation, Modélisation, Poste à haute-tension, Interférences électromagnétiques

ANALYSIS AND MODELLING OF RADIO FREQUENCY INTERFERENCES INDUCED BY ELECTRIC ARC DISCHARGES IN HIGH VOLTAGE SUBSTATIONS

Minh AU

ABSTRACT

In the context of the next generation of electric grids, called smart grids, the use of modern and advanced communication systems in high-voltage substations can significantly improve the efficiency, reliability and safety of the electric power grid. Indeed, the deployment of intelligent sensor networks allows for the development of a more efficient, rapid, and automated remote monitoring, control and diagnosis in major pieces of high-voltage equipment in substations: current, potential, and power transformers, circuit breakers, and high-voltage disconnectors. Wireless sensor networks offer significant benefits in this area. Unfortunately, high-voltage substations are harsh and hostile environments whose wireless communication systems can be interfered to such an extent as to render their performances severely degraded. This work consists of the identification, characterization, and modelling of electromagnetic interferences in substations for the deployment of wireless sensor networks.

In the first part, we propose a radio frequency measurement setup for electromagnetic interferences identification and characterization in the frequency range of 800 MHz to 5 GHz in substations. The majority of interference sources comes from radiations caused by partial discharges. The induced signals are characterized by strong transient impulses whose such events follow a cyclostationary process. Next, a characterization process is proposed, by which physical characteristics of partial discharge can be measured in terms of first- and second-order statistics.

In the second part, we investigate the modelling of electromagnetic interferences caused by partial discharge sources. First, we propose complete and coherent approach model that links physical characteristics of high-voltage installations to the induced radio-interference spectra of partial discharge sources. The goodness-of-fit of the proposed physical model has been measured based on some interesting statistical metrics. This allows us to assess the effectiveness of our approach in terms of first- and second-order statistics.

Finally, a generalized radio-noise model for substations is proposed, in which there are many discharges sources that are randomly distributed over space and time according to the Poisson field of interferers approach. This allows for the identification of some interesting statistical properties of moments, cumulants and probability distributions. These can, in turn, be utilized in signal processing algorithms for rapid partial discharge's identification, localization, and impulsive noise mitigation techniques in wireless communications in substations.

Keywords: Partial discharges, Impulsive noise, Characterization, Modelling, High-voltage substations, Electromagnetic interferences

TABLE OF CONTENTS

Page

INTRODUCTION 1

CHAPTER 1 CHARACTERIZATION AND MODELLING EMI FROM ELECTRIC DISCHARGES: A LITERATURE REVIEW 7
1.1 Introduction 7
1.2 Concept of electromagnetic interferences and classification 9
1.2.1 Definition of EMI sources 9
1.2.2 Natural noise sources 10
1.2.3 Man-made noise sources 10
1.2.4 Communication channels in presence of impulsive noise 11
1.3 Characterization and impulsive noise models 12
1.3.1 A statistical characterization of impulsive noise 12
1.3.2 Impulsive noise models 13
1.3.3 Probability models of impulsive noise 15
1.3.3.1 Memoryless models 16
1.3.3.2 Impulsive noise with memory: Burst noise 19
1.4 The electromagnetic interferences in substations 22
1.4.1 Ionization process and electrical discharge in gases 22
1.4.2 Partial discharges mechanism 23
1.4.3 Measurements and characterization of partial discharge sources 25
1.4.3.1 Measurement techniques 25
1.4.3.2 Characterization of PD impulses 28
1.4.4 Partial discharge modelling 29
1.4.4.1 Physical PD models 30
1.4.4.2 Statistical PD models for wireless channels 30
1.5 Discussion and conclusion 32
1.5.1 Proposed research plan 35

CHAPTER 2 MEASUREMENT AND CHARACTERIZATION OF EMI FROM PD ACTIVITY IN HIGH-VOLTAGE SUBSTATIONS 37
2.1 Introduction 37
2.2 The measurement setup 38
2.3 An experimental characterization of the discharge sources 39
2.3.1 Amplitude of measured signals 39
2.3.2 Signal processing tools for impulsive noise measurement 40
2.3.2.1 The Denoising process 40
2.3.2.2 Short-time analysis for impulsive signals 42
2.3.2.3 Temporal location of an impulse 42
2.3.3 Characterization metrics definition 43
2.3.3.1 Characterization based on first-order statistics 44

2.3.3.2 Characterization based on second-order statistics 44
2.4 Measurements in substations 46
2.4.1 Description of the environment 46
2.4.2 First-order statistics 47
2.4.2.1 PRPD representation 47
2.4.2.2 Statistical distribution of PD characteristics 49
2.4.3 Waveforms and second-order statistics 51
2.4.3.1 Typical waveform and spectrogram 51
2.4.3.2 Power spectral density 52
2.5 Conclusion 54

CHAPTER 3 A PHYSICAL MODEL OF EMI INDUCED BY A PARTIAL DISCHARGE SOURCE 57
3.1 Introduction 57
3.2 Partial discharge phenomenon and its mechanism 59
3.3 The physical model of partial discharge source 60
3.3.1 Electric field stress 60
3.3.2 Discharge process 62
3.3.3 Current and charge density 65
3.4 The electromagnetic radiation of the interference source induced by partial discharge 66
3.4.1 Electric dipole formulation 66
3.4.2 Power radiation of the interference source received at the antenna 68
3.4.3 Modelling impulsive waveforms and PSD 68
3.4.4 Brief summary of interference induced by discharge source 69
3.5 Experimental characterization process of the interference source 70
3.5.1 Definition of characterization metrics 70
3.5.2 Denoising process 72
3.5.3 Short-time analysis process 72
3.6 Experimental validation 73
3.6.1 Brief description of measurement setup 73
3.6.1.1 The measurement setup 73
3.6.1.2 PD sources from stator bar 74
3.6.2 Simulation setup 74
3.6.2.1 Calculation of the electric field along the surface 75
3.6.2.2 Discharge process in air cavity parameters 76
3.6.2.3 Stochastic property of the emitted radiations of PD sources 77
3.6.3 Simulation-measurement comparison 78
3.6.3.1 PRPD comparison 78
3.6.3.2 Statistical distributions comparison 80
3.6.3.3 PSD and waveforms of impulses 82
3.7 Conclusion 84

CHAPTER 4 ANALYSIS AND MODELLING OF WIDEBAND RF IMPULSIVE SIGNALS INDUCED BY PARTIAL DISCHARGES USING SECOND-ORDER STATISTICS 87
4.1 Introduction 87
4.1.1 Motivation and prior related work 87
4.1.2 Main contribution and organization 89
4.2 Measurement setup 90
4.3 Conjectures and mathematical formulation of EM waves 91
4.3.1 Second-order statistics 91
4.3.1.1 Time-frequency analysis 91
4.3.1.2 Autocorrelation function 92
4.3.1.3 Results from the measurement campaigns 92
4.3.2 A physical interpretation 94
4.4 The proposed model 95
4.4.1 Theory of filters and its relationship with time series models 95
4.4.2 Definition of the time series model 96
4.4.3 Tests for unit roots 98
4.4.4 Estimation and selection 100
4.5 The goodness-of-fit 101
4.5.1 Analysis of the residuals 101
4.5.1.1 Residuals of fitted ARMA(7,2) 102
4.5.1.2 Residuals of fitted ARMA(4,1) 104
4.5.2 Tests for heteroskedasticity 105
4.5.3 Analysis of the residuals of the improved models 108
4.5.4 Summary 111
4.6 Simulation and results 112
4.6.1 Simulation parameters 112
4.6.2 A comparison of measurement vs. simulation results 112
4.6.3 Analysis of simulated impulsive waveforms 113
4.6.4 Advantages and limitations of the proposed model 114
4.7 Conclusion 116

CHAPTER 5 A STATISTICAL ANALYSIS OF IMPULSIVE NOISE IN A POISSON FIELD OF INTERFERERS IN SUBSTATION ENVIRONMENTS 119
5.1 Introduction 119
5.1.1 Prior and related work 119
5.1.1.1 EMIs in substation environments 119
5.1.1.2 Partial discharge diagnostics 120
5.1.1.3 Communication in substation environments 121
5.1.2 Contribution and organization 122
5.2 A mathematical formulation of multiple PD interference sources 123
5.2.1 Electromagnetic radiations of multiple PD sources 123

5.2.1.1 The emission of the PD impulses 123
5.2.1.2 Basic assumptions of spatial and temporal PD events 123
5.2.2 Propagation of EM waves induced by PD sources 124
5.2.2.1 The noise process observed by the receiver 125
5.2.2.2 A generic temporal impulsive waveform from PD 126
5.2.2.3 The attenuation factor 126
5.2.3 Spatial and temporal distribution of PD sources 127
5.3 Statistical analysis 129
5.3.1 Probability density function of the instantaneous amplitude 129
5.3.2 Amplitude probability distribution 134
5.3.3 Tails and moments 134
5.3.3.1 Moments of α-stable distributions 135
5.3.3.2 Moments of shot-noise processes 136
5.3.4 A summary of important findings 137
5.4 Experimental and simulation results 138
5.4.1 Measurements in substations 138
5.4.2 A procedure for estimation 139
5.4.3 Measurement-simulation comparison 140
5.4.3.1 First-order statistics 141
5.4.3.2 Second-order statistics 144
5.5 A rapid identification of PD sources using blind source separation 145
5.5.1 Motivation and contribution 146
5.5.2 System model 147
5.5.3 Blind source separation via generalized eigenvalue decomposition 149
5.5.4 Simulation and results 150
5.6 Conclusion 153

CONCLUSION 157

BIBLIOGRAPHY 164

LIST OF TABLES

Page

Table 1.1 The goodness-of-fit of impulsive noise models 32

Table 2.1 Summary of statistical quantities 48

Table 3.1 Dimensions and electrical properties of PD process 75

Table 3.2 The Goodness-of-fit: Measurement vs. simulation 82

Table 4.1 Results of PP test obtained from the measured impulsive noises 100

Table 4.2 Results of Ljung-Box Q-test for residual autocorrelation 111

Table 4.3 Results of Ljung-Box Q-test for squared residual autocorrelation 111

Table 5.1 The Goodness-of-fit: Measurement vs. impulsive noise models 143

LIST OF FIGURES

Page

Figure 1.1 Typical example of impulsive noise with background Gaussian noise 13

Figure 1.2 Impulsive noise modelled by a filter 14

Figure 1.3 Markov-Middleton impulsive noise model with 3 states of Markov chain 20

Figure 1.4 Partitioned Markov chain for asynchronous impulsive noise 21

Figure 1.5 Current-voltage relationship in prebreakdown region 23

Figure 1.6 Typical behaviour of impulsive noise induced by a discharge source 24

Figure 1.7 Test circuit for partial discharge detection 26

Figure 1.8 Typical measurement setup using UHF PD detection 27

Figure 1.9 PRPD pattern of slot PD measured on a stator bar 29

Figure 1.10 Impulsive noise with fitted statistical models 32

Figure 2.1 Denoising process using wavelets 41

Figure 2.2 Characterization process 43

Figure 2.3 Typical HV equipment in the 735 kV substation 46

Figure 2.4 PRPD of EMI from PD activity in a 735 kV substation 48

Figure 2.5 Power density distribution 49

Figure 2.6 Inter-arrival time distribution 50

Figure 2.7 Time occurrence distribution 50

Figure 2.8 Typical impulsive waveform 52

Figure 2.9 Waveforms and PSD of an impulse 53

Figure 2.10 Average power spectral density 54

Figure 3.1 Typical behaviour of discharge process under AC voltage stress Taken from Bartnikas and McMahon (1979) 60

Figure 3.2 Dielectric between a pair of HV electrodes and its equivalent circuit 61

Figure 3.3 Stator bar and measurement configuration 74

Figure 3.4 The surface of a stator bar with modelled air cavities 75

Figure 3.5 Tangential electric field distribution 77

Figure 3.6 Phase Resolved Partial Discharge 16 kVrms 79

Figure 3.7 Power density distribution 81

Figure 3.8 Inter-arrival time distribution 81

Figure 3.9 Time occurrence distribution 82

Figure 3.10 PSD Comparison: Measurement vs. simulation 83

Figure 3.11 Waveforms and PSD of an impulse 84

Figure 4.1 Waveform measured from PTT 93

Figure 4.2 Waveform measured from CTT 93

Figure 4.3 Analysis of the residuals of fitted ARMA(7,2) model 103

Figure 4.4 Results of Ljung-Box Q-test for residual autocorrelation of the ARMA(7,2) 103

Figure 4.5 Analysis of the residuals of fitted ARMA(4,1) model 104

Figure 4.6 Results of Ljung-Box Q-test for residual autocorrelation of the ARMA(4,1) 105

Figure 4.7 Results of Ljung-Box Q-test for squared residual autocorrelation of the ARMA(7,2) 107

Figure 4.8 Results of Ljung-Box Q-test for squared residual autocorrelation of the ARMA(4,1) 108

Figure 4.9 Results of Engle test for residual heteroskadasticity of the ARMA(7,2) 108

Figure 4.10 Results of Engle test for residual heteroskadasticity of the ARMA(4,1) 109

Figure 4.11 Analysis of the residuals of fitted *Model* 1 110

Figure 4.12 Analysis of the residuals of fitted *Model* 2 110

Figure 4.13 Comparison of waveforms : PTT vs. *Model* 1 113

Figure 4.14 Comparison of waveforms : CTT vs. *Model* 2 114

Figure 4.15 Waveform obtained with the *Model* 1 115

Figure 4.16 Waveform obtained with the *Model* 2 115

Figure 5.1 Impulsive waveform obtained by simulation 141

Figure 5.2 Physical shot-noise process X 142

Figure 5.3 Probability distributions of the noise process 143

Figure 5.4 Second-order statistics: average PSD 146

Figure 5.5 Overview of the system model 148

Figure 5.6 Probability of error vs. Γ_{dB}. Based on PPP model: Avg. PD source density $\lambda_s = 4$ sources per unit volume or surface, avg. emission density $\lambda_e = 5$ discharges per unit time per sources, NB. obs. $M = 20 > N$ 152

Figure 5.7 Probability of error vs. Γ_{dB} with various Nb. obs. M. Based on PPP model: Avg. PD source density $\lambda_s = 4$ sources per unit volume or surface, avg. emission density $\lambda_e = 5$ discharges per unit time per sources 153

LIST OF ABBREVIATIONS

AC	Alternative Current
ACF	Autocorrelation Function
AR	Autoregressive
ARCH	Autoregressive Conditional Heteroskedastic
ARIMA	Autoregressive Integrated Moving Average
ARMA	Autoregressive Moving Average
CCDF	Complementary Cumulative Distribution Function
CDF	Cumulative Distribution Function
c.f	Characteristic Function
EGARCH	Exponential Generalized Autoregressive Conditional Heteroskedastic
EID	Electronic Intelligent Device
EM	Electromagnetic
EMI	Electromagnetic Interference
GARCH	Generalized Autoregressive Conditional Heteroskedastic
HV	High voltage
IAT	Inter-Arrival Time
IEEE	Institute of Electrical and Electronics Engineers
iid	Independent and Identically Distributed
IREQ	Institute of Research Hydro-Québec

KL	Kullback-Leibler
LTI	Linear Time Invariant
MLE	Maximum Likelihood
PACF	Partial Autocorrelation Function
PD	Partial Discharge
PDF	Probability Density Function
PPP	Poisson Point Process
PRPD	Phase Resolved Partial Discharge
PSD	Power Spectral Density
RF	Radio Frequency
UHF	Ultra High Frequency
WIED	Wireless Intelligent Electronic Device

INTRODUCTION

Two of the most pressing contemporary environmental issues are climate change and the management of scarce energy resources. The increased awareness of these issues encourages the electricity industry to deploy advanced communication technologies within the electric grid for the next generation of electric grids, called smart grids (Yan *et al.*, 2013; Gungor *et al.*, 2011; Amin and Wollenberg, 2005). Since the early 21st century, this novel concept has emerged to manage the increasing demand for energy resources while maintaining economic growth and environmental sustainability. This new paradigm allows for decentralized production by integrating renewable energy resources and enhancing consumer empowerment for sustainable development (Farhangi, 2010; US Department of Energy Office, 2007a,b).

Over the last few years, the development of smart grid has become a promising area of research for both industrial and academic researchers. We mention the development of:

- new information and communication technologies for better electricity management;
- battery energy storage systems for improving the power quality, reliability and energy efficiency of the electric grid;
- smart grid interoperability for the integration of renewable energy resources.

Potential applications and benefits of the smart grid have been summarized by (Farhangi, 2010; Gungor *et al.*, 2010; Gungor and Lambert, 2006; Amin and Wollenberg, 2005).

Within this context, Hydro-Québec has one of the most extensive electric grids in North America. As of 2016, more than 500 substations are located in strategically-important locations. Workers and maintenance supervisors on these sites require more information from major high voltage (HV) equipment, such as power transformers and circuit breakers, to be collected via a network of electronic intelligent devices, or EIDs (Riendeau *et al.*, 2009b; Riendeau and Béland, 2009; Riendeau *et al.*, 2009a; Pater, 2009). However, using wired sensor networks might be complex to manage in terms of wiring complexity, cost reduction and ease of deployment.

Power-line communication (PLC) can be used as an alternative as mentioned in (Riendeau *et al.*, 2009a,b). This alternative is out of the scope of this thesis. Wireless communication technologies might be relevant in substations (Gungor *et al.*, 2011; Gungor and Lambert, 2006). However, the transmitted signal can be degraded due to electromagnetic interferences (EMI) in the environment.

Although wireless sensor networks avoid some constraints induced by wires, their deployments require the study and analysis of the electromagnetic environment, especially in high-voltage substations, which can be considered harsh and hostile environments. Indeed, the high-voltage installations can produce discharge mechanisms in which the electromagnetic (EM) radiations can interfere with the transmitted signal. Therefore, these installations have to be taken into consideration to evaluate their impact on wireless communications. In addition, the multiple reflectors induced by metallic structures in substations can produce destructive and constructive interferences, which can impact the transmitted signal.

Motivations and objectives

Our research objective is to propose characterization methods of EMI phenomena in substations. Next, a generic model for wireless channel models is proposed. This may be used in the design of new remote control and monitoring systems via wireless IED (WIED), as well as for the performance analysis of wireless communications. This work may contribute to the deployment of wireless communication systems in substations where significant improvement in protection, control, automation and monitoring applications in HV equipment can be achieved.

In this document, EMIs induced by discharges in HV installations are particularly focused. Partial discharges (PD) in the air are the predominant EMIs phenomena in which their activity can take place in HV equipment: along the insulation surface or in an air gap located between two separated conductors. When the local electric field is sufficiently high, the charged particles can collide, which produces an electron avalanche process in which electric discharges

can occur. The induced charges and the currents generate high impulsive electromagnetic radiations.

In this thesis, the main contribution is to propose: a full characterization of EMIs produced by PDs and a generic impulsive noise model for wireless channels in substations. The proposed model is a complete and coherent approach that links physical characteristics of PDs to the induced radio interference spectrum. It allows for the performance analysis of wireless communication systems as well as the design of robust receivers corrupted by impulsive noises in substations. This work is based on three major axes of research, namely: *i*) the characterization of radio frequency (RF) signals from PD activity in HV equipment; *ii*) the formulation of a generic RF impulsive noise model induced by PD; *iii*) the statistical analysis of the model in the presence of multiple PD sources.

Thesis organization

This document is organized in five chapters as follows:

Chapter 1 is a literature review of the characterization and interference modelling of radio noise. Then, impulsive radio noise in high voltage substations is particularly emphasized. It is shown that impulsive noise is mainly produced by PD sources in substations. The study of PD is a well-developed field of research, even though electromagnetic radiation and its resultant impact on wireless communication systems have been largely ignored in recent papers. PD Measurement, detection and impulsive noise models induced by PD are summarized. In conclusion, our research objectives and the methodologies employed are detailed in the rest of the document.

In Chapter 2, we develop a measurement setup using a wideband antenna to capture electromagnetic radiation induced by PDs in a frequency range of 800 MHz to 5 GHz which covers frequency bands of conventional wireless communications. Then, signal processing tools are developed for the first-order characterization of RF signals from PD activity in the air. EMIs

induced by PDs are measured and characterized in a 735 kV substation. This chapter is mostly based on our published conference paper (Au *et al.*, 2013).

In Chapter 3, we propose first a coherent, detailed and validated PD model that links the physical characteristics of HV installations to the induced radio interference spectrum. PD sources are generated experimentally in a 16 kV stator bar in the IREQ laboratory. Using our proposed characterization process described in Chapter 2, our proposed model is validated by comparing measurement results to the results of simulations. This chapter is based on our published journal paper (Au *et al.*, 2015b).

In Chapter 4, a general RF impulsive noise waveform model is proposed based on second-order statistics. Time series models are used to estimate spectrum characteristics of RF impulsive signals from PDs with a reasonable number of parameters. It is shown that residuals from fitted time series models are stochastic processes in which the variance is not constant over time. A heteroskedastic white Gaussian noise is used to reproduce the random behaviour of transient impulsive waveforms. Measurement results and simulation results show that our RF impulsive noise waveform model fits measurements accurately. This chapter is based on our submitted journal paper (Au *et al.*, 2015b)

In Chapter 5, the RF impulsive noise model is generalized in the presence of multiple PD sources. A spatial and temporal Poisson point process (the Poisson field of interferers) is used to emulate an environment typical of substations. This generalized model can take into account physical-statistical parameters estimated from data. We employ our proposed RF impulsive noise waveform model to reproduce typical impulsive noise waveforms in which parameters are estimated from the measurements that were presented in Chapter 4. Moreover, the first-order characteristics of PD such as power density, inter-arrival time and occurrence distributions from data can be used. In this chapter, the statistical properties of the generalized model can be derived based on practical assumptions. Therefore, signal processing algorithms can be implemented for rapid PD identification, localization, and impulsive noise mitigation techniques. These can in turn be utilized in wireless communications in substations. This chapter

is a summary of our research based on our proposed and published papers (Au *et al.*, 2015a; Ali *et al.*, 2015; Au *et al.*, 2015e).

Finally, we conclude this document with a summary of our work and a discussion of important findings.

List of contributions

The majority of these works have been published or submitted to international conferences and journals. They are listed as follows:

Conference papers

- an Experimental Characterization of Substation Impulsive Noise for an RF Channel Model in Progress in Electromagnetics Research Symposium (Au *et al.*, 2013);
- Mitigation of Impulsive Interference in Power Substation with Multi-Antenna Systems in IEEE International Conference on Ubiquitous Wireless Broadband (Ali *et al.*, 2015).

Journal papers

- a Model of Electromagnetic Interferences Induced by Corona Discharges for Wireless Channels in Substation Environments in IEEE Transactions on Electromagnetic Compatibility (Au *et al.*, 2015b);
- Analysis and Modelling of Wideband RF Impulsive Signals Induced by Partial Discharges using Second-Order Statistics in IEEE Transaction on Electromagnetic Compatibility (submitted) (Au *et al.*, 2015d);
- a Fast Identification of Partial Discharge Sources using Blind Source Separation and Kurtosis in Electronic Letters IET (Au *et al.*, 2015e).

CHAPTER 1

CHARACTERIZATION AND MODELLING EMI FROM ELECTRIC DISCHARGES: A LITERATURE REVIEW

1.1 Introduction

Communications technology for smart grid applications is an area of growing interest as mentioned in many publications (Yan *et al.*, 2013; Gungor *et al.*, 2011, 2010; Gungor and Lambert, 2006; Amin and Wollenberg, 2005). Indeed, its deployment can significantly improve the efficiency, reliability and safety of the electric power grid (Gungor *et al.*, 2010). This communications technology can be classified into four types: power-line communications, satellite communications, wireless communications and optical fiber communications. Of these technologies, wireless communications offers potential benefits for the implementation of smart grids, such as rapid deployment, low installation cost, and mobility. However, in industrial environments, the transmitted signal quality can be degraded due to various electromagnetic interferences. As a result, it is necessary to evaluate the communication performance in such environments.

Channel models are valuable tools for characterizing interference phenomena, performing communications analyses, and designing and optimizing communication systems in harsh and hostile environments. An accurate channel model can be provided through an experimental characterization of the interference sources that are produced mainly by electromagnetic, electrostatic or non-electric sources. For conventional wireless communication systems, interferences often come from external electromagnetic sources. The deployment of wireless sensor networks has been investigated by Gungor *et al.* (2010) and Gungor and Lambert (2006), along with associated opportunities and challenges. While propagation channel measurements in substations are presented, high-voltage installations can generate electromagnetic radiation in instances when the spectrum can be measured above a few GHz, as is mentioned in several publications (Portugués *et al.*, 2003; Moore *et al.*, 2006; Judd *et al.*, 1996a; Sarathi *et al.*, 2008; Moose and O'dwyer, 1986). These electromagnetic interference (EMI) sources are highly im-

pulsive with short durations generally caused by electric arc discharges and partial discharges sources. Under such conditions, the conventional wireless communication systems listed in Gungor *et al.* (2010) and Gungor and Lambert (2006) can be interfered to such an extent as to render their performances severely degraded.

The subject of partial discharges (PD) is an intensive research area in which physical mechanisms, measurement and characterization have been investigated for many years (Bartnikas, 2002; Bartnikas and McMahon, 1979; Florkowska and Wlodek, 1993; Judd *et al.*, 1996a; Trichel, 1939). The interest in partial discharges can be explained by the harmful effects these discharges have been observed to have on electrical insulations, including irreversible damage and possible failure. Moreover, electromagnetic radiations can also interfere with radio communication devices such as TV or FM radio (CIGRÉ, 1974; Arai *et al.*, 1985).

This chapter gives a general overview of EMIs and describes the measurement and characterization methods associated with them, in keeping with the latest research. Impulsive noise phenomenon in substations are particularly emphasized and existing impulsive noise models are discussed. The chapter is organized as follows: Section 1.2 introduces, defines, and classifies the concept of EMI sources. A review of related literature shows the impact of impulsive EMI sources; namely, that performance can be severely degraded in these special environments. Many papers show that the performance can be severely degraded in these special environments. In Section 1.3, the characterization and existing impulsive noise models for communication channels are presented. In Section 1.4, the emphasis is on how EMIs are generated mainly by partial discharge sources in substations. The physical mechanisms, measurements, detection methods and existing PD models are reviewed. Section 1.5 concludes this chapter with a brief summary and discussion of our proposed research. Through the literature review, we will show that existing PD characterization methods do not assess if electromagnetic radiation from PD activity is a source of interference for the radio communication systems operating in the industrial, scientific and medical (ISM) radio bands and existing impulsive noise models cannot link the physical characteristics of high-voltage installations to the induced radio interference spectrum neither.

1.2 Concept of electromagnetic interferences and classification

This section presents a general overview of EMI, which can be classified into two categories: natural noise sources and man-made noise sources. In high-voltage substations, man-made noise sources are caused mainly by electric arc discharges in which electromagnetic radiations are sources of interference for conventional wireless communication systems.

1.2.1 Definition of EMI sources

Electromagnetic interferences are observed when external sources interfere with any other devices. Their tolerance to unwanted electromagnetic (EM) radiation should be analysed and characterized in order to assess the electromagnetic compatibility (EMC) of interference sources with any other electronic devices (Kaiser, 2005; Vasilescu, 2005).

We may distinguish intrinsic noise sources inherently generated by the electronic device itself and the external noise generated by interferences. Intrinsic noise sources are generated inside the device. A typical example of intrinsic noise is thermal noise. It comes from the motion of free electrons inside a conductive material, which is inherently random and unavoidable. The resulting signal amplitude fluctuates randomly. This can be modelled as Gaussian noise in which the mean value is zero and its variance is given by:

$$v_n^2 = 4k_B T R \Delta f \tag{1.1}$$

where k_B is Boltzmann's constant, T is the temperature, R is the resistance of the material and Δf is the bandwidth of the measurement system that has been employed.

External noise sources are unwanted signals in which EM waves come from undesired sources. In the literature (Kaiser, 2005; Vasilescu, 2005), these interferences are classified into natural noise sources (*e.g.* atmospheric noise, cosmic noise, etc.) or man-made noise sources (*e.g.* industrial noise, arc welding, switches, etc.).

1.2.2 Natural noise sources

These noise sources are produced by charged particles that are either present or produced naturally in the environment. The waveform can be modelled as Gaussian noise (*e.g.* cosmic noise) or as transient impulsive noise (*e.g.* lightning discharges). The emitted radiations can occupy a wide range of frequencies; typically, they can reach a few GHz.

Atmospheric noises are generated by lightning discharges in thunderstorms. They are characterized by fast transient waveforms and rapid time decay (10 to 100 μs). The current amplitude can be 20 kA for an average arc discharge and 300 kA for a very high-arc discharge. They are mostly harmful to humans and damage electronic devices embedded in aircraft. The frequency spectrum can be up to 20 MHz and the spectral density has a form of $\sim 1/f$ (Vasilescu, 2005). This spectrum content explains why a natural noise sources are generally considered less troublesome than man-made noise sources, which covers a much broader band.

1.2.3 Man-made noise sources

Electromagnetic man-made noise sources are generated by human activities via any electrical or electronic devices that may be located in industrial, residential or business areas. These sources can generate various type of waveforms like stationary random signals, non-stationary random signals (*e.g.* impulsive noise), and/or modulated signals from undesired communication systems.

Interference sources can affect the reliability of communications systems and also damage electronic devices when the amplitude of the current is very high. These sources can be intentional interferences (jammers) and/or unintentional interferences. The latter could come from EM sources induced by the normal operation of any electronic device. As a result, it is necessary to characterize and to quantify their impact on communication systems.

Among man-made noise sources, impulsive noise can be generated by automotive ignition systems, arc welding, power-line distribution systems, high-voltage transmission lines or HV

equipment in substations. The amplitude associated with such sources is very high and has short durations compared to background noise: 50 to 310 μs in power-line distribution systems (Zimmermann and Dostert, 2002; Degardin *et al.*, 2002), and 50 to 200 ns in HV transmission lines as reported in (CIGRÉ, 1974; Gary, 1998). The impulse repetition rate can range from 50 to 200 kHz in power-line distributions and around 50 to 100 kHz in HV transmission lines. When impulsive noise is significant, communication performances can be severely degraded.

1.2.4 Communication channels in presence of impulsive noise

For several years, there has been a growing interest in both broadband power-line communications and wireless communications within industrial environments. Unfortunately, various EMIs especially impulsive noise can interfere with communication systems. Many papers show that the receivers perform poorly (Madi *et al.*, 2011, 2010; Shan *et al.*, 2007; Ma *et al.*, 2005; Haring and Vinck, 2000; Ghosh, 1996; Spaulding and Middleton, 1977). Due to extensive research, more robust optimum and suboptimum receivers that function even in the presence of impulsive noise have been developed, along with mitigation techniques (Ling *et al.*, 2013; Ndo *et al.*, 2013; Tsihrintzis and Nikias, 1995; Ambike and Hatzinakos, 1994; Spaulding and Middleton, 1977).

Typically, communication channels include a transmitted signal and additive interferences such that the received signal is written as:

$$x(t) = s(t) + n(t) + \sum_{k} u_k(\theta_k, t) \tag{1.2}$$

where $s(t)$ is the transmitted signal, $n(t)$ is the receiver's thermal noise and $u_k(\theta_k,t)$ is the k^{th} interferer where θ is a set of random variables characterizing the interference. If we assume that $x(t)$ is a sequence of independent and identically distributed (*iid*) random variables with the same expected value and a finite variance, then, the sum of overall received signals converges in distribution to a Gaussian distribution. From this assumption, classical coding theory is well-known (Proakis and Salehi, 2008; Goldsmith, 2005). However, when the receiver is corrupted

by impulsive interferers, the probability density is heavy tailed. Therefore, the assumption of Gaussian distribution no longer applies and the classical decoding scheme and detection rules for additive white Gaussian noise (AWGN) channel fail to recover the transmitted message from $s(t)$.

1.3 Characterization and impulsive noise models

In the literature, models for impulsive noise are widely developed and used to extend the existing knowledge regarding the nature of impulsive noise sources and communication performance analysis. In this section, characterization methods and existing impulsive models are reviewed.

1.3.1 A statistical characterization of impulsive noise

In practice, measured impulsive noise consists of impulsive events and additive background noise. The latter is produced by thermal noise from the measurement setup as well as ambient noise, which is generated by many interferences below the level of impulses as depicted in Figure 1.1. Since these impulsive waveforms are characterized by their short duration and high amplitude, they can be detected using a simple threshold. A more sophisticated technique can be used to extract impulses from overall background noise to yield an estimation of power spectral density. This will be detailed in Chapter 2.

Impulsive interferences can be characterized in one of two ways. Using first-order statistics, statistical distribution can be calculated using duration, the inter-arrival time between two consecutive impulses, amplitude, and energy. Assuming that impulsive noise is a non-stationary random process, short-time analysis is used in the analysis of first-order statistics. Second-order statistics utilizes power spectral densities, and a Spectrogram, a Wigner-Ville distribution, or a scalogram can be used to estimate PSD, (Mallat, 1998; Hammond and White, 1996; Priestley, 1967).

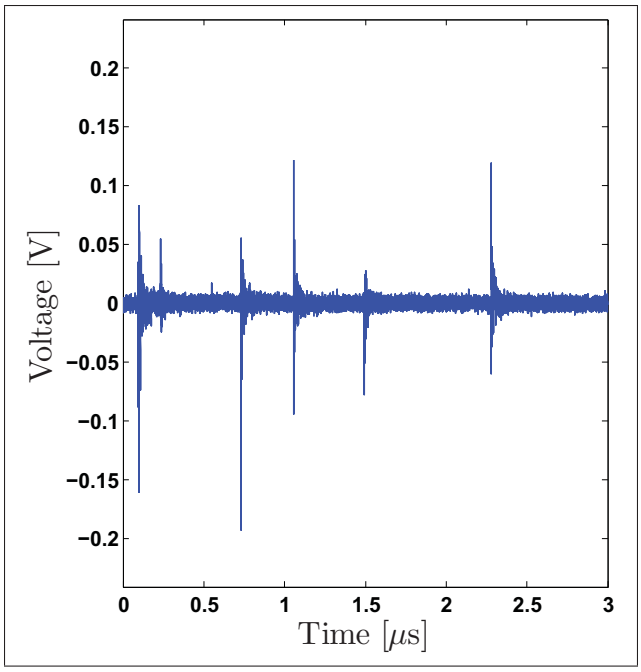

Figure 1.1 Typical example of impulsive noise with background Gaussian noise

1.3.2 Impulsive noise models

Impulsive noise can be modelled as a succession of short impulse waveforms with background noise over a large observation time. Various approaches can be used to represent impulsive waveforms. Middleton (1999) classifies these interferences into three categories as follows:

- EMIs can produce negligible transient waveforms in a typical receiver. It is denoted by Class A noise. In terms of receiver bandwidth Δf_R and duration of interference sources T_U, the Class A noise assume that:

$$T_U \Delta f_R \gg 1 \tag{1.3}$$

- when EMIs are characterized by transient effects, they are denoted by Class B noise when the receiver bandwidth and the duration of interference sources are:

$$T_U \Delta f_R \ll 1 \tag{1.4}$$

- class C is a mixture of Class A and B in which Class B is predominant compared to Class A.

An impulse can be modelled as a unit-impulse function $u(t) = \delta(t)$ with an infinitesimal time width or duration. The integral of the impulse is given by:

$$\int_{-T_U/2}^{T_U/2} \delta(t)dt = \begin{cases} 1, & -T_U/2 < t < T_U/2. \\ 0, & \text{otherwise.} \end{cases} \tag{1.5}$$

The Fourier transform is given by:

$$\delta(f) = \int_{\mathbb{R}} \delta(t)e^{-j2\pi ft}dt = 1 \tag{1.6}$$

where f is the frequency domain of an arbitrary function. However, the unit-impulse function with an infinitesimal time duration does not exist in practice because impulsive interferences have a non-zero finite duration in real-life.

A channel response impulse can be used to model various impulsive noise waveforms such as damped oscillation with transient effects, etc. As presented in Figure 1.2, a typical impulsive waveform can be modelled by using a filter in which the input model is an ideal impulse. In this condition, a power spectral density can be determined.

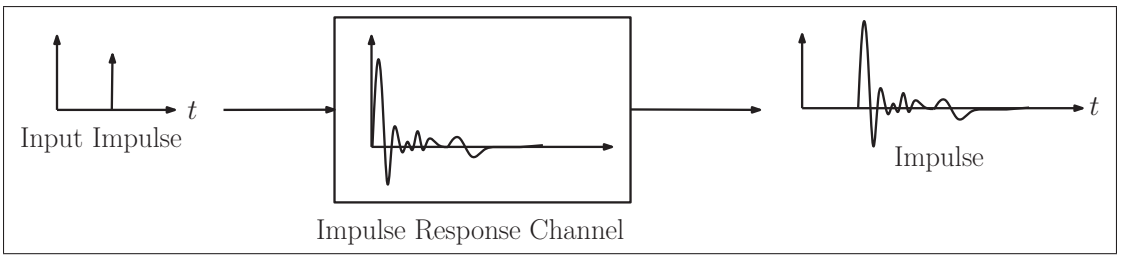

Figure 1.2 Impulsive noise modelled by a filter

For a given impulse time-occurrence t_n, the resulting waveform can be written as a convolution product between the input impulse and the filter, such that:

$$u(t) = h_m(t) * \delta(t - t_n) \tag{1.7}$$

where the impulse response of the filter is given by $h_m(t)$ and $*$ is the convolution product operator. Physically, the impulse response includes the propagation channel, the impulse response of both the emitted source and the measurement setup. The power spectral density of the resulting impulse is only determined by the power spectral density of this filter.

1.3.3 Probability models of impulsive noise

Impulsive noise can be characterized and modelled by its instantaneous amplitude probability density function. This representation is commonly used in the study of communication performance. Over a long observation time, the resulting noise is a superposition of many independent sources with a random number of impulsive radiations and their locations are randomly distributed in space. From Equation (1.2), without any signals to be transmitted at the receiver ($s(t) = 0$) and assuming that background noise $n(t)$ is modelled as a Gaussian noise process, the overall noise is given by:

$$x(t) = \sum_k u_k(\theta_k, t) + n(t) \tag{1.8}$$

In the literature, many existing impulsive noise models have been developed, (Middleton, 1999; Zimmermann and Dostert, 2002; Ndo *et al.*, 2013; Vaseghi, 2008) . They can be classified as either memoryless noise or memory noise models, (Vaseghi, 2008).

1.3.3.1 Memoryless models

Poisson-Gaussian noise

We assume the overall noise to be a superposition of independent EMI emissions modelled as a Poisson process for a large observation time T, while the amplitude distribution of impulses is a Gaussian noise process. From Equation (1.8), the resulting noise is given by:

$$x(t) = \sum_{k=1}^{N_I(t)} a_k \delta(t - t_k) + n(t) \tag{1.9}$$

where a_k is the random amplitude of the impulse k^{th} and the impulsive event is given by t_k. $N_I(t)$ is the number of impulses driven by a homogeneous Poisson process. The probability occurrence of the k^{th} impulse in the observation time T is given by:

$$f(k;\lambda) = \Pr\left[N_I(t+T) - N_I(t) = k\right] = \frac{e^{-\lambda T}(\lambda T)^k}{k!} \tag{1.10}$$

where λT is the average number of emissions occurring within the observation time and λ is the density of emissions. The probability density function (PDF) of impulsive noise is given in (Vaseghi, 2008) in a small time interval Δt by:

$$f_I(u) = (1 - \lambda \Delta t)\,\delta(u) + \lambda \Delta t \frac{1}{\sqrt{2\pi}\sigma_u} e^{-u^2/2\sigma_u^2} \tag{1.11}$$

where σ_u is the variance of the impulsive component. Since the background noise and impulsive noise are a sum of independent random processes, the resulting PDF is written as the convolution product of the background noise PDF and the impulsive noise PDF such that:

$$f_{P+G}(x) = f_I(x) * f_n(x) \tag{1.12}$$

where $f_n(x)$ is the Gaussian distribution of the background noise; and

$$f_n(x) = \frac{1}{\sqrt{2\pi}\sigma_n} e^{-x^2/2\sigma_n^2} \tag{1.13}$$

where σ_n is the variance of the background noise component.

Middleton Class A and B noise

Extended to Poisson-Gaussian models, physical-statistical impulsive noise models are proposed by Middleton (1999, 1983, 1977). Based on the Poisson field of interferers, the resulting noise is a superposition of independent EMI sources randomly distributed in space which results in emissions that can be activated within a given observation time T. The PDF of overall noise can be derived for Class A noise as:

$$f_{P+G}(x) = e^{-A} \sum_{m=0}^{\infty} \frac{A^m}{m!\sqrt{2\pi\sigma_m^2}} e^{-x^2/2\sigma_m^2} \tag{1.14}$$

where $\sigma_m^2 = \frac{m/A+\Gamma}{1+\Gamma}$.

- the parameter A is the impulse index. This is the average number of emissions for a given observation time. From Equation (1.10), $A = \lambda T$ where $A \in \left[10^{-2}, 1\right]$;
- the parameter Γ is the ratio between the level of the background noise and the level of the impulsive noise component where $\Gamma \in \left[10^{-6}, 1\right]$.

The Class A PDF can be seen as a weighted sum of Gaussian probability densities. This model is widely used due to its canonical form, and accordingly, this is an analytically tractable model for narrowband interferences in which the transients in the typical receiver can be neglected.

Class B interferences with transient effects is a broadband noise model which is thus more complex than the Class A noise model (Middleton, 1999). The interference noise model is physically coherent, due the presence of the Gaussian noise component (background noise).

However, six parameters and an empirical parameter have to be considered in this model, which is more difficult to use.

α-stable noise

As an alternative to the Class B interference model, α-stable noise model is used to approximate the Middleton Class B model (Nikias and Shao, 1995). The α-stable distribution was introduced by Lévy (1925) in his study of normalized sums of *iid* random variables. Let X be a stable random variable such that $X \sim S_\alpha(\sigma,\beta,\mu)$. The noise model is defined by its characteristic function (c.f) $\mathscr{M}_X(j\xi)$ given by:

$$\mathscr{M}_X(j\xi) = \mathbb{E}\left[e^{j\xi X}\right] = \begin{cases} \exp\left\{j\xi\mu - |\sigma\xi|^\alpha\left(1 - j\beta\,\mathrm{sign}(\xi)\tan(\pi\alpha/2)\right)\right\}, & \alpha \neq 1. \\ \exp\left\{j\xi\mu - |\sigma\xi|^\alpha\left(1 - j\beta\,\mathrm{sign}(\xi)\frac{2}{\pi}\log|\xi|\right)\right\}, & \alpha = 1. \end{cases} \tag{1.15}$$

where $\mathbb{E}[\cdot]$ denotes the expectation, $0 < \alpha < 2$ is the stability index, μ is a location parameter real value, $\sigma \geq 0$ is a scale factor and β is the skewness parameter where $-1 \leq \beta \leq 1$. The model can take into consideration the heavy-tailed behaviour induced by impulsive events in the distribution. By using the inverse Fourier transform, the PDF is obtained. However, closed forms are difficult to derive. Only a few stable distributions can be written in closed forms for specific parameters of α for:

- $\alpha = 2$, the PDF is the Gaussian distribution, $X \sim S_2(\sigma,0,\mu)$, where the mean is given by μ and its variance is 2σ. Note that the scale factor σ is not the same as the variance of the Gaussian noise;
- $\alpha = 1$, the PDF is the Cauchy distribution, $X \sim S_1(\sigma,0,\mu)$ and
- $\alpha = 1/2$, the PDF is the Levy distribution, $X \sim S_{1/2}(\sigma,1,\mu)$.

Middleton (1999) notes that the α-stable model is physically incomplete since the background noise modelled as a Gaussian noise is not considered. These memoryless models have the

advantage of being analytically tractable when parameters of these PDFs can be estimated by using statistical methods (Zabin and Poor, 1991, 1989; Tsihrintzis and Nikias, 1996; Middleton, 1983; Chambers *et al.*, 1976). Based on these impulsive noise models, performance analysis of communication systems have been investigated (Tsihrintzis and Nikias, 1995; Spaulding and Middleton, 1977; Wiklundh *et al.*, 2009; Wang *et al.*, 2011).

1.3.3.2 Impulsive noise with memory: Burst noise

Markov-Middleton

Memoryless impulsive noise models generate *iid* noise samples when time correlation is not taken into account. In practice, most environments, such as high-voltage substations or power-line distribution systems, experience impulsive noise in bursts, (Portugués *et al.*, 2003; Zimmermann and Dostert, 2002; Moore *et al.*, 2006). Markov chains have been investigated for impulsive noise modelling in instances when this bursty behaviour of impulsive noise can be reproduced.

Recently, a Markov-Middleton model has been proposed in (Ndo *et al.*, 2013). This model uses the Middleton Class A noise model but includes an extra parameter to ensure the presence of impulse memory with a hidden Markov model, as shown in Figure 1.3. A transition state is considered when duration within the state is null. The correlation between noise samples is ensured by the probability p_x, which is independent of Middleton Class A parameters. The entering state $m = \{0,1,2,3,\cdots\}$ from the transition state is ensured by the probability p_m such that:

$$p_m = \frac{p'_m}{\sum_{m=0} p'_m} \tag{1.16}$$

where $p'_m = e^{-A}A^m/m!$, according to the Middleton Class A PDF model. Each state generates noise samples from a zero-mean Gaussian noise where its variance is given by $\sigma_m^2 = \frac{m/A+\Gamma}{1+\Gamma}$.

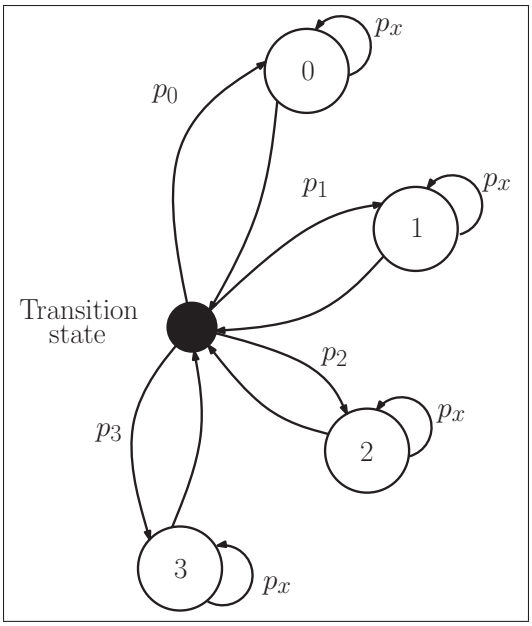

Figure 1.3 Markov-Middleton impulsive noise model with 3 states of Markov chain
Taken from Ndo *et al.* (2013)

The model has the same Middleton Class A PDF, which is analytically tractable, and the time correlation of bursty impulsive noise is taken into consideration. However, the number of states in Markov chains might be difficult to define, and the resulting impulsive noise samples are still uncorrelated. Therefore, transient and damped oscillation effects are neglected.

Partitioned Markov chain

Alternatively, partitioned Markov chain (PMC) models can be used to reproduce memory effects of impulsive noise. A PMC model has been developed for broadband power-line communications in (Zimmermann and Dostert, 2002). This model can reproduce the bursty behaviour of impulsive noise in PLC. Simulation results show that the model fits measurements. An example of PMC for asynchronous impulsive noise is depicted in Figure 1.4. The K states are partitioned into two groups; A denotes the absence of an impulsive component, and B, the presence of an impulse event. This is the generalization of the Gilbert-Elliot model for bursty impulsive noise modelling (Gilbert, 1960; Elliot, 1963). The latter considers only two states

of the Markov chain. The two groups can be described independently by transition probability matrices for free impulses states and for impulse states. In addition, transition states are introduced in order to regulate the transition from free impulses states to impulse states and vice versa. However, the definition of a suitable number of states in the Markov chain can be challenging and the estimation procedure are complex, (Sacuto *et al.*, 2013; Ndo *et al.*, 2013). Using these models can also drastically increase computational complexity, (Zimmermann and Dostert, 2002; Sacuto *et al.*, 2013).

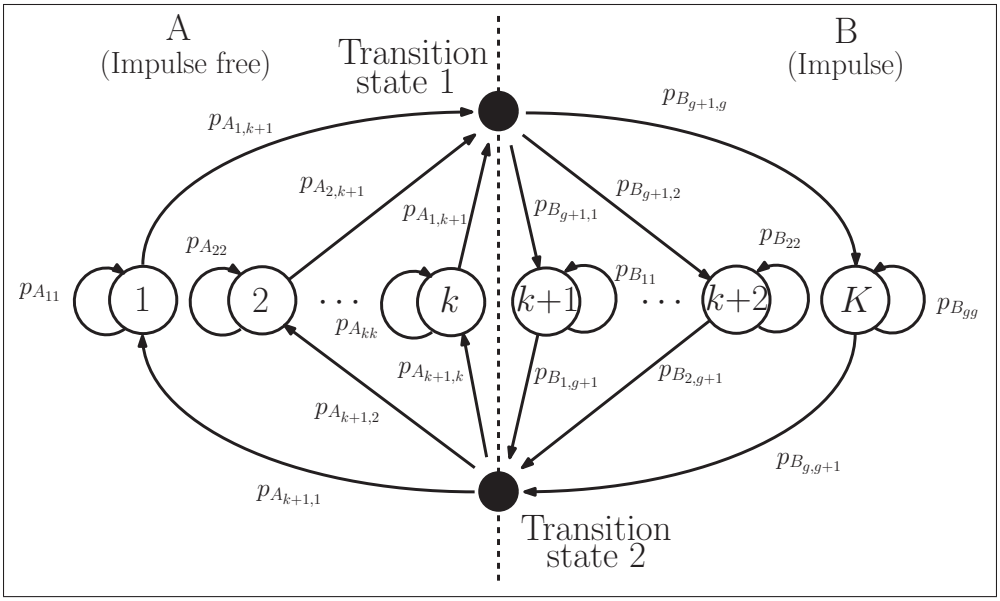

Figure 1.4 Partitionned Markov chain for asynchronous impulsive noise
Taken from Zimmermann and Dostert (2002)

These statistical impulsive noise models can reproduce EMIs in various impulsive environments. However, they do not take into account the specificity of the electromagnetic environment in substations; In other words, they cannot provide any information linking the physical characteristics of HV installations to the induced radio interference spectrum. The next section focuses on the electromagnetic interferences in substations.

1.4 The electromagnetic interferences in substations

In high-voltage substations, electric arc discharges can be generated in HV equipment, either along insulation surfaces or in an air gap between a pair of electrodes. Their electromagnetic radiations are man-made noise in which the amplitude is highly impulsive. Electric arc discharges have been investigated for several years to understand the physical mechanisms involved and to assess their impact on electrical insulation. These discharge are also EMI sources for radio communications systems.

1.4.1 Ionization process and electrical discharge in gases

Discharges in gases are related to a partial or complete breakdown of a gas phenomenon. They occur when an applied electric field is sufficiently high. In such instances, due to a strong acceleration of free electrons, other neutral molecules and atoms become excited or ionized by collisions in which kinetic energies are exchanged. An ionization process in gases can take place by avalanche effect. Depending on the nature of the gas, the ionization process can be significant when densities of electrons are high (Kuffel *et al.*, 2000; Loeb, 1965; Bartnikas and McMahon, 1979). Townsend (1910) found that the current through a uniform field air gap, grows exponentially when the applied voltage is sufficiently high, as shown in Figure 1.5. A pair of electrodes is separated by an air gap of a length d, and the electric field $\mathbf{E}$ between the electrodes is generated by an applied voltage. At voltages higher than V_2, the current growth is due to ionization by electron collision in the gas (Townsend, 1910).

Various ionization phenomena can be observed during an electric discharge, such as photoionization and/or thermal ionization processes. Deionization by recombination and/or diffusion can also be observed (Kuffel *et al.*, 2000). In addition to a high field stress, an initiatory-free electron rate can affect discharge events by a random time lag which depends on the amount of pre-ionization or irradiation of the gap (Meek and Craggs, 1953).

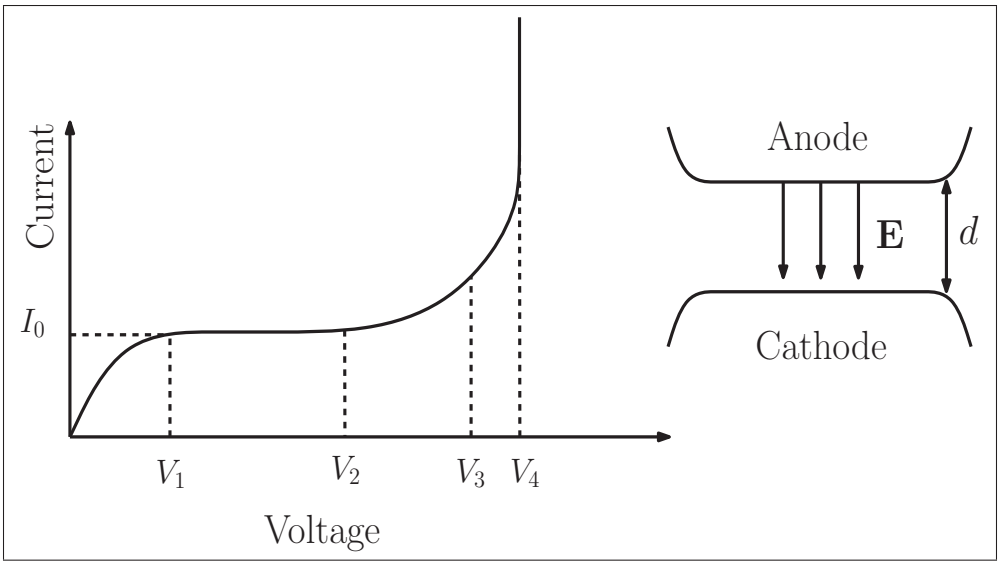

Figure 1.5 Current-voltage relationship in prebreakdown region
Taken from Kuffel *et al.* (2000)

1.4.2 Partial discharges mechanism

Three major types of discharges can be distinguished (Lemke, 2008). The first is internal discharge, which refers to discharge within dielectric insulation caused by gaseous inclusion or gas bubbles in liquids. The second major type of discharge is external discharge. Often known as corona discharge, it takes place in ambient air. The third type occurs along solid dielectric surfaces in ambient air. These discharges may bridge in a long gap distance and can erode solid insulation surfaces due to the high temperature in the discharge site (Lemke, 2008; Hudon and Bélec, 2005). Their physical mechanism is related to the ionization processes induced by electron-avalanches as observed in (Townsend, 1910; Loeb and Meek, 1940).

PD phenomena are represented as stochastic processes in which amplitude, inter-arrival time between two successive impulses, and time occurrence are random variables. This can be explained by the variability of physical mechanisms such as the presence of ionizing radiation, fluctuations in gas density or gas decomposition in cavities or dielectric surfaces, (Brunt and Kulkarni, 1990; Brunt, 1991). Under AC voltages, PDs occur on every half-cycle of the applied volt-

age. Typical behaviours of impulsive noise from PD activity are presented in Figure 1.6. PD events are superimposed upon the AC voltage.

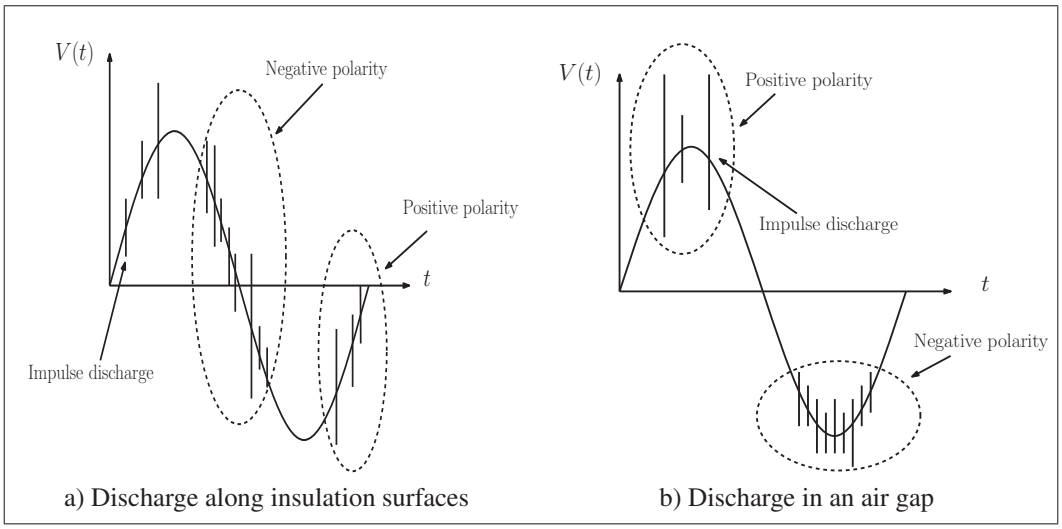

Figure 1.6 Typical behaviour of impulsive noise induced by a discharge source

When PDs take place along insulation surfaces, an asymmetric behaviour between polarities can be observed (Levesque *et al.*, 2010; Hudon and Bélec, 2005). Their amplitude and occurrence are higher at negative polarity than at positive as depicted in Figure 1.6.(a). This behaviour can be found during slot discharge, surface tracking or gap-type discharge events (Hudon and Bélec, 2005; Lemke, 2008; Levesque *et al.*, 2010). For PDs in an air gap, the process occurs at the peak region of the applied AC voltage. At the negative polarity, impulses, known as Trichel impulses, can be observed with high repetition rates (between 50 and 100 kHz) and low amplitude, while impulses at the positive polarity, known as a pre-breakdown streamer, have low repetition rates with high amplitude as illustrated in Figure 1.6.(b). This behaviour can be found in overhead power-lines (Pakala and Chartier, 1971; Pakala *et al.*, 1968; Chartier *et al.*, 1986; Gary, 1998; CIGRÉ, 1974).

These discharges can cause degradation and possible mechanical failure of electrical insulations (Lemke, 2008; Kuffel *et al.*, 2000; Bartnikas and McMahon, 1979). They are also in-

terference sources for TV and FM radio (CIGRÉ, 1974; Arai *et al.*, 1985). Over the last four decades, PD detection and characterization methods have become important in the study of aging mechanisms and life-time analysis of HV equipment.

1.4.3 Measurements and characterization of partial discharge sources

1.4.3.1 Measurement techniques

Partial discharges can generate electrical pulse currents, dielectric losses, electromagnetic radiations, chemical reactions, and more. In this chapter, we present methods for PD detection and measurement based on impulse currents and electromagnetic radiation. These two methods are commonly used (Kuffel *et al.*, 2000).

PD currents impulses

PD impulse currents can be measured by connecting the test object to a high-voltage source. The circuit for a PD test includes an impedance Z and a coupling capacitor C_k in parallel to the test object as depicted in Figure 1.7. The test object can be seen as a capacitor C_t. During the short period of the partial discharge, C_k is a storage capacitor which can release a PD current impulse $I_{pd}(t)$ between C_k and the test object C_t.

The PD pulse apparent charge q can is given by:

$$q = \int I_{pd}(t)dt \tag{1.17}$$

when $C_k \gg C_t$. It is said apparent because the measured charge q is not equal to the charge locally involved at the discharge site (Kuffel *et al.*, 2000; IEC-60270, 2000). Thus, the true charge cannot be measured directly. However, a calibration procedure can be used to improve the measurement of PD quantities.

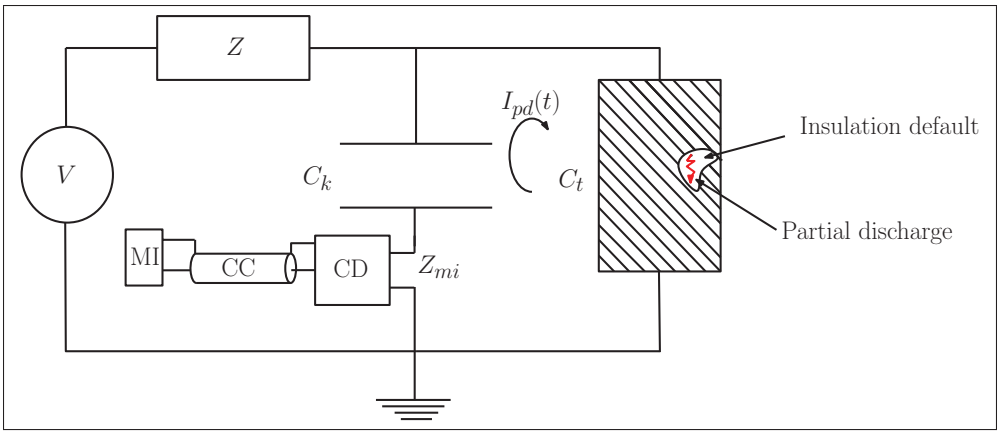

Figure 1.7 Test circuit for partial discharge detection
Taken from IEC-60270 (2000)

Most PD measurement systems based on PD impulse currents are integrated into the test circuit as shown in Figure 1.7. The circuit includes a coupling device with its impedance Z_{mi}, and the measurement instrument is linked by a connecting cable. The coupling device can be a passive filter, such as a parallel RLC resonance circuit as was used by Bartnikas and McMahon (1979). The input current and the output voltage are linked by the impedance of the filter when the apparent charge of PD pulse can be measured. Low- and high-frequency currents can be filtered by adjusting the parameters of the RLC circuit.

PD electromagnetic radiations

EM radiations from PD activity can be detected by passive devices such as antennas or sensors. They can be detected in the ultra high frequency (UHF) range (Hikita *et al.*, 1998; Hoek *et al.*, 2012; Tenbohlen *et al.*, 2008; Judd *et al.*, 2005; Portugués *et al.*, 2003; Pearson *et al.*, 1991). There are several advantages to these methods: sensors do not need electrical connection to the high voltage circuit, they ensure a better signal-to-noise ratio, and their use allows failure location to be determined by using PD localization methods (Tenbohlen *et al.*, 2008). UHF PD measuring methods are mostly used in gas-insulated substations (GIS) in which HV equipment is contained in a sealed environment with sulfure hexafluoride gas (SF6). A typical measure-

ment setup is presented in Figure 1.8. Signals from the UHF sensor are filtered, amplified by RF stages and digitized by digitizing hardware to extract PD quantities.

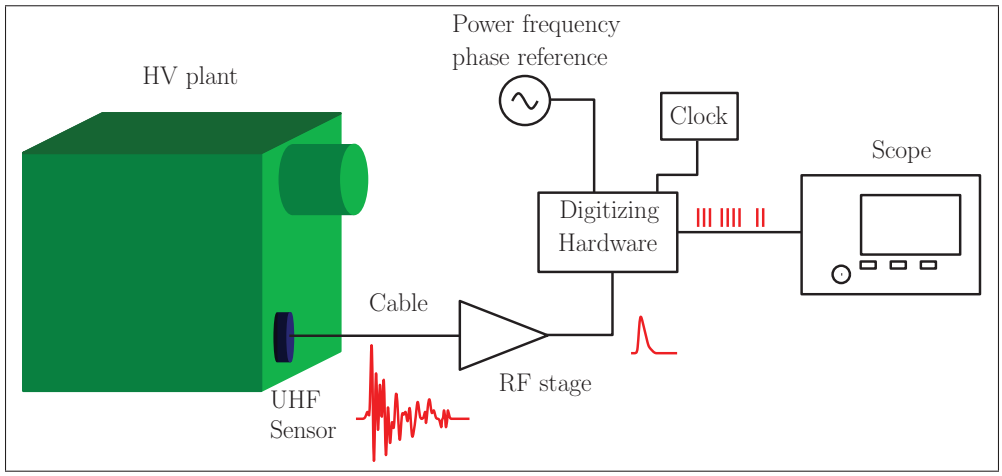

Figure 1.8 Typical measurement setup using UHF PD detection
Taken from Judd *et al.* (2005)

Electromagnetic radiations from PD can be measured using antennas. A typical measurement setup includes a wideband antenna, RF filters and amplifiers. Impulses are recorded by a scope over a very large frequency range. Pakala and Chartier (1971); Pakala *et al.* (1968) use a wideband antenna to measure corona and gap-type discharges in a 60 Hz to 10 GHz frequency range on 2.4 kV to 765 kV overhead power-lines under AC voltages. It has been found that the power spectral density (PSD) of these interferences have a form of $1/f^{\gamma}$ where γ is the exponent characterizing the decay over frequency (Pakala and Chartier, 1971; Pakala *et al.*, 1968; Portugués *et al.*, 2003). The waveform is impulsive with transient effects (Portugués *et al.*, 2003; Portugués and Moore, 2006; Moore *et al.*, 2005).

These discharges are also EMI sources for RF communications (Arai *et al.*, 1985; Babnik *et al.*, 2003; Trinh, 2001; Madi *et al.*, 2010). PD measurement and detection methods using antennas are appropriate for RF channel characterization in substation environments. In the literature, the physical mechanism of PD and its electromagnetic radiation is not explicit and the characterization is often incomplete. For example, in (Pakala and Chartier, 1971) and

(Pakala *et al.*, 1968), information about the inter-arrival time, duration and occurrence of PD is not provided. In (Portugués *et al.*, 2003) (Portugués and Moore, 2006) and (Moore *et al.*, 2005), RF signals are measured in the frequency range 100 MHz to 1 GHz, which does not cover the frequency range of conventional communication systems, which is 800 MHz to 5 GHz.

1.4.3.2 Characterization of PD impulses

PD phenomena are a category of stochastic processes whose characteristics can be described as time-dependent random variables (Brunt, 1991). PD impulses are then characterized by:

- the repetition rate, which is the total number of PD impulses occurring within an arbitrary time interval. With AC voltages, this time interval can be a cycle of the applied voltage. Thus, the repetition rate is defined as the number of PD impulses per cycle. The repetition rate can be also defined as the number of impulses during the positive or the negative polarity of the AC voltage;
- the inter-arrival time (IAT), which is the time between two consecutive PD impulses. Under AC voltages, IAT can be measured at the positive or at the negative polarity;
- the occurrence which is the time in which a PD occurs under the operating voltage. Under AC voltages, the PD process is cyclostationary as the PD occurs at every half-cycle of the applied voltage;
- the duration of an impulse. PD can have different physical processes in which the duration can be variable;
- the amplitude of a discharge, which can be measured by the apparent charge of the PD phenomena as recommended by the standard IEC 60270 in (IEC-60270, 2000). In this case, impulse currents measurement methods are used. For electromagnetic radiations, the average energy can be calculated.

Under AC voltages, phase-resolved partial discharge (PRPD) representation is commonly used in PD characterization (Brunt, 1991; Levesque *et al.*, 2010; Hudon and Bélec, 2005). This is a three-dimensional statistical representation of a PD process in which probability distributions of PD events and amplitude are plotted on the phase of the operating voltage. One can identify typical patterns of PDs with PRPD as depicted in Figure 1.9. PD measured on a stator bar in which PDs occur at every half cycle of the applied voltage. The PD impulse currents measurement method is used in this figure.

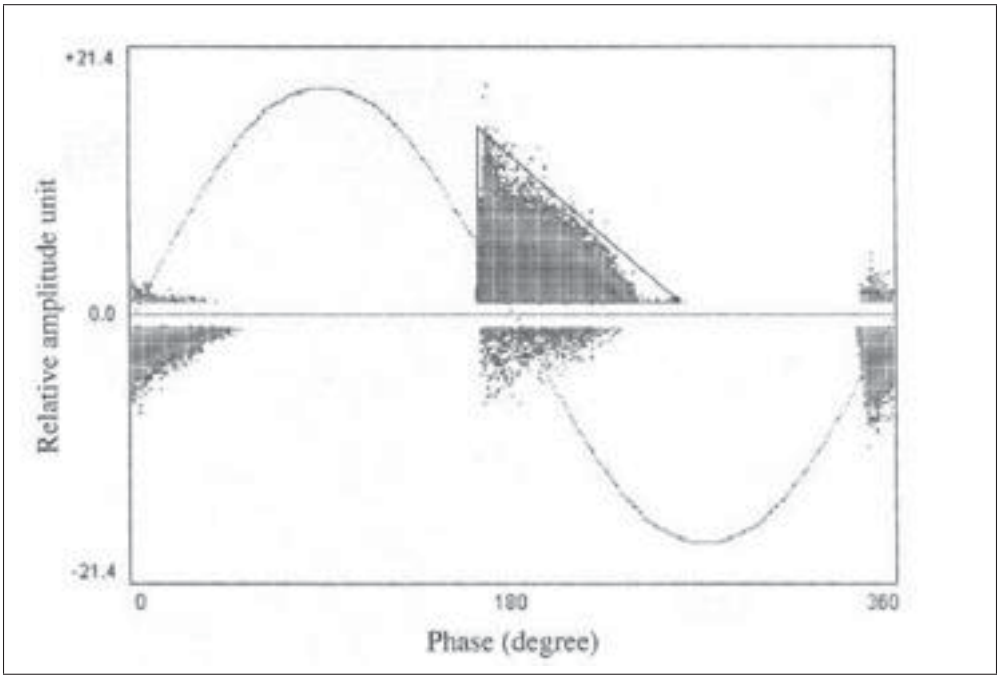

Figure 1.9 PRPD pattern of PD measured on a stator bar
Taken from Hudon and Bélec (2005)

1.4.4 Partial discharge modelling

PD modelling is an extensive research area in which physical and statistical models have been investigated (Niemeyer, 1995; Gutfleisch and Niemeyer, 1995; Levesque *et al.*, 2013; Bhatti *et al.*, 2009; Madi *et al.*, 2011). PD models can be classified as either physical PD models or statistical PD models.

1.4.4.1 Physical PD models

Physical PD models have been developed to extend knowledge about the evolution of PD activity. Researchers have shown that these models use the physical approach in which PD activities are simulated in spherical voids (Niemeyer, 1995; Gutfleisch and Niemeyer, 1995), or in stator bars (Levesque *et al.*, 2013). Essentially, the electric field in the PD site is calculated by numerical methods in each model. Based on physical criteria such as temperature, pressure and the radius of the cavity, the critical value for discharge is determined. When the electric field in a given PD site is higher than the critical value, a discharge occurs in which PD charge amplitude can be calculated physically. These models can reproduce the cyclostationary process under AC voltages. However, the PD charge amplitude cannot provide any information about the induced electromagnetic radiations. Waveforms and spectra of RF signals from the PD are not taken into consideration.

1.4.4.2 Statistical PD models for wireless channels

Middleton Class A and α-stable noise models are commonly used to reproduce EMIs from PD in wireless communication channels (Bhatti *et al.*, 2009; Madi *et al.*, 2011). Based on measurement campaigns in substations or in laboratories, statistical parameters are estimated from data using statistical methods (Zabin and Poor, 1991, 1989; Tsihrintzis and Nikias, 1996; Middleton, 1983; Chambers *et al.*, 1976). The resulting probability distributions are compared to the experimental results. The Kullback–Leibler (KL) divergence is used to quantify the difference between two probability density (Kullback and Leiber, 1951). This is a non-symmetric measure of the distance between two arbitrary probability densities f_1 and f_2. For discrete probability densities, the KL divergence of f_2 from f_1 is defined by:

$$D_{\mathrm{KL}} = \sum_i f_1(i) \ln \frac{f_1(i)}{f_2(i)} \tag{1.18}$$

If f_1 and f_2 are identical, then $D_{\mathrm{KL}} = 0$. In addition, a Kolmogorov-Smirnov (KS) test for the null hypothesis that two sample data are from the same distribution. The test statistic is:

$$D_{\mathrm{KS}} = \sup_x |F_1(x) - F_2(x)| \tag{1.19}$$

where $F_1(x)$ and $F_2(x)$ are the empirical cumulative distribution functions (CDF). $\sup_x$ is the supremum. If two sample data are from the same distribution, then D_{KS} converges to zero (Massey, 1951).

An example of a typical PD impulse measured in a substation is depicted in Figure 1.10. Gaussian, Middleton Class A and α-stable noise models are used to reproduce data. Parameters are estimated from the data using statistical methods (Zabin and Poor, 1991, 1989; Tsihrintzis and Nikias, 1996; Middleton, 1983; Chambers *et al.*, 1976). PDFs and resulting noise samples are plotted for comparison. It can be seen that impulsive noise produces a heavy-tailed distribution. Contrary to the Gaussian distribution, the heavy-tailed behaviour is taken into account in Middleton Class A and α-stable noise models. Therefore, the KL divergence values are smaller than those in the fitted Gaussian noise model as seen in Table 1.1. However, the KS test has been conducted for a significance level of 5%, in which the p-values can be derived from the test statistics values in the table (Massey, 1951). These p-values are lower than 0.05 for all of these noise samples impulsive noise models. As a result, the test indicates the rejection of the null hypothesis that noise samples from these statistical impulsive noise models and the measured impulsive noise cannot come from the same distributions at a 95% confidence interval. Moreover, these statistical models exhibit lack-of-fit because the resulting waveforms generate *iid* noise samples which are not observed in the data. Indeed, we can see that the PD impulse occurs in bursts with transient effects and damped oscillation. Using KL divergence to validate statistical models from measurements is not accurate because the spectrum characteristics of EMIs are not taken into account.

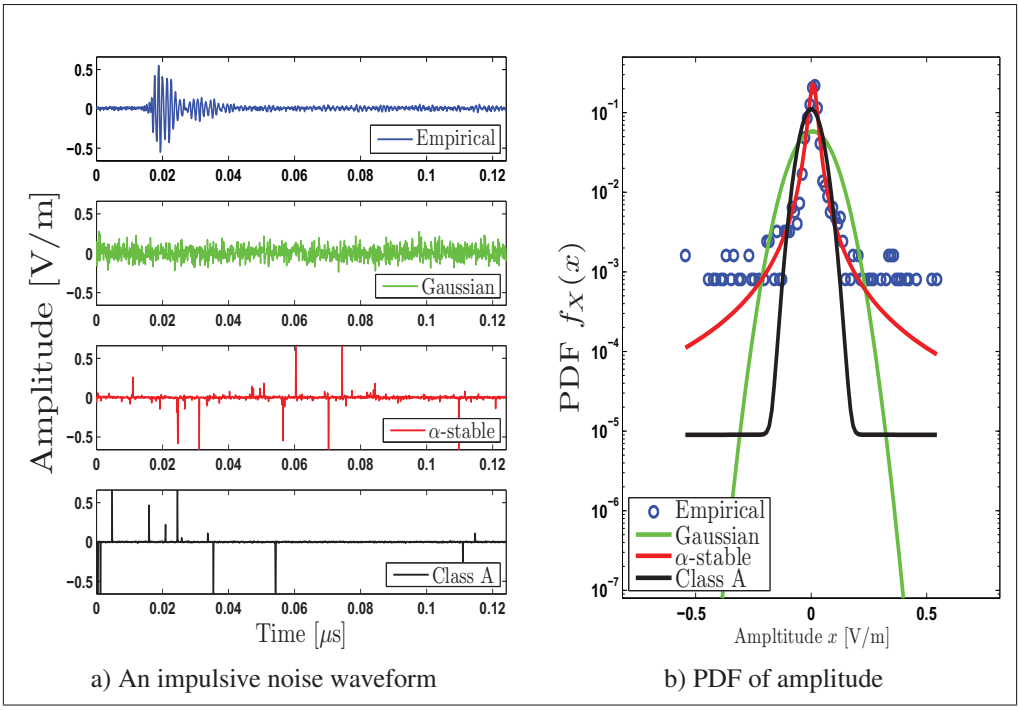

a) An impulsive noise waveform b) PDF of amplitude

Figure 1.10 Impulsive noise with fitted statistical models

Table 1.1 The goodness-of-fit of impulsive noise models

Test statistics	**Gaussian**	**Middleton Class A**	**α-stable**
D_{KL}	1.18	0.596	0.08
D_{KS}	0.56	0.24	0.195

1.5 Discussion and conclusion

In this chapter, impulsive noise measurements, characterization and modelling are reviewed. Power-line distribution systems, high-voltage transmission lines and HV equipment in substations can generate impulsive EMIs. Performance of conventional wireless communication systems can be degraded drastically due to impulsive noise. Therefore, substation environments can pose challenges to the reliability of wireless sensor networks due to various man-made noise sources such as discharge phenomena. A performance analysis and the design of ro-

bust receivers in this special environment can be provided based on accurate impulsive noise models. To do so, it is necessary to identify and characterize these interference sources.

Impulsive noise in substation environments are generated by PDs when their occurrences follow cyclostationary processes due to AC voltages. When insulations are subjected to intense electric stress, an ionization process is generated by an electron-avalanche effect in the medium, such as an air gap. A conductive channel in the air gap can create an electrical discharge. As defined in (IEC-60270, 2000), a PD is characterized by an electric discharge that does not completely bridge the space between two conducting electrodes. When this occurs, PD can be measured and detected using coupling devices via its impulse current or by sensors and wideband antennas via its electromagnetic radiations. PD phenomena are inherently stochastic processes in which amplitude, inter-arrival time and occurrence can be described by time-dependent random variables. It has been shown in literature that wideband RF signals from PD activity have transient behaviour with damped oscillation when the power spectral density has a form of $1/(f-f_0)^{\gamma}$, where f_0 is a resonant frequency and γ is the exponent characterizing the decay over frequency.

Our research objectives are to characterize and model RF signals from PD activity for wireless communication channels. Several limitations from the literature review, show the current state-of-the-art:

Measurement and characterization of EMI from PD

Although EMIs from PD activity have been measured using a wideband antenna on overhead power-lines in the frequency range of 60 Hz to 10 GHz (Pakala and Chartier, 1971; Pakala *et al.*, 1968), these EMI sources are not fully characterized. For example, the inter-arrival time, duration and occurrence of PD are not provided. Moreover, PD activity can also take place in much HV equipment such as power transformers, bushbars or circuit breakers. Wideband RF signals are measured in the frequency range of 100 MHz to 1 GHz when conventional

wireless communications, such as cellular networks IEEE 802.11 and 802.15.4 do not operate in practice (Portugués *et al.*, 2003; Portugués and Moore, 2006; Moore *et al.*, 2005).

Impulsive noise models

Physical PD models describe fundamental mechanisms of partial discharge and their impact on electrical insulations. However, they have not been adapted for wireless channel modelling because the physical mechanism of PD and its electromagnetic radiation are not linked. Statistical impulsive noise models for communication systems such as memoryless impulsive noise models are commonly used to reproduce EMIs in substation environments (Bhatti *et al.*, 2009; Madi *et al.*, 2011). Their canonical forms and their analytic tractability can offer elegant solutions to combat impulsive noise. However, it has been shown that these statistical models generate *iid* noise samples which have not been observed in practice. Indeed, RF signals from PD have transient effects with damped oscillation. PMC models can be used alternatively in order to account for the transient effect of impulsive noise, as developed by Zimmermann and Dostert (2002), Gilbert (1960), and Elliot (1963). However, the Markovian nature of these models makes the analysis complex, because the definition of the number of states can be challenging and the computational complexity can increase drastically. Statistical impulsive noise models are physically limited because their parameters cannot provide any information about physical characteristics of HV installations and the induced radio interference spectrum.

To our knowledge, as of 2016, we do not have a complete and coherent impulsive noise model that link physical characteristics of high-voltage installations to the induced radio interference spectrum. Our proposed research plan consists of the characterization of EMI impulsive noise induced by PD sources as well as the formalization of a coherent model, detailed and validated linking the discharge process to the induced far-field wave propagation.

1.5.1 Proposed research plan

In the following chapters, we will investigate the characterization and the modelling of EMI impulsive noise induced by PD sources for wireless RF channels.

A proposed characterization process of EMI induced by PD

A measurement setup will be employed to capture the electromagnetic radiations from PD sources in substations, and a wideband antenna will be used to cover the frequency range of conventional wireless communications, which is 800 MHz to 5 GHz. A characterization process is proposed using short-time analysis in which impulsive interferences can be fully characterized in terms of first- and second-order statistics. Under this condition, statistical distributions of PD quantities can be represented over time (*e.g.* PRPD) and frequency (*e.g.* PSD).

A physical model of EMI induced by PD

We propose the first model of impulsive EMIs, which is characterized by the cyclostationary process under AC voltages. We formally link the physical characteristics of PD to the induced electromagnetic radiations. Assuming a PD source as an electric dipole, the ionization process leads to a conducting channel in which currents and charges generate electromagnetic wave radiations. Therefore, there is a magnetic potential vector source and an electric scalar potential source in which potentials can be expressed by solving Lorenz gauge condition equations in the far-field region. Using our proposed characterization process, experimental results are compared to the results of simulations to validate the effectiveness of our approach.

A generalized model of impulsive EMI in substations

We propose a generalized model of impulsive EMI in substations using second-order statistics. Measurements in substations show that impulsive noise from PD activity are transient impulsive waveforms. Moreover, in the far-field region, the presence of multiple reflectors produces

multiple reflected EM waves. As a result, the impulsive waveforms measured by an antenna are distorted both by the propagation of the EM waves and the discharge source itself. Hence, we may assume that PDs in HV equipment have a spectral signature whose the interference radio spectra are distorted by multipath propagation effects. Time series models can approximate the spectral characteristics of PDs from data with a reasonable number of parameters. We have proposed a validation procedure to check the adequacy of the time series models (the goodness-of-fit). The latter is measured by a statistical analysis of the residuals. We show that the random behaviour of a transient impulsive waveform can be simulated using a heteroskedastic, white Gaussian noise. To validate our approach, experimental results are compared to the results of simulations.

A complete generalized model of impulsive EMI induced by PDs is proposed by using a spatial and temporal Poisson point process (the Poisson field of interferers) in which transient impulsive waveforms are emulated by our proposed time series models with first-order statistics of PDs obtained from data. The Poisson field of interferers model allows for the identification of some interesting statistical properties of moments, cumulants and probability distributions. These can, in turn, be utilized in signal processing algorithms for fast PD identification, localization, and impulsive noise mitigation techniques in wireless communications in substations.

CHAPTER 2

MEASUREMENT AND CHARACTERIZATION OF EMI FROM PD ACTIVITY IN HIGH-VOLTAGE SUBSTATIONS

2.1 Introduction

The phenomenon of impulsive noise is generated by PD sources in high-voltage substations. A PD generates a current impulse, acoustic noise, visible and ultraviolet (UV) light and electromagnetic radiation, and accordingly its presence can be detected via several measurement methods. In this chapter, PD measurement methods that are based on the detection of electromagnetic radiations. These PD instrument detectors have the advantage to be non-invasive measurement methods for the HV equipment as well as one can assess impulsive EMI threats to wireless communication systems.

This specific radio noise is a source of interference for the radio communication systems. In the literature, electromagnetic radiations from PD activity have been measured in several substations (Pakala and Chartier, 1971; Pakala *et al.*, 1968; Portugués *et al.*, 2003; Portugués and Moore, 2006; Shan *et al.*, 2011). However, the measurement setup employed does not cover the frequency range used by conventional wireless communications, and so the impulsive noise characterization is often incomplete. Inspired by related works in PD current measurements and characterization (Brunt and Kulkarni, 1990; Brunt, 1991; Levesque *et al.*, 2010; Hudon and Bélec, 2005), we have developed a characterization process in which the impulsive electromagnetic radiations from PD activity are fully characterized by the amplitude of the power density, inter-arrival time, occurrence and spectrum.

The main objective in this chapter is to provide a non-invasive measurement and detection method for the characterization of the electromagnetic radiations induced by PDs. This information can then be applied towards the development of rapid on-line remote monitoring and diagnostic tools in HV equipment, and/or for characterizing and modelling wireless channels in substations. These impulsive interferences are measured using a wideband antenna surrounded

by HV equipment in normal operation. This work is based on Au *et al.* (2013), in which results are extended to the second-order of characterization (spectrum).

The first-order statistics are obtained from the measured data based on short-time analysis using a spectrogram and detection peak in instances when the power densities and occurrences of these impulses have been estimated. A denoising process, based on wavelet transform and a threshold, is implemented to improve the PD detection. Under these conditions, a full PD characterization can be achieved by using the phase-resolved partial discharge (PRPD) representation and other first-order statistical distributions. The waveforms and spectral characteristics of these impulses can be analysed based on autocorrelation function (ACF) and spectrogram.

This chapter is organized as follows: in Section 2.2, the measurement setup that has been employed is presented. A wideband antenna is used to measure and characterize impulsive noise that is induced by PDs in the frequency range of 800 MHz to 5 GHz. In Section 2.3, signal processing tools are presented for PD characterization in substations. In Section 2.4, measurement campaigns in a 735 kV outdoor substation are presented. The proposed characterization process is applied to the measurements in the substation when significant characteristics of these PD impulses can be identified. Section 2.5 concludes this chapter with a brief summary of our findings and suggestions for possible improvements in PD characterization methods.

2.2 The measurement setup

A wideband antenna is used for PD characterization in substations. The measurement setup is as follows:

- a wideband log-periodic antenna from Rhode and Schwartz (HL050) in the frequency range of 800 MHz to 26 GHz, in which the antenna gain is 8.5 dBi;
- a passband filter in the frequency range of 780 MHz to 3.2 GHz, in which the loss is less than 1 dB. It allows for the reduction of unwanted signals below approximatively 800 MHz;

- a radio frequency amplifier in the frequency range of 30 MHz to 3 GHz. The output signal power of the filter can reach 12.8 dBm to ensure a better signal-to-noise ratio. The gain is around 20 dB;
- a broadband limiter to protect our oscilloscope against unwanted signals up to 2.5 W in the frequency range of 30 Hz to 6 GHz;
- a serial data analyser from LeCroy to capture signals up to a maximum of 256 million samples. The maximum sample rate is 40 Gs/s.

In the measurement campaign, the observation time is 20 ms and the sample rate is $F_s = 10$ Gs/s. Hence, 200 M samples are recorded. The electromagnetic radio noise in substations can be measured in the frequency range of 800 MHz to 5 GHz. The measurement campaign has been conducted in specific locations in the substations when radiations from PD sources are significant.

2.3 An experimental characterization of the discharge sources

2.3.1 Amplitude of measured signals

Electromagnetic radiations generated by PD sources are characterized by any RF gain in the measurement setup by removing the antenna factor. As a result, the amplitude of the measured signal in voltage (V) is converted into electric field strength in (V/m).

We denote $u(\theta,t)$ as the impulsive noise waveform measured in electric field strength (V/m), where θ is a set of random variables characterizing its duration, occurrence and other physical parameters. By denoting $u_m(\theta,t)$ as the impulsive waveform measured in voltage (V), we have:

$$u(\theta,t) = u_m(\theta,t)\sqrt{\frac{Z_0 4\pi}{RG_r\lambda^2}} \tag{2.1}$$

where R is the load resistance and G_r is the gain of the RF system including the filter, the RF amplifier and the antenna. $Z_0 = 120\pi\ \Omega$ is the freespace impedance and λ is the wavelength

of wideband antenna. Note that this relationship is valid in far-field conditions. In practice, PD sources and the antenna are separated by several meters, thereby establishing far-field conditions.

2.3.2 Signal processing tools for impulsive noise measurement

2.3.2.1 The Denoising process

In practice, the measured signals consist of overall background noise produced by thermal noise in RF components, interleaving artefacts, clock feedthrough noise in the scope and RF signals which come from cellular phones at 1.7 and 1.9 GHz. The resulting noise received by the antenna is written as:

$$x(\theta,t) = \sum_{k} u_k(\theta,t) + n(t) \tag{2.2}$$

where $n(t)$ is the signal of the overall background noise. Over a long observation time, the presence of many impulses is a superposition of impulsive transient waveforms, where the occurrences are randomly distributed over this interval of time.

By using a denoising process, the overall background noise can be removed to ensure a better temporal and frequency location of each impulse. We use the wavelet transform to which a threshold has been applied to remove low wavelet coefficients. The wavelet transform is used to decompose a signal on a wavelet orthonormal basis. It defines a multi-resolution representation of the signal (Mallat, 1998).

The discrete wavelet transform is based on the convolution of the signal with a pair of quadrature mirror filters. The signal is decomposed by these filters successively. Since impulsive components are above the background noise component, their wavelet coefficients are higher than the background noise (Mallat, 1998). Low coefficient values can be set to zero by a hard threshold defined by Donoho (Donoho and Johnstone, 1994) such that the threshold T_h is given by:

$$T_h = \sigma_i \sqrt{2\log(M_i)} \tag{2.3}$$

where σ_i^2 is the variance of the background noise and M_i is the number of samples for a given level of decomposition i. Krim *et al.* (1999); Donoho and Johnstone (1994) have shown that the background noise standard deviation is estimated by:

$$\sigma_i = \frac{\text{Med}_i}{0.6745} \tag{2.4}$$

where Med_i is the estimated median value of the signal. Next, impulses are extracted by rescaling the threshold value at each decomposition level, and the reconstructed signal is obtained by the inverse of the wavelet transform. The denoising process can be summarized by Figure 2.1. The wavelet decomposition is applied to our measurements $x(\theta,t)$, where low wavelet coefficient values are set to zero by hard threshold T_h at each level of decomposition. Impulsive components can be estimated by using the inverse of wavelet transform. An extensive analysis on denoising PD signals shows that a suitable estimation of impulsive transient-noise waveforms can be performed using Daubechies wavelets with 8 vanishing moments for 30 levels of decomposition, (Ma *et al.*, 2002; Satish and Nazneen, 2003; Au *et al.*, 2013).

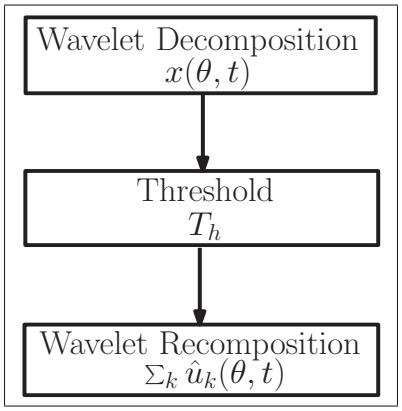

Figure 2.1 Denoising process using wavelets

2.3.2.2 Short-time analysis for impulsive signals

Over a long observation time, many impulses can be observed in our measurements with different time occurrences. When their amplitude is significant, it is reasonable to say that the process is non-stationary. In such instances, it may be useful to conduct a short-time analysis to preserve information regarding the time-frequency location of impulse events.

Spectrograms can be used to yield a time-frequency representation of measured signals. Based on the short-time Fourier transform, impulses can be written as follows:

$$U(\theta, t_w, f) = \int_{-\infty}^{+\infty} u(\theta, t) w(t - t_w) e^{-j2\pi f t} dt \tag{2.5}$$

where $w(t) \in \mathscr{L}^2(\mathbb{R})$ is a square-integrable temporal window function with a length of t_w. The spectrogram can be computed by the squared magnitude of the STFT as:

$$S_{uu}(\theta, t_w, f) = \frac{1}{Z_0} |U(\theta, t_w, f)|^2 \tag{2.6}$$

where each segment $S_{uu}(t_w, f)$ is the power density of the process located in (t_w, f). To ensure a better time-frequency localisation, we have to define properly the window function, the number of samples that overlap between adjoining sections and the number of FFT. These parameters will be defined in the next section.

2.3.2.3 Temporal location of an impulse

PD quantities can be estimated while maintaining their temporal locations. This allows for the study of first-order statistics in terms of power density, inter-arrival time and time occurrence.

The power density of PD sources can be estimated using the marginal time condition in a selected bandwidth Δf near a given resonant frequency f_0, as follows:

$$S_{uu}(\theta, t_w) = \frac{1}{Z_0} \int_{f_0 - \Delta f/2}^{f_0 + \Delta f/2} \frac{\left| U(\theta, t_w, f) \right|^2}{\langle w(t), w(t) \rangle} df \tag{2.7}$$

where $\langle w(t), w(t) \rangle$ is defined by:

$$\langle w(t), w(t) \rangle = \int_{-\infty}^{+\infty} w(t) w^*(t) dt \tag{2.8}$$

and $w^*(t)$ is the complex conjugate of $w(t)$.

An impulse detector is used for an experimental characterization of PD sources as illustrated in Figure 2.2. First, impulsive noise emitted by PD sources is extracted from overall background noise via a denoising process. Next, the power density of each impulse is calculated using the short-time Fourier analysis. We use peak detection to measure the power density value at t_w, denoted as P_d. PD sources can be characterized in terms of their power spectral density.

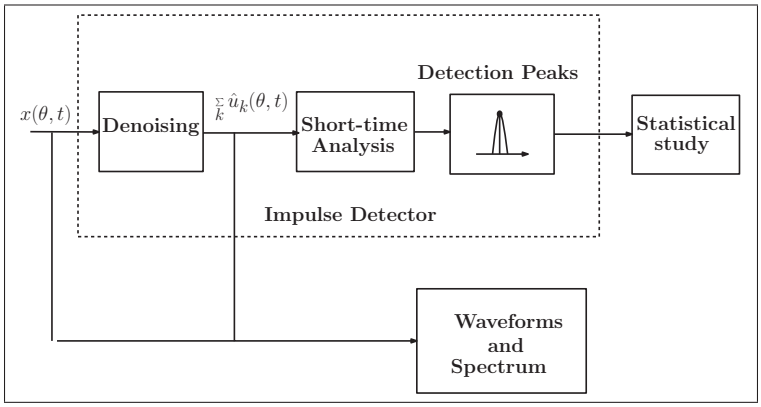

Figure 2.2 Characterization process

2.3.3 Characterization metrics definition

We define characterization metrics based on the probability distributions of some physical parameters such as amplitude, inter-arrival time and occurrence (first-order statistics), as well as power spectral density and autocorrelation function (second-order statistics).

2.3.3.1 Characterization based on first-order statistics

Inspired by related research projects (Shan *et al.*, 2011; Portugués *et al.*, 2003; Au *et al.*, 2013), we define the first-order characterization metrics for the PD sources under AC voltages in terms of:

- the power density of impulsive noise radiations P_d distribution (W/m^2);
- the discharge occurrence t_n distribution (s);
- the inter-arrival time Δt distribution (s).

These metrics are expressed as $p(x)dx$, which shows the probability that a discharge event has a value between x and $x+dx$, independent of previous events. The phase-resolved partial discharge (PRPD) representation is useful to show the power density distribution in a restricted interval time between t_{i-1} and t_i where $\delta t_i = t_i - t_{i-1}$ (Brunt, 1991). PRPD is expressed as:

$$p(P_d|\delta t_i) = \int_{t_{i-1}}^{t_i} p(t_n)p(P_d)|t_n)dt_n \tag{2.9}$$

where $p(t_n)$ is the probability per time unit of an impulse occurrence at $t_n \in [t_{i-1}, t_i]$. $p(P_d|t_n)$ determines the probability of a discharge event having a power density P_d if its occurrence is t_n. The PRPD representation is widely used in the study and analysis of these discharge sources on insulation systems (Levesque *et al.*, 2010; Bartnikas, 2002; Hudon *et al.*, 2008; Levesque *et al.*, 2013). Because these sources are typically generated by AC voltages, the processes are cyclostationary. Therefore, the PRPD representation can be used to characterize the occurrences and power densities of these EMI sources per unit time or phase.

2.3.3.2 Characterization based on second-order statistics

Second-order statistics are defined by power spectral density (PSD) and autocorrelation function (ACF). It might be difficult to characterize non-stationary random processes of real-valued

functions using second-order statistics. Nevertheless, PSD and ACF can be estimated using numerical methods. By taking our measurements as a discrete-time signal $u(n)$, the relationship between the time variables t and n is given by:

$$t = nT_s \tag{2.10}$$

where T_s is the sampling period. Moreover, we assume that a characterization using second-order statistics is restricted to a single impulse delimited by its duration. The length of the measured discrete-time signal is given by M. As a result, an estimation of PSD and sample ACF can be provided. The estimated PSD can be obtained by using the periodogram via discrete Fourier transform. For an impulse $u(n)$ sampled at Fs samples per unit time, the estimated PSD is given by:

$$P_{uu}(f_k) = \frac{1}{M}\left|\sum_{n=1}^{M} u(n)e^{-2\pi n f_k}\right|^2 \tag{2.11}$$

where the frequency is given by $f_k = k/M$, where $k = \{0,1,\cdots,M-1\}$, and M is the number of observations.

The ACF can be found by taking the covariance of $u(n)$ and $u(n-i)$. We define the autocorrelation for a lag i as r_i such that:

$$r_i = \frac{\sum_{n=i+1}^{M}(u(n)-\bar{u})(u(n-i)-\bar{u})}{\sum_{n=1}^{M}(u(n)-\bar{u})^2} \tag{2.12}$$

where $\bar{u}$ is the estimated mean value of the measured impulse. The ACF is used to check whether samples noises are correlated when an impulse is observed. Accordingly, it allows us to select an approach to modelling impulsive noise waveforms that fits our measurements using a discrete-time filter.

2.4 Measurements in substations

In this section, measurements from a 735 kV substation are presented. Although many measurements were made in different locations within the substation, only one location is presented in this thesis. These interference sources are randomly located in space and can be characterized based on our proposed metrics.We used AC power-lines in the scope to synchronize our measurements. Since these PD sources are also generated by the three-phase AC voltages, the measured occurrences can undergo a phase shift. Waveforms are captured periodically at the beginning of each cycle of the AC power line.

2.4.1 Description of the environment

The antenna is surrounded by HV pylons with 735 kV overhead power-lines, circuit breakers, a transformer and bush bars. Measurements were made in an outdoor substation where the atmospheric pressure is 102 khPa, and the temperature is 20°C. An environment typical of a 735 kV substation is shown in Figure 2.3. In this substation, 30 waveforms are captured. The observation time is 20 ms sampled at 10 Gs/s.

Figure 2.3 Typical HV equipment in the 735 kV substation

The measurement data consist of a train of impulses randomly located in time. The spectrogram is used to detect each impulse for which power density, occurrence, and inter-arrival time can be calculated. For a suitable time-frequency localisation, we use a Hamming window whose length is set according to the average duration of impulses. In this measurement point, the average duration is approximately 80 ns. As a result, the Hamming window length is set at 1024 samples, *i.e* 102.4 ns. The length of the FFT is $N_{\text{fft}} = 2048$ and 50% overlap is used. The power density of each impulse is calculated in the bandwidth range of 0.2 to 5 GHz by using the marginal time condition (see Equation (2.7)). Since the power density of the ambient noise without any discharges is about -43.65 dBW/m^2, $P_d(t_w)$ value is located at each signal peak above -39.03 dBW/m^2.

2.4.2 First-order statistics

PD processes can be characterized by first-order statistics such as amplitude, inter-arrival time and occurrence. These parameters provide relevant information regarding the PD mechanism, its physical process and electrical aging of HV equipment. These statistical quantities are useful for the characterization of wireless channels in substations.

2.4.2.1 PRPD representation

EMI from PD can be characterized using PRPD representation, as depicted in Figure 2.4. It is clear that PD characteristics can be described in terms of time-dependent random variables when PD activity can follow the cyclostationary process induced by AC voltages. The power density of these impulses are randomly distributed such that some PDs can reach 15 mW/m^2. Impulsive events occur randomly over time, even though they take place at every half-cycle of the AC voltage. Note that since we have used the AC power-line of the scope to capture impulses periodically, the measurement setup is not synchronized with AC voltages applied to PD sources. Thus, a phase shift is observed in the PRPD.

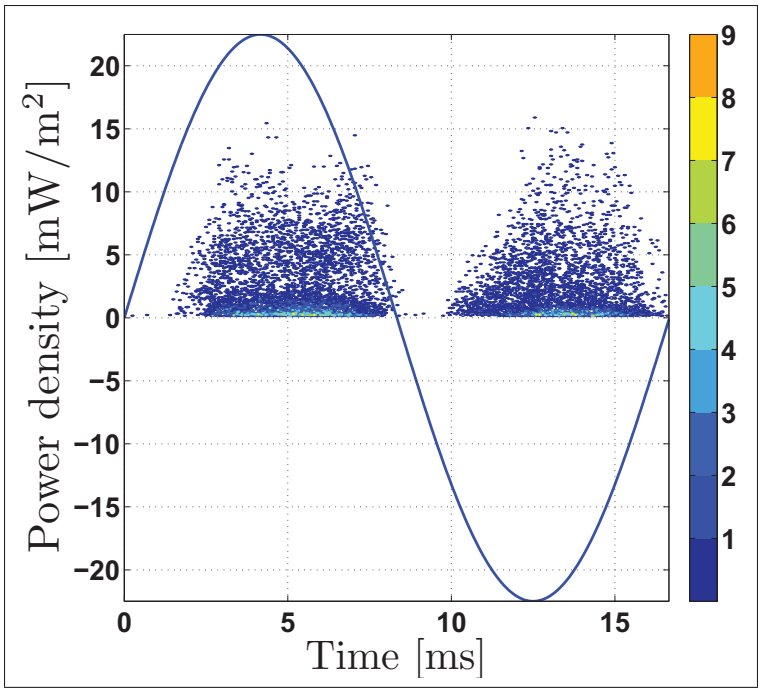

Figure 2.4 PRPD of EMI from PD activity in a 735 kV substation

The total PD rate is 408 discharges per cycle when the number of PD events is more predominant during the first half-cycle, *i.e* within the time interval of 1 to 9.5 ms. Indeed, the PD rate is 235 discharges per cycle during the first half-cycle whereas the PD rate is 129 discharges per cycle during the second one. The average total power density is 1.4655 mW/m^2. The average power density during the first half-cycle is 0.7891 mW/m^2 and the second one is 0.5637 mW/m^2. These measured quantities are summarized in Table 2.1.

Table 2.1 Summary of statistical quantities

	Total PD	**PD first half-cycle**	**PD second half-cycle**
Rate (disch. per cycle)	408	235	129
Avg. power density (mW/m^2)	1.4655	0.7891	0.5637

2.4.2.2 Statistical distribution of PD characteristics

PD characteristics can be presented in terms of statistical distributions, such as PDFs and complementary cumulative distribution functions (CCDFs) of power density, inter-arrival time and time occurrence. The CCDF is given by:

$$\bar{F}_X(x) = 1 - \int_{-\infty}^{x} f_X(\tau) d\tau \tag{2.13}$$

where f_X is the PDF of random variables produced by PD activity. PDFs and CCDFs are depicted in Figures 2.5 to 2.7. Power density and IAT distributions follow power law distributions with a fast decay (see Figures 2.5 and 2.6). The average power density is $\bar{P}_d = 1.4655$ mW/m^2 and the average IAT is $\bar{\Delta}t = 47\mu$s. PD occurrence distribution within a cycle has two separate Gaussian distributions. Under AC voltage, PD discharges occur at every half-cycle because the critical value for a discharge is reached when the local electric field in the PD site is intense. This critical value and the intensity of the electric field affect amplitude, IAT and occurrence of PD processes. On average, the majority of discharges take place at 6.2 ms during the first half-cycle of the AC voltage and at 12.56 ms during the second one.

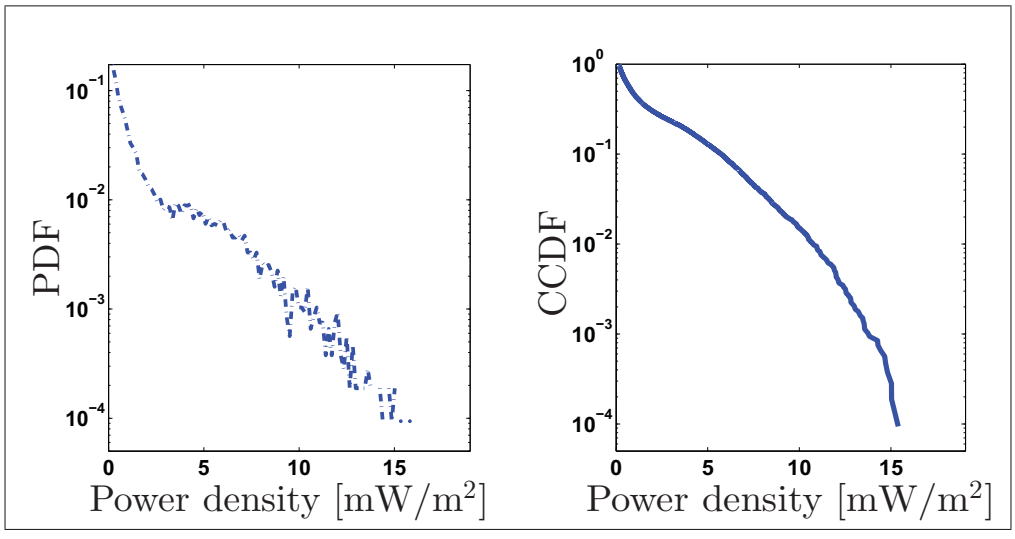

Figure 2.5 Power density distribution

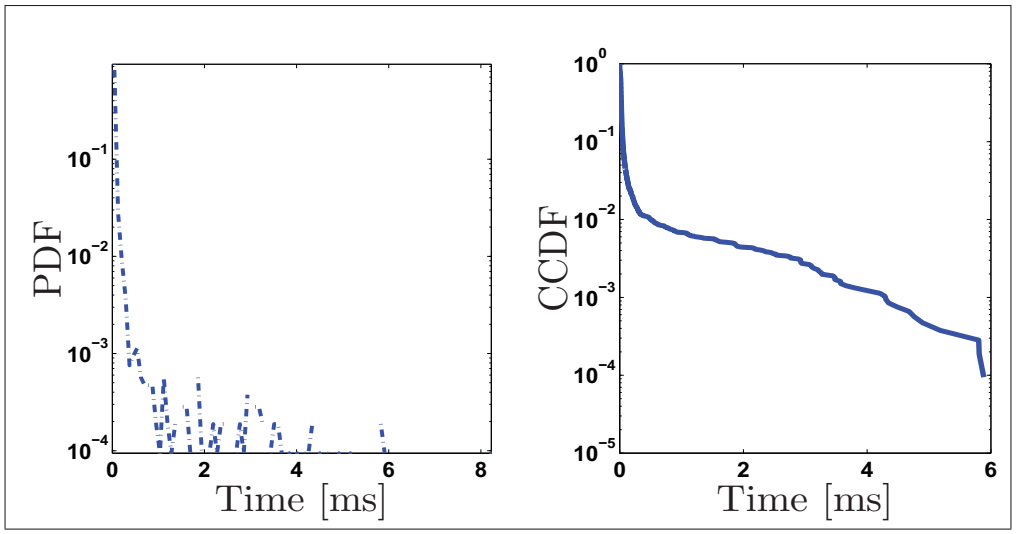

Figure 2.6 Inter-arrival time distribution

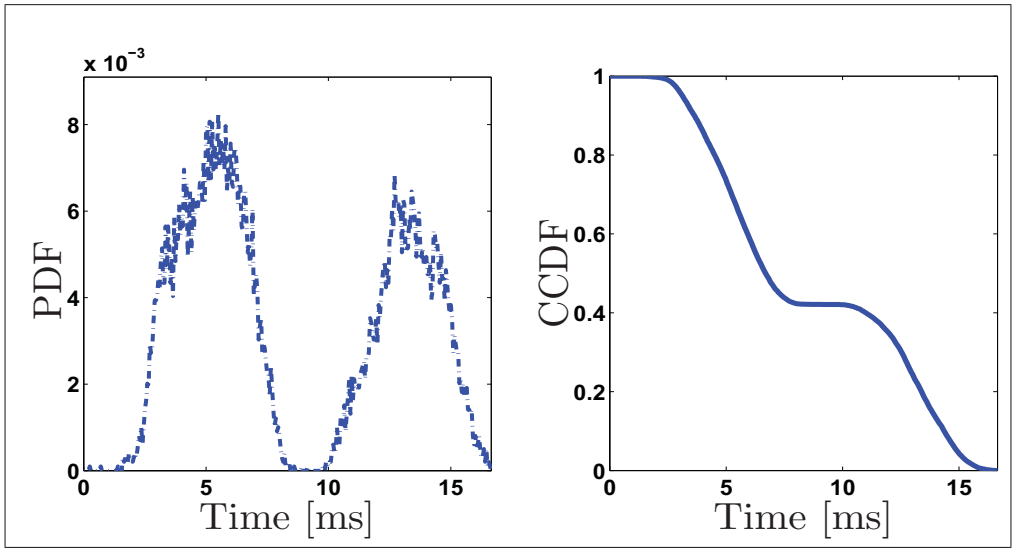

Figure 2.7 Time occurrence distribution

EMIs induced by PD sources are measured from 800 MHz to 5 GHz. As a result, they can be interference sources for wireless communications. Such events follow a cyclostationary process due to AC voltages. The received signal emitted by a transmitter can be corrupted by several impulses with high amplitude. The deployment of wireless sensor networks in substations can pose several problems pertaining to their reliability due to the typical EMIs that are emitted by PD sources.

2.4.3 Waveforms and second-order statistics

Second-order statistics can be useful in characterizing RF signals from PD activity. It allows for the analysis of the statistical distributions of an EMI's power density over frequencies, and also facilitates the identification of their spectral characteristics.

2.4.3.1 Typical waveform and spectrogram

A typical waveform from PD activity measured in the substation is depicted in Figure 2.8. The PSD, the ACF and the spectrogram are used to represent the RF signal. To have a suitable time-frequency resolution of the impulse, we use a Hamming window of $t_w = 3.2$ ns length. The FFT length is $N_{\text{fft}} = 512$ and 70% overlap is used.

The waveform of a discharge is characterized by a short rise time (4 ns), a long fall time (50 ns) with damped oscillation around $f_0 = 800$ MHz, and high amplitude, maximal amplitude 0.75 V/m. During the rise time, the discharge can cover a large frequency range of 800 MHz to 3 GHz when the discharge amplitude is high. During the fall time, it covers a frequency range of 800 MHz to 1 GHz. The ACF exhibits a damped oscillation decay due to the damped oscillation and transient effect of the measured impulse.

An impulse generated by a PD can be approximated by a damped harmonic oscillator such that:

$$u(t) = u_0(e^{-at} - e^{-bt})\sin(2\pi f_0 t + \varphi) \tag{2.14}$$

where u_0 is the amplitude of the impulse, a and b are respectively rise time and fall time decay, f_0 is the resonant frequency and φ is the phase shift of the measured impulse.

The ACF of $u(t)$ in Equation (2.14) can be approximated by:

$$R_{uu}(\tau) = \mathbb{E}[u(t)u(t+\tau)] \approx \frac{u_0^2}{2}(e^{-a\tau} + e^{-b\tau})\cos(2\pi f_0 \tau) \tag{2.15}$$

where τ is the time lag.

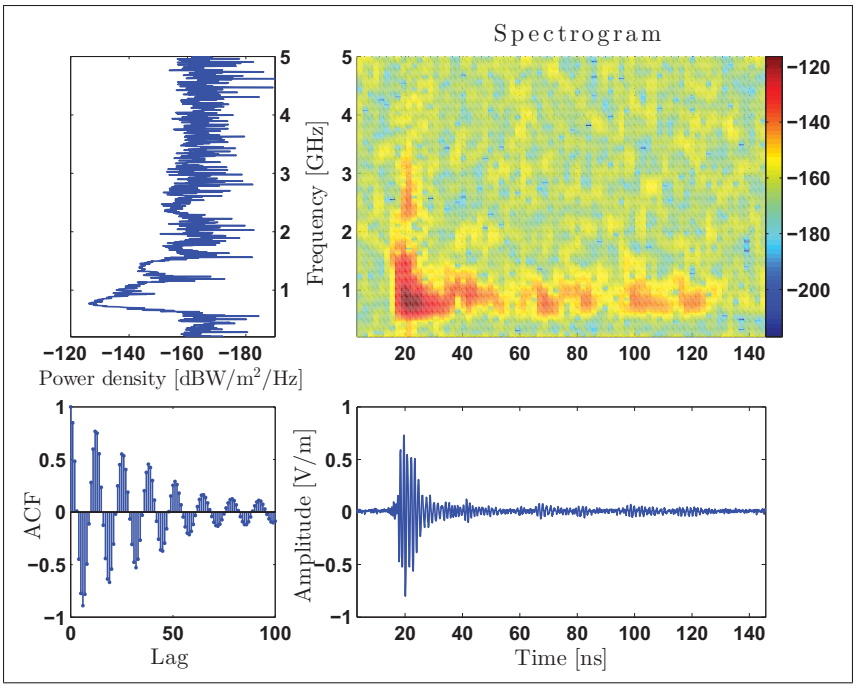

Figure 2.8 Typical impulsive waveform

From these measurements, one can conclude that memoryless impulsive noise models can be limited. Indeed, these noise models generate impulses in one sample in which the resulting noise process is *iid*. Impulses from PD activity exhibit bursty behaviour and the ACF indicates that, in the presence of transient impulsive noise induced by PD, samples are highly correlated (see damped oscillated decay in the ACF).

2.4.3.2 Power spectral density

The spectral characteristics of PD impulses can be provided via second-order statistics. The periodogram is used to estimate the PSD of these impulses in this work.

Power spectral density of an impulse

The PSD of measured PD impulse before and after the denoising process are depicted in Figure 2.9. When the wavelet transform is applied to the measurements, low wavelet coefficients are considered to be ambient noise components. The hard threshold removes them and keeps

high wavelet coefficients, *i.e* impulsive components. As a result, we have a good estimation of the spectral characteristics of an PD impulse. Furthermore, deep fades can be observed at some frequencies. This might be due to the presence of multipath effects in which multiple reflections of EM waves are observed by the antenna.

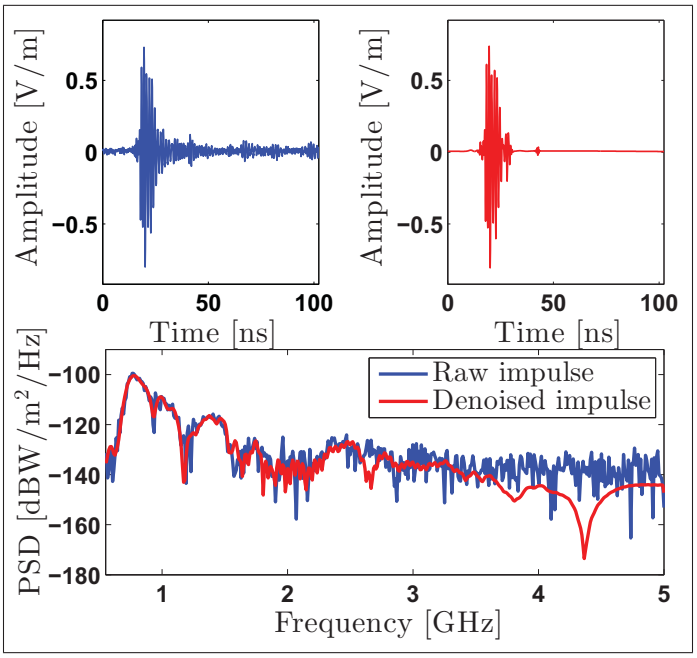

Figure 2.9 Waveforms and PSD of an impulse

Average Power spectral density

Based on the total number of $N_{\text{disch}} = 12,400$ measured discharges, the average PSD is estimated by using the periodogram in Equation (2.11) as:

$$\begin{aligned}\bar{P}_{xx}(f) &= \mathbb{E}\left[P_{xx}(\theta, f)\right] \\ &= \frac{1}{N_{\text{disch}}} \sum_{l=1}^{N_{\text{disch}}} \frac{1}{M} \left| \sum_{n=1}^{M} x(\theta_l, n) e^{-2\pi n f} \right|^2\end{aligned} \tag{2.16}$$

where $x(\theta_l, n)$ is raw or denoised data. M is the number of observations. This has to be larger than the duration of impulses. The average PSD is depicted in Figure 2.10 where $M = 1024$

samples, *i.e* 10.24 μs. In Figure 2.10.(a), the average PSD is calculated from noisy data. The green curve is the measured ambient noise PSD. RF communications can be seen around 900 MHz and around 1.9 GHz. Harmonics at 1.25, 2.5 and 3.75 GHz are created by interleaving artefacts and clock feedthrough from the oscilloscope. On average, PD impulses can cover a frequency range of 800 MHz to 2 GHz.

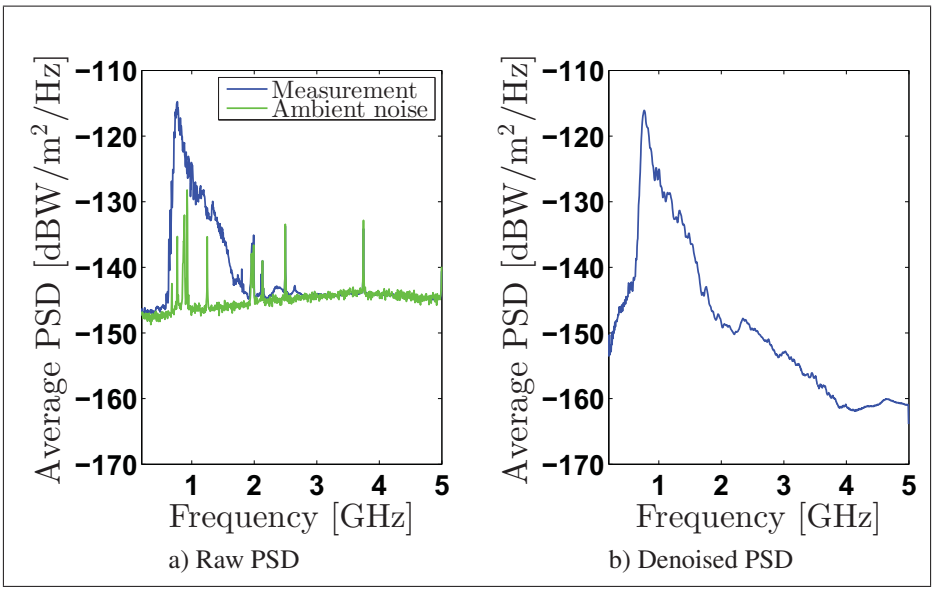

Figure 2.10 Average power spectral density

2.5 Conclusion

In this chapter, a non-invasive PD measurement using wideband antenna was proposed for EMIs induced by PDs in substations. The measurement setup still requires an AC power-line to synchronize with AC voltages in substations. In addition, signal processing tools using short-time analysis are presented for a full PD characterization by their electromagnetic radiations from which first-order and second-order statistics can be derived. These tools can be implemented into any wireless electronic devices using antennas for a rapid and on-line PD diagnostic in HV equipment. By using short-time analysis, the user has to define the time window $w(t)$, its length t_w and the length of the FFT to ensure a suitable time-frequency resolution

of impulses. Compared to Pakala and Chartier (1971), Pakala *et al.* (1968), Portugués *et al.* (2003), Portugués and Moore (2006) and Shan *et al.* (2011), our proposed characterization metrics are relevant because the physical characteristics of HV equipment and the induced PD electromagnetic radiations are taken into account.

These signal processing tools are also valuable for the characterization of wireless communication channels in the presence of impulsive noise in substations. From the measurement campaign in a 735 kV substation, within a frequency range of 800 MHz to 5 GHz, we have seen that the spectrum of the impulsive EMIs can cover a large frequency range of 800 MHz to 2 GHz on average. Thus, conventional communications systems, such as IEEE 802.15.4 which uses 915 MHz in the Americas and 868 MHz in Europe, ISM bands can be interfered by PD impulses. One remarkable characteristic of PD is that the rise-time is very rapid so that the spectrum can be up to 3 GHz, which can overlap communication systems operating at 2.4 GHz. Indeed, researchers have shown experimentally that performances of conventional wireless communication systems using 2.4 GHz ISM bands are degraded by PDs (Sacuto *et al.*, 2012; Madi *et al.*, 2011; Bhatti *et al.*, 2009, 2012; Shan *et al.*, 2008b).

From our observations, EMIs induced by PD activity can be summarized as follows:

Random behaviour of PD

In substations, PDs take place under AC voltages in HV installations. When the electric field is sufficiently high, the ionization process along the insulation surface of HV equipment leads to PD. Their electromagnetic radiations can be detected by antennas in which conventional wireless communications operate. PD processes can be seen as time-dependent random processes in which their occurrences follow a cyclostationary process due to AC voltages. Their occurrences, inter-arrival times and power densities are random processes due to fluctuations in gas density, ionizing radiation, gas decomposition in cavities or dielectric surfaces, or because of several other physical mechanisms.

Transient impulsive noise

RF signals from PD activity create fast transient impulsive noise with high amplitude highly above the average ambient noise power density. According to our measurements, they are characterized by damped oscillations around 800 MHz with a rapid rise time (few ns) and a fall time of 100 ns. They can be seen as non-stationary random processes due to the presence of multiple reflections of EM waves.

In future work, an antenna array can be used in our measurement setup for PD localisation and identification. Under this condition, one can estimate the number of PD sources and their locations. Our proposed PD characterization process can be applied so that PRPD can be plotted for each PD source located in different HV equipment.

In the next chapter, a physical PD model is proposed based on physical mechanisms to which the induced electromagnetic radiation can be linked. The measurement setup and the proposed characterization process are used to demonstrate the efficiency of our approach by comparing measurement and simulation results.

CHAPTER 3

A PHYSICAL MODEL OF EMI INDUCED BY A PARTIAL DISCHARGE SOURCE

3.1 Introduction

Electromagnetic interferences (EMIs) can be categorized as either natural or man-made noise. Impulsive noise can predominate naturally within atmospheric noise, such as lightning discharges or cosmic radiations. It may also occur in man-made noise sources, such as power-line distribution and transmission networks or ignition systems. Modelling these phenomena is an active research area due significant impact of EMIs on the performance of communication systems (Ndo *et al.*, 2013; Madi *et al.*, 2011; Shinde and Gupta, 1974; Zimmermann and Dostert, 2002; Moose and O'dwyer, 1986; Meng *et al.*, 2005; Middleton, 1977). In substation environments, electromagnetic interferences are induced by corona discharges. They take place within or along the insulation surface of high-voltage equipment like transformers, powerlines, bushing bars, etc. The high voltages applied to electrodes that are separated by air cavities and air gaps can lead to discharges when the dielectric strength of the air is surpassed. Currents and charges induced by the discharge mechanism generate electromagnetic radiations (Rao *et al.*, 2007; Okazaki *et al.*, 2005; Bartlett *et al.*, 1999; Minegishi *et al.*, 1989). The electromagnetic waves interfere with conventional wireless communication systems that use radio frequency such as TV, FM bands (CIGRÉ, 1974; Arai *et al.*, 1985), and/or industrial, scientific and medical (ISM) bands (Madi *et al.*, 2011; Shan *et al.*, 2007; Bhatti *et al.*, 2009). Regarding the latter, the authors describe the impact on performances of conventional systems, and how they are severely degraded by emissions of these electromagnetic interferences, which are induced by discharges.

The primary interest in this chapter[1] is to formalize a coherent, detailed, and validated model that links the discharge process to the induced far-field wave propagation. To our knowledge,

[1] This chapter is based on the published journal paper "A model of Electromagnetic Interferences Induced by Corona Discharges for Wireless Channels in Substation Environments" in IEEE Transaction on Electromagnetic Compatibility, Vol. 57, No. 3 2015.

this is the first complete and coherent approach model that links physical characteristics of high-voltage installations to the induced radio-interference spectrum. The majority of the discharge processes may be caused by partial discharges. This behaviour is distinct from other classical models in the literature. Indeed, in substation environments, the applied voltage is generally AC. As a result, occurrences of discharge events are cyclostationary processes which vary according to the cycle of the AC voltage. Moreover, the emitted radiations occupy a wide range of frequencies. The waveforms received through antennas are transient damped oscillations whose their high amplitude far exceeds above background noise (Shan *et al.*, 2008a; Moore *et al.*, 2006; Shan *et al.*, 2011; Portugués *et al.*, 2003; Au *et al.*, 2013).

In this chapter, we propose the first model of these impulsive electromagnetic interferences whose impulse events are cyclostationary processes and waveforms are transient impulses. We adopt a physical approach to simulate partial discharges in which charge and current densities of interference sources are deducted. The proposed model is inspired by models described in Niemeyer (1995), Gutfleisch and Niemeyer (1995), and Fruth and Niemeyer (1992) in which fundamental aspects of the discharge process have been taken into account. Then, the electromagnetic radiations from charge and current densities can be derived by using an electric dipole approach of interference sources.

The chapter is structured as follows: in Section 3.2 and 3.3, we briefly describe the physical aspect of the partial discharges (PD) process that takes place along the insulation surface. Then, in Section 3.4, we model an electromagnetic (EM) radiation emitted by a partial discharge source as an electrical dipole in which the interfering source's current of charge density radiates electromagnetic waves. A theoretical formalisation of these EM radiations is defined by using retarded potential equations. Inspired by previous works (Shan *et al.*, 2011; Portugués *et al.*, 2003; Au *et al.*, 2013), we have defined characterization metrics to compare measurements and the simulation results to validate the model in Section 3.5. Measurements are made in the laboratory with a stator bar. Radiations emitted by partial discharge sources are characterized by the phase-resolved partial discharge (PRPD), statistical distributions of power density, inter-arrival time and occurrences. PD sources can also be characterized by power-spectral density

(PSD) and impulsive waveforms. Results are discussed in Section 3.6 by comparing simulation results and measurements with PD generated by a stator bar at 16 kVrms.

3.2 Partial discharge phenomenon and its mechanism

A partial discharge is an electrical discharge which partially bridges the insulation between conductors. It is caused by imperfections within or along the insulation surface. These defects could be gaseous inclusions containing voids, cracks in solid materials or bubbles in liquids. From a physical point of view, PD is related to partial electrical breakdown phenomena. When an electric field applied to a dielectric is sufficiently intense, an ionization process occurs and leads to discharge. In addition to a high field stress, an initiatory electron is required to discharge. Hence, a discharge occurs randomly in time, and has a time lag. Several sources provide more thorough treatment of the discharge process (Niemeyer, 1995; Gutfleisch and Niemeyer, 1995; Fruth and Niemeyer, 1992; Bartnikas, 2002; Townsend, 1910; Loeb and Meek, 1940; Meek and Craggs, 1953).

A PD is characterized by a sudden drop in the local electric field due to the flow of electric charges, causing a short current-impulse discharge. Radiations emitted by partial discharge sources are random processes in terms of amplitude, the inter-arrival time between two successive impulses and time occurrence. The random character of the process is explained by complex physical mechanisms such as the presence of ionizing radiation, fluctuations in gas density or gas decomposition, etc. (Brunt and Kulkarni, 1990; Brunt, 1991). In AC voltages, impulsive events are cyclostationary and occur at every half-cycle of the applied voltage. An example of a basic PD mechanism is shown in Figure 3.1. When the electric field is sufficiently high to reach an exceeded value defined by E_{inc}, a PD occurs. The impulse train is driven by an AC voltage in this example. Δt_i is the inter-arrival time of subsequent PD events.

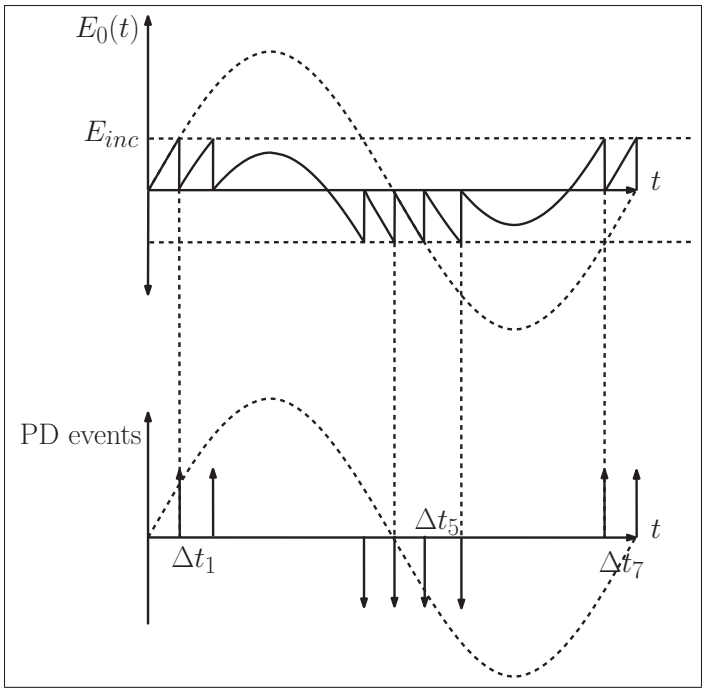

Figure 3.1 Typical behaviour of discharge process under AC voltage stress
Taken from Bartnikas and McMahon (1979)

3.3 The physical model of partial discharge source

Two physical parameters are required to initiate a discharge: the electric field stress amplitude and the critical value that leads to the ionization process. In this section, we describe a physical model of the discharge process using models of the electric field stress and the discharge occurrence in the ambient air.

3.3.1 Electric field stress

The amplitude of the electric field determines the amplitudes and rate of a PD. Depending on the arrangement of electrodes and the presence of the space charge, the electric field distribution can be strongly non-uniform. PDs in substations are formed by non-uniform field distributions due to asperities such as air cavities on insulation surface that have been degraded by PD activities and high stress fields. The electric field along the insulation surface can be

determined by an equivalent circuit a telegrapher's equations and illustrated in Figure 3.2. The presence of space charge is not considered.

Without space charges, the dielectric is represented by its conductivity at the interface of dielectric surface-air, modelled by a resistance r_s per unit length. Its permittivity is modelled by a capacitance c_o per unit length. The term ℓ denotes the width of the air gap.

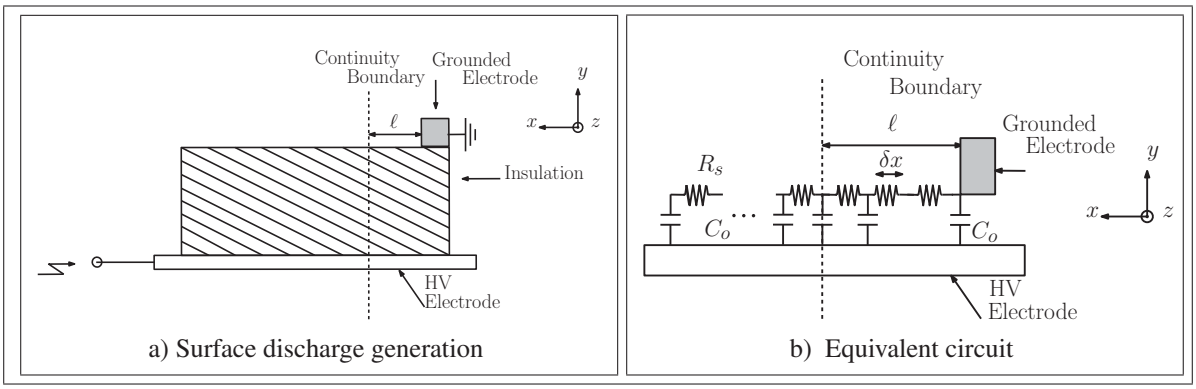

Figure 3.2 Dielectric between a pair of HV electrodes and its equivalent circuit

In the equivalent circuit, the electric field that is tangential to the insulation surface at the x coordinate can be defined by the following equations:

$$\frac{\partial U(x,t)}{\partial x} = -r_s I(x,t) \tag{3.1}$$

$$\frac{\partial I(x,t)}{\partial x} = -c_o \frac{\partial U(x,t)}{\partial t} \tag{3.2}$$

Let U^* be the potential at the dielectric surface noted as:

$$U^* = U_0 e^{j\omega t} \tag{3.3}$$

where U^* is a periodic harmonic potential $\in \mathbb{C}$, and U_0 is the magnetude of the AC voltage. Introducing boundary conditions, such that $U(0) = 0$ and $U(\ell) = U_0$ (Kogan *et al.*, 1995;

David and Lamarre, 2006). In a given direction, x, the tangential electric field on the insulation is expressed as:

$$\begin{aligned} E_{\parallel}(x,t) &= -\frac{\partial U^{*}(x,t)}{\partial x} \\ E_{\parallel}(x,t) &= -\alpha U_0 \frac{\cosh\left[(\ell - x)\alpha\right]}{\sinh\left[\ell\alpha\right]} \end{aligned} \tag{3.4}$$

with $\alpha = \sqrt{j\omega r_s c_o}$. If there are regions in which the electric field exceeds the E_{inc} value, an ionization process takes place and PD activity is observed. Furthermore, for a fixed value of c_o, when $r_s \to 1/c_o$, the field distribution becomes uniform in the cavity and the local field becomes $E \simeq U_0/\ell$. We assume the applied electric field $\mathbf{E}_0(\mathbf{r},t)$ where $\mathbf{r} = (x,y,z) \in \mathbb{R}^3$ is determined by the tangential electric field.

3.3.2 Discharge process

The area of the ionization process of air is defined when the amplitude of the electric field is higher than the critical value. Electrons are released from the surface or at the cathode. The deposited charges on the dielectric surface reduce the local field. As a result, the contribution of PD events to the electric field is given by:

$$\mathbf{E}_i(\mathbf{r},t) = \mathbf{E}_0(\mathbf{r},t) - \mathbf{E}_{pd}(\mathbf{r},t) \tag{3.5}$$

where $\mathbf{E}_0$ is the local field due to the applied voltage between electrodes, $\mathbf{E}_{pd}(\mathbf{r},t)$ is the reduced local field related to the discharge process. From Equation (3.5), PD activity is approximated by:

$$\mathbf{E}_{pd}(\mathbf{r},t) = \sum_{n=0}^{\infty} E_{q_n} \delta_{pd}(\mathbf{r}, t - \Delta t_n) \tag{3.6}$$

where $\delta_{pd}(\mathbf{r},t)$ is a space-time function related to the electric field reduction during the discharge process. E_{q_n} is the contribution of the n^{th} PD, and Δt_n is the inter-arrival time between two consecutive PD events. The critical value E_{cr} depends on a number of factors, such as discharge type, the presence of a cavity or gap, the nature of gas or pressure temperature (Levesque

et al., 2013). The critical value of a streamer discharge in a void can be used to initiate a discharge, although PD does not take place in a spherical void, in keeping with related research (Levesque *et al.*, 2013; Niemeyer, 1995; Gutfleisch and Niemeyer, 1995). The threshold value is a suitable approximation of the PD inception field. This is expressed as:

$$E_{inc} = (E/P)_{cr} P \left[1 + \frac{B}{\sqrt{2P\ell}} \right] \tag{3.7}$$

where $(E/P)_{cr} = 25.2$ VPa^{-1}m^{-1} and $B = 8.6$ m$^{1/2}$ are constant values for the air (Gutfleisch and Niemeyer, 1995). P is the atmospheric pressure and ℓ is related to air gap width. Thus, PD occurs whenever the local field reaches E_{inc}. Then, during the discharge process, the local field is reduced until its residual field E_{res} is reached. This value is approximately proportional to the critical field (Niemeyer, 1995; Gallimberti *et al.*, 1985), such that:

$$E_{res} = \gamma (E/P)_{cr} P \tag{3.8}$$

where γ is the dimensionless factor. Different values of γ can be assumed at different polarities (Niemeyer, 1995). Under these conditions, by knowing E_{inc} and E_{res}, the local field reduction due to PD activity is expressed as:

$$E_q = E_{inc} - E_{res} \tag{3.9}$$

A high field stress is a necessary but insufficient condition to initiate a discharge. The presence of an initiatory electron is required for a PD event. These electrons are produced from surfaces. They are derived from a combination of physical processes such as field emission from cathodic conductors, detrapping of electrons from traps at the insulator surface, collisions between ions, or photo-ionization processes (Niemeyer, 1995). The surface emission can be modelled by using the Richardson-Schottky formula (Levesque *et al.*, 2013; Niemeyer, 1995) to model PD

activity at insulation surfaces in the following equation:

$$N_e = \frac{A}{e} S_m \exp\left[-\frac{\Phi - \sqrt{eE/(4\pi\varepsilon_0)}}{k_B T}\right] \tag{3.10}$$

where N_e is the emitted electron rate from the surface of area A. e is the elementary charge, Φ is an effective work function, E the electric field at the emitting surface, k_B the Boltzmann constant and T the temperature. S_m is the material surface state. Depending on the insulation part or the conductive part, S_m can be written as:

$$S_{m_c} = C_{th} T^2 \tag{3.11}$$

$$S_{m_i} = \nu_0 \frac{q}{A} \tag{3.12}$$

where S_{m_c} is the characterization of the conducting part where $C_{th} = 1.2 \cdot 10^6$ $\mathrm{Am^{-2}K^{-2}}$ is an universal constant. S_{m_i} is the characterization of the insulation part where $\nu_0 \simeq 10^{14}$ $\mathrm{s^{-1}}$ is the fundamental phonon frequency and q is the deposited charge on the insulation by previous PD events (Levesque *et al.*, 2013; Niemeyer, 1995). The availability of initiatory electrons on the surface determines the average delay between the time when the field reaches the critical value E_{inc} and the excess value required to initiate a discharge. Thus, PD occurrence can be delayed due to these electrons emitted from the surface. The average time delay is expressed as:

$$\tau_e = \frac{1}{N_e} \tag{3.13}$$

The contribution of the surface emission gives stochastic properties of PD events. The calculation of this time delay was made by von Laue (1925). It determines the probability that a discharge will occur after the time when the field strength exceeds its critical value. This effect is explained by the presence of free electrons which start an electron avalanche process. Statistical properties, such as amplitude and time occurrence distributions of the PD activity, are determined by these electrons. The number of the released electrons is assumed to be a random value following the Poisson distribution law (Niemeyer, 1995; Brunt, 1991). Therefore,

the probability of a PD occurrence is given by:

$$p_{pd} = 1 - p_{\tau_e} \tag{3.14}$$

where p_{pd} is the probability of a PD occurrence and p_{τ_e} the probability of delayed electron emission from the surface.

3.3.3 Current and charge density

When a PD occurs, charged particles move from cathode to anode via a conductive spark streamer channel or electrical arc. During the discharge process, the electrical arc is seen as a conductor. Under this condition, the current density $\mathbf{J}(\mathbf{r},t)$ flows uniformly in the conductor. We assume the ionized air to be a plasma (Chang *et al.*, 1991). We link the current density with the electric field reduction and the plasma conductivity σ by:

$$\mathbf{J}(\mathbf{r},t) = \sigma \mathbf{E}_{pd}(\mathbf{r},t) \tag{3.15}$$

The plasma conductivity is written as:

$$\sigma = \frac{Ne^2}{m_e \nu_c} \tag{3.16}$$

where N is the density of electrons, e is the elementary charge, m_e is the electron mass and $1/\nu_c$ is the mean scattering time between subsequent charge collisions. The charge density induced by a discharge can be written using the expression of the electric field induced by the discharge process in keeping with Gauss's law, such that:

$$\rho(\mathbf{r},t) = \varepsilon_0 \nabla \cdot \mathbf{E}_{pd}(\mathbf{r},t) \tag{3.17}$$

where $\nabla\cdot$ is the divergence operator and ε_0 the vacuum permittivity.

3.4 The electromagnetic radiation of the interference source induced by partial discharge

Due to the local ionization process, the ionized air becomes a conductor. Hence, charges and currents are produced from the interference source. From the Lorenz gauge equation, electromagnetic radiations can be derived from current and charge densities. In this section, we assume a PD source to be an electric dipole. In the far field region, EM radiations and power density are derived from the retarded potentials equations. Inspired by models in Rao *et al.* (2007) and Moose and O'dwyer (1986), as well as many experimental results in Okazaki *et al.* (2005), Minegishi *et al.* (1989), and Pakala *et al.* (1968), we propose a coherent approach to model electromagnetic impulsive transient noise interferences induced by corona discharges on high-voltage installations.

3.4.1 Electric dipole formulation

Due to the movement of charges, we assume that the ionization process leads to a conducting channel in which currents and charges generate electromagnetic wave radiations. Therefore, from the local ionization area, there is a magnetic potential vector source and an electric scalar potential source produced by a current density and a charge density, respectively. From an antenna located at a point $\mathbf{r}$ in the three-dimensional space in the far field region, potentials are written by solving Lorenz gauge condition equations defined by:

$$\nabla \cdot A(\mathbf{r},t) + \varepsilon\mu \frac{\partial V(\mathbf{r},t)}{\partial t} = 0 \tag{3.18}$$

where $A(\mathbf{r},t)$ and $V(\mathbf{r},t)$ are respectively the magnetic vector potential and the electric potential. By assuming the harmonic time dependence, potentials $\mathbf{A}(\mathbf{r},t)$ and $V(\mathbf{r},t)$ are written from the solution to the Equation (3.18) respectively as:

$$\mathbf{A}(\mathbf{r},t) = \frac{\mu}{4\pi} \int_{\mathbf{v}'} \mathbf{J}(\mathbf{r}',t-t') \frac{e^{-j\omega\sqrt{\varepsilon\mu}|\mathbf{r}-\mathbf{r}'|}}{|\mathbf{r}-\mathbf{r}'|} d\mathbf{v}' \tag{3.19}$$

$$V(\mathbf{r},t) = \frac{1}{4\pi\varepsilon}\int_{\mathbf{v}'}\rho(\mathbf{r}',t-t')\frac{e^{-j\omega\sqrt{\varepsilon\mu}|\mathbf{r}-\mathbf{r}'|}}{|\mathbf{r}-\mathbf{r}'|}d\mathbf{v}' \tag{3.20}$$

where $\mathbf{J}(\mathbf{r},t)$ is the current density and $\rho(\mathbf{r},t)$ the charge density produced by the interference source. The delayed time propagation from the interference source to an antenna respectively positioned at $\mathbf{r}'$ and $\mathbf{r}$ is represented by $t' = |\mathbf{r}^{'} - \mathbf{r}|/c$, where c is the speed of light in vacuum. These retarded potentials equations can be seen as spatial convolution products by Green's functions.

It is worth remembering that during the discharge process, an electrical arc is a conducting channel where charge and current densities generate electromagnetic waves. Consequently, it is seen as a wire conductor when its length ζ is lower than the wavelength λ. Based on Equation (3.6), the expression of the current impulse $I_{pd}(t)$ produced by the interference source is written as:

$$I_{pd}(t) = \sum_{n=0}^{\infty}\sigma E_{q_n}\delta_{pd}(t-\Delta t_n) \tag{3.21}$$

The integration in Equation (3.19) allows us to link the expression of the current $I_{pd}(t)$ and the length of the wire conductor ζ by $I_{pd}(t)\zeta$. Now, the magnetic- and electric-radiated fields can be determined by using:

$$\mathbf{H}_r(\mathbf{r},t) = \frac{1}{\mu}\nabla\times\mathbf{A}(\mathbf{r},t) \tag{3.22}$$

$$\mathbf{E}_r(\mathbf{r},t) = -\nabla V(\mathbf{r},t) - \frac{\partial\mathbf{A}(\mathbf{r},t)}{\partial t} \tag{3.23}$$

We place an antenna in the far field region where $r \gg \lambda$. The radiated fields by PD activity in spherical coordinates $\mathbf{e}_{sph} = (\mathbf{e}_r, \mathbf{e}_\theta, \mathbf{e}_\varphi)$ are:

$$\mathbf{H}_r(r,\theta,t) = \frac{j\beta_0 I_{pd}(t)\zeta}{4\pi r}\sin\theta e^{-j\beta_0 r}\cdot\mathbf{e}_\varphi \tag{3.24}$$

$$\mathbf{E}_r(r,\theta,t) = \sqrt{\frac{\mu_0}{\varepsilon_0}}\frac{j\beta_0 I_{pd}(t)\zeta}{4\pi r}\sin\theta e^{-j\beta_0 r}\cdot\mathbf{e}_\theta \tag{3.25}$$

where $\beta_0 = \omega\sqrt{\varepsilon_0\mu_0}$.

3.4.2 Power radiation of the interference source received at the antenna

By assuming isotropic radiations in the far field region, the Poynting theorem allows for the expression of the instantaneous power radiation emitted by the interference source as:

$$\begin{aligned} P_{pd}(t) &= \int_S \mathbf{S}(r,\theta,t)dS \\ &= \int_0^{2\pi} d\varphi \int_0^{\pi} Z_0 |I_{pd}(t)|^2 \left(\frac{\beta_0 \zeta}{4\pi r}\right)^2 \sin^3\theta r^2 d\theta \\ &= 2\pi Z_0 \frac{|I_{pd}(t)|^2}{3} \left(\frac{\zeta}{\lambda}\right)^2 \end{aligned} \tag{3.26}$$

where $\mathbf{S}(r,\theta,t) = \mathbf{E}_r(r,\theta,t) \times \mathbf{H}_r^*(r,\theta,t)$ is the Poynting vector of PD radiation and $Z_0 = \sqrt{\mu_0/\varepsilon_0} = 120\pi\ \Omega$. Since impulsive noise radiations are characterized by a fast transient component, each impulse can be determined by its power density $P_d(t_n)$ such that:

$$P_d(t_n) = \frac{1}{4\pi r^2} \int_{t_n - t_w/2}^{t_n + t_w/2} P_{pd}(t)dt \tag{3.27}$$

where r is the distance between the interference source and the antenna, t_w is the duration of each impulse and t_n is the time occurrence. If the observation point is an electric dipole such as an antenna, the radiative power received depends on its effective surface or effective aperture A_e, defined by:

$$P_r(\theta,\varphi) = A_e(\theta,\varphi)P_d \tag{3.28}$$

where θ and φ are angular coordinates of the beam.

3.4.3 Modelling impulsive waveforms and PSD

Impulsive waveforms emitted by partial discharges can be modelled numerically by using a linear time-invariant (LTI) filter, defined in the z-domain as:

$$U(z) = H_m(z)\varepsilon(z) \tag{3.29}$$

where $\varepsilon(z)$ is the input of the LTI defined as a Dirac impulse, $U(z)$ is the resulting impulsive waveform and $H_m(z)$ is the LTI filter. The latter includes both the frequency response of the measurement setup and the discharge. We have interpolated the frequency response of the measurement setup according to data sheets. $H_m(z)$ is approximated by a digital resonator written as:

$$H_m(z) = G\frac{1-z^{-2}}{1-(2b_0\cos\omega_0)z^{-1}+b_0^2z^{-2}}H_{ms}(z) \tag{3.30}$$

where $H_{ms}(z)$ is given by the frequency response of the measurement setup, ω_0 is the resonant frequency, b_0 gives the bandwidth and G is the normalization gain of the filter given by:

$$G = \frac{(1-b_0)\sqrt{1+b_0^2-2b_0\cos\ 2\omega_0}}{\sqrt{2(1-\cos\ 2\omega_0)}} \tag{3.31}$$

Parameters of $H_m(z)$ will be set. The model will be compared to experimental results in terms of average power spectral density (PSD) and waveforms in the discussion.

3.4.4 Brief summary of interference induced by discharge source

The interference source can be summarized by the following statements:

- a high electric field stress and an initiatory first electron are required to initiate discharges;
- the availability of these delayed electron emissions affects the stochastic properties of impulses in terms of power radiation, time occurrence and inter-arrival time;
- a PD activity reduces the local electric field due to deposited charges;
- discharge events follow the cyclostationary process when an AC voltage is applied;
- during the discharge process, charge and the current densities are produced by an electrical arc;
- the electromagnetic radiations are derived from charge and the current densities during the discharge process. An antenna can receive these radiations as an impulsive transient noise.

An example of a computation of a PD process occurring at every rise of the AC voltage is illustrated in Algorithm 3.1, with the presence of a first electron to initiate discharges. The following notations are introduced for the implementation of partial discharges :

- l is the number of the cycle of the AC voltage;
- t_{inc^+} and t_{inc^-} are the time of the first PD occurrence during the first half-cycle and the second, respectively;
- t_n is the time occurrence of the n^{th} impulse;
- $E_0(t)$ is the local field applied to the electrodes, which is a AC voltage;
- $E_q = E_{inc} - E_{res}$ is the local field reduction due to the PD process;
- $\Delta E = E_{inc} + E_{res}$ corresponds to the contribution of the electric field between the last PD event and the first impulse at the last half-cycle;
- $\mathbf{S}(r, \theta, t)$ is the Poynting vector;
- $P_{pd}(t)$ is the power density of impulsive radiations emitted by a partial discharge source.

3.5 Experimental characterization process of the interference source

3.5.1 Definition of characterization metrics

Based on Chapter 2, the proposed model can be validated according to the characterization of PD sources as follows:

- power density of impulsive noise radiations P_d distribution (mW/m^2);
- PD occurrence t_n distribution (s);
- inter-arrival time Δt distribution (s).

Algorithm 3.1 Computation of PD process sequence during the first half-cycle

Data: E_{inc}, E_{res} and $E_0(t)$
Result: Compute $P_{pd}(t)$ of PD process

Ensure $\exists t_{n-1} \in t = \left[t_{inc^-}\ ;\ (2l-1)\pi + \frac{\pi}{2}\right]$, a PD impulse exists for $l > 0$;
if $l > 0$ **then**
  if $\exists t_n \in t = \left[t_{n-1}\ ;\ 2l\pi + \frac{\pi}{2}\right]$, $E_0(t_n) - E_0(t_{n-1}) = \Delta E$ **then**
    $P_{pd}(t_n) \leftarrow \int_S \mathbf{S}(r,\theta,t_n)dS$;
  end
  $n \leftarrow n+1$
end
while $t_{n-1} < t \leq 2l\pi + \frac{\pi}{2}$ **do**
  if $t_n, \in t, E_0(t_n) - E_0(t_{n-1}) = E_q$ **then**
    $P_{pd}(t_n) \leftarrow \int_S \mathbf{S}(r,\theta,t_n)dS$;
    $n \leftarrow n+1$;
  else
    $P_{pd}(t) \leftarrow 0$;
  end
end

These first order statistics give PD occurrence and its power density distribution per unit time or phase. For an isotropic antenna, the measured signal in voltage $V_m(t)$ is converted into electric field strength $x_m(t)$ defined by:

$$x_m(t) = V_m(t)\sqrt{\frac{Z_0 4\pi}{RG_r\lambda^2}} \tag{3.32}$$

where R is the load resistance, G_r the gain of the RF system and λ the wavelength of the wide-band antenna. In practice, the measured signal contains impulsive noise emitted by discharges and the overall background noise. An impulse detector is used for an experimental characterization of PD. First, impulsive noise emitted by partial discharge sources is extracted from the overall noise via a denoising process using a threshold applied to wavelet coefficients. Then, the power density of each impulse is calculated by using a short-time Fourier analysis. PD processes are characterized in terms of statistical distributions and also in terms of power spectral density (dBW/m^2/Hz).

3.5.2 Denoising process

The power spectral density of the radiations that are received from partial discharge sources can be estimated properly by using a denoising process that extract impulses from the overall noise. The extraction procedure is based on wavelet transform. Then, a threshold is applied to wavelet coefficients. By estimating the background noise level such as in Donoho and Johnstone (1994), impulses are extracted by rescaling the threshold values at each decomposition level and the obtained signal is reconstructed by the inverse of wavelet transform. In the denoising process, Daubechies wavelets are used with eight vanishing moments and for 30 levels of decomposition to yield a suitable estimation of impulsive transient noise waveforms (Au *et al.*, 2013).

3.5.3 Short-time analysis process

The measurement data contain a train of impulses located randomly in time. PD can be detected by using a short-time analysis of the spectrogram of the waveform $X_m(t_w, f)$ defined by:

$$X_m(t_w, f) = \int_{\mathbb{R}} x_m(t) w(t - t_w) e^{-j2\pi ft} dt \tag{3.33}$$

where $w(t)$ is the time window and t_w is the window length parameter. The spectrogram is useful in localizing fast transient signals in frequency and time. In Equation (3.33), each segment contains a power spectral density value. Therefore, PD can be localized in time by the high value of the PSD in the segment. The power density of PD can be estimated by using the marginal time condition. In order to determine the contribution of these impulses in RF range, the power is calculated in a selected bandwidth Δf near a given resonant frequency f_0 based on Equation (3.34).

$$P_d(t_w) = \frac{1}{Z_0} \int_{f_0 - \Delta f/2}^{f_0 + \Delta f/2} \frac{\left| X_m(t_w, f) \right|^2}{\langle w(t), w(t) \rangle} df \tag{3.34}$$

To analyse each impulse in a given impulse train, we use a wide band spectrogram with a Hamming window of $t_w = 6.4$ ns length. The length of the FFT is $N_{\text{fft}} = 2048$ and 50% overlap

is used. Under this condition, the measured power of the ambient noise without discharges is about -53.20 dBW/m^2. The power density of each impulse is calculated in the bandwidth range of 0.2 to 5 GHz. $P_d(t_n)$ value is located at each signal peak above -47 dBW/m^2 to ensure the detection of significant impulsive noise emitted from partial discharge sources.

3.6 Experimental validation

In this section, the experimental validation is based on the comparison of measurement campaign and the simulation results. The following subsections describe the measurement setup including the PD sources produced by a stator bar. Then, the simulation parameters are adapted according to measurement conditions. Note that the measurement setup, follows Chapter 2.

3.6.1 Brief description of measurement setup

3.6.1.1 The measurement setup

The following measurement setup includes:

- a wideband log periodic antenna from $0.8-26$ GHz;
- a high pass filter from $780-3200$ MHz;
- an RF amplifier is employed from $30-3000$ MHz;
- a broadband limiter to protect RF equipment;
- an oscilloscope used for data acquisition, a serial data analyser.

The observation time is 20 ms at a 10 Gs/s sample rate (200 M samples). The oscilloscope is synchronized to the HV voltage generator. Waveforms are captured periodically at the beginning of each cycle of the AC voltage. Using this configuration, 30 waveforms are captured. The antenna is positioned at $d = 3$ m from the stator bar in the far field region.

3.6.1.2 PD sources from stator bar

A stator bar is used to generate PDs along the insulation surface. A main PD site is located on the insulation surface as illustrated in Figure 3.3. In the middle of the bar, the semi-conducting coating has been removed to expose the epoxy-mica insulation. An air gap between insulation and grounded electrode, including the semi-conducting coating, can be seen. The Dimensions and electrical properties of the dielectric and air cavities used are summarized in Table 3.1 and Figure 3.4. The conductivity of the insulation surface is attributed to the presence of epoxy-mica. Levesque *et al.* (2010) have measured the conductivity of the epoxy-mica. It can be found that σ_i can be $\sim 10^{-16}$ S/m for unaged dielectric, and $\sim 10^{-9}$ S/m for aged dielectric. The air cavity is represented by the thickness of the semi-conducting coating on the bar. Thus, when the electric stress is sufficiently high, PD activities can take place at the end of the semi-conducting coating. A HV generator is applied to the stator bar. Surface discharges are predominant in this experimentation. PDs are generated by an AC high voltage of 16 kVrms at 60 Hz.

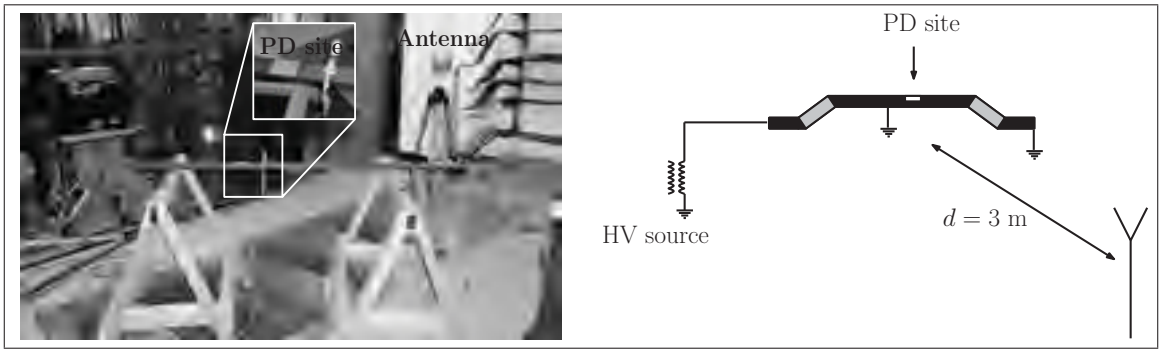

Figure 3.3 Stator bar and measurement configuration

3.6.2 Simulation setup

Simulation parameters are defined by the following steps:

Table 3.1 Dimensions and electrical properties of PD process

	Dimensions			**Relative permittivity**	**Conductivity**
Model	Height (mm)	Width (mm)	Depth (mm)	ε_r	σ_i (S/m)
Air cavity	0.25	2.5	2	1	0
Dielectric	3.6	55	58	4	$2.8 \cdot 10^{-9}$

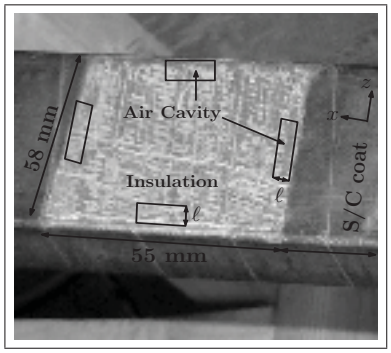

a) PD site with modelled air gap cavities

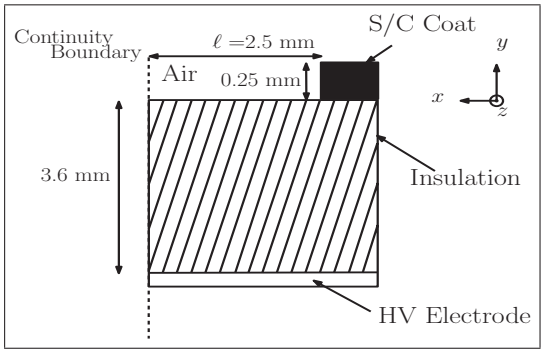

b) Dimensions of stator bar with an air cavity

Figure 3.4 The surface of a stator bar with modelled air cavities

3.6.2.1 Calculation of the electric field along the surface

The electric field inside air cavities is calculated from the equivalent circuit where r_s and c_0 are the resistance of the insulation surface and the capacitance of the grounded wall, respectively. Depending on the orientation of air cavities, ℓ is in the x or z coordinate. These components are written as:

$$\begin{aligned} r_s &= \frac{1}{\sigma_i A_r} \\ c_0 &= \frac{\varepsilon_0 \varepsilon_r A_c}{\eta \, \delta x} \end{aligned} \tag{3.35}$$

with $\delta x = \delta z = 0.5$ mm, calculating the cross sectional area of the resistance A_r is the product of the depth of the dielectric (58 mm) and its height (3.6 mm), the calculated resistance per

unit length is $r_s = 1.72$ TΩ/m. Calculating the overlapping surface area of the plates A_c as the product of δx and the depth of the dielectric (58 mm). Since η is the height of the dielectric (3.6 mm), the capacitance of the insulation is $c_0 = 0.604$ nF/m. By applying an AC voltage at 16 kVrms, the tangential electric field is calculated from Equation (3.4). Since the tangential electric field is complex, we use the absolute value to determine its amplitude.

3.6.2.2 Discharge process in air cavity parameters

These parameters have been set in keeping with several related works (Niemeyer, 1995; Gutfleisch and Niemeyer, 1995; Fruth and Niemeyer, 1992). PD activities take place on either side of the air gap between the end of the semi-conducting coating and the insulation surface. In Figure 3.4, four air cavities are considered. Although many PD sources can take place randomly in these air cavities, four PD sources are assumed for each. PD sources are located in the middle of the high-stress region. At 16 kVrms voltage, the electric field amplitude at $x = 0$ is 12.45 kV/mm as depicted in Figure 3.5. From Equation (3.7), under normal temperature and pressure, the critical value to initiate a discharge is $E_{inc} = 3.96$ kV/mm. Since the calculated electric field amplitude is higher than the E_{inc}, PD activity is observed.

We characterize PD amplitudes by the local field reduction, as defined in Equations (3.6) and (3.9). The reduction depends on the deposited charges in the air cavity. Previous discharges and other discharges in the vicinity of the air cavity can also affect this local field reduction (Levesque *et al.*, 2013; Brunt, 1991). The latter determine the behaviour of the inter-arrival time and also the amplitude of the field reduction. We assume that E_q is a random value following an exponential distribution, where the average value is:

$$\begin{aligned} E_{q^+} &= E_{inc} - \gamma_+ (E/P)_{cr} P \\ E_{q^-} &= E_{inc} - \gamma_- (E/P)_{cr} P \end{aligned} \tag{3.36}$$

where E_{q^+} and E_{q^-} are the local field reduction value of the conductive part and the insulation part, respectively, where $\gamma_+ = 0.01$ and $\gamma_+ = 1.2$.

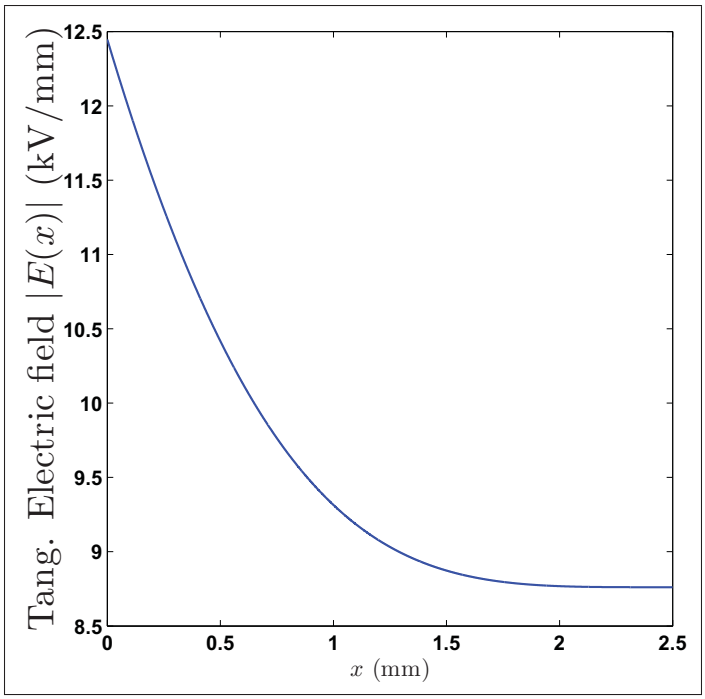

Figure 3.5 Tangential electric field distribution

The release of free electrons from surfaces is given by Equation (3.10). We define the conductive part and the insulation part by their work functions Φ_c and Φ_i, respectively. Although emission surface parameters could not be measured directly, they have been adapted to reproduce measurements. We use $\Phi_c = 1.20\ e$V, $\tau_{e_c} \simeq 36\ \mu$s and $\Phi_i = 1.38\ e$V, $\tau_{e_s} \simeq 21\ \mu$s.

3.6.2.3 Stochastic property of the emitted radiations of PD sources

Due to the reduction of the local field, each air cavity generates charge and current density according to Equations (3.15) and (3.17). The retarded potentials equations allow us to determine the induced electromagnetic radiations from partial discharge sources, as defined in Equation (3.27). The amplitude of the electromagnetic field is derived from the currents and the length of the electric arc, $I_{pd}(t)\zeta$. The amplitude of the current impulse depends on the local field reduction value E_q and the conductivity of the ionized air σ as seen in the Equation (3.21).

The conductivity σ as defined in Equation (3.16) depends on the collision frequency between species and the density of electrons. We assume that the combination of many PD sources

affects the plasma conductivity randomly and independently. Moreover, due to the applied voltage, the discharge process is time-dependent in terms of amplitude and occurrence. Therefore, we express the plasma conductivity σ as:

$$\begin{aligned} \sigma^{+}(\sigma_0^{+},t) &= \sigma_0^{+} f^{+}(t) \\ \sigma^{-}(\sigma_0^{-},t) &= \sigma_0^{-} f^{-}(t) \end{aligned} \tag{3.37}$$

where σ_0^{+} and σ_0^{-} are the average random values. $f^{+}(t)$ and $f^{-}(t)$ are deterministic time-dependent functions related to the influence of the electric field stress on charge density and the mean scattering time. These functions determine the time occurrence distribution of PD events. It maybe challenging to obtain parameters of plasma conductivity. Inspired by relevant models (Zimmermann and Dostert, 2002; Moose and O'dwyer, 1986; Shan *et al.*, 2011), we have adapted these parameters with observations from the measurement campaign. Thus, we choose that the quantity $\zeta\sigma$ can be considered as a random value according to Weibull distributions. Parameters of the distribution are estimated from empirical data obtained from the measurement campaign. In addition, we have decided that time-dependent functions $f^{+}(t)$ and $f^{-}(t)$ are Gaussian functions. The antenna is located 3 m from the source, and 30 cycles of the 60 Hz are considered.

3.6.3 Simulation-measurement comparison

3.6.3.1 PRPD comparison

The measurement campaign is conducted using voltage of 12 kVrms and 16 kVrms. In this chapter, the discussion is restricted to the comparison at 16 kVrms. The power density of these impulsive radiations and their occurrences can be compared in terms of the measurement and simulation results by PRPD illustrated in Figure 3.6. According to measurements, PD events occur at every half cycle of the AC voltage. These results show the cyclostationary process of PD sources generated by an AC voltage. The impulse rate and the power density in the negative part is higher compared to what occurs in the positive part. This is due to the number

of deposited charges on the insulation surface. They can be explained by a low value of the electric field reduction on the cavity $E_q^- < E_q^+$ and a higher value of the air conductivity due to the ionization process.

A high probability of having a PD with low amplitude of power density is observed and the probability of having a high amplitude of power density is lower. This is because the local field of PD activity has yielded a low value of reduction. Moreover, the emission of electrons from surfaces influences the amplitude of the power density and the rate of PD events. When the critical field stress E_{inc} is reached, the presence of the initiatory electrons is not sufficient to discharge. Consequently, a time delay is observed due to the excessive electric field stress-to-discharge process, which causes the power density of impulsive radiations to increase. The obtained PRPD from the simulation results matches with measurement results. Both results indicate that the cyclostationary process of PD events are induced by the applied voltage. The occurrence of discharge events is predominant at the negative polarity compared to the positive one.

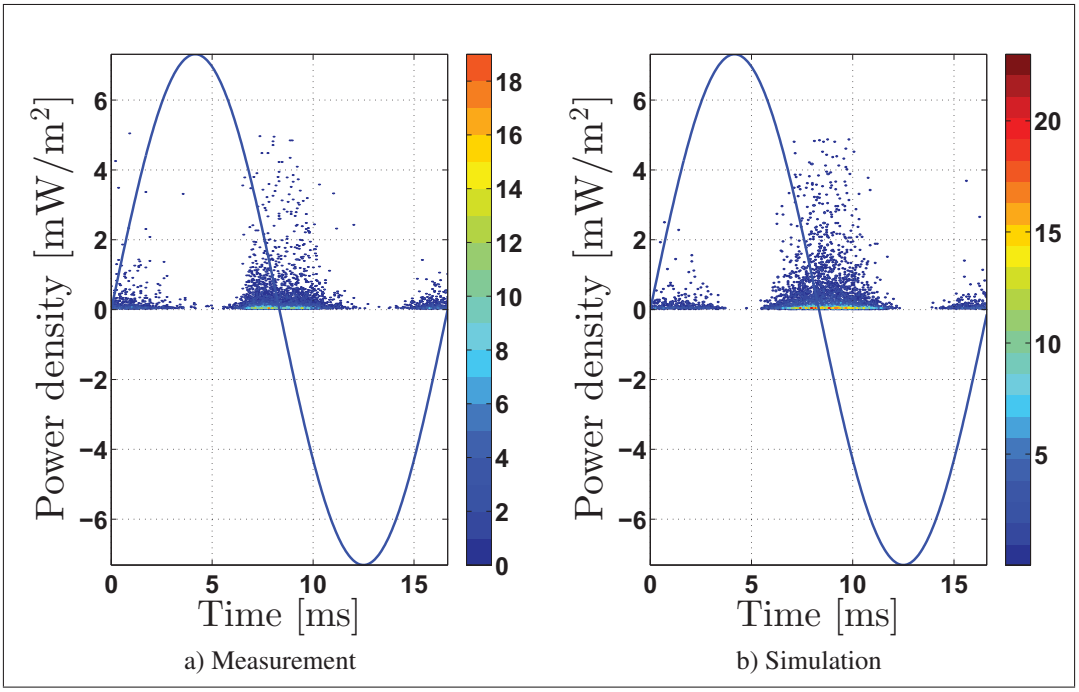

Figure 3.6 Phase Resolved Partial Discharge 16 kVrms

3.6.3.2 Statistical distributions comparison

The statistical distributions of power density, inter-arrival time and time occurrence for measurements and the simulation at 16 kVrms are presented as an empirical probability density function (PDF) and empirical complementary cumulative density function (CCDF) in Figure 3.7, Figure 3.8 and Figure 3.9. Statistical results shows that PD events can be described as random processes in terms of power density amplitude, inter-arrival time and time occurrence.

Stochastic properties of PD events are explained by physical interactions between charged particles, such when these particles recombine in order to reach their equilibrium state. These interactions can take place because of previous discharges or as a result of the PD activities of other sources. The excessive electric field stress of the applied voltage increases the probability of releasing free electrons and charged particles by collision into the air. As a result, the air becomes ionized.

Figure 3.7 shows power density distributions of measurement and simulation. The probability of a high amplitude of power density decreases exponentially. The inter-arrival time distributions follow exponential distributions in measurement and simulation results (see Figure 3.8). Figure 3.9 shows time occurrence distributions. PD events are observed as the applied voltage rises and falls. They follow the cyclostationary process induced by the frequency of the applied voltage. The probability of observing a discharge at the negative polarity is higher than the positive. Time occurrence PDF describes two Gaussian distributions. We compare measurement and simulation results by plotting the empirical CCDF, measuring the Kullback-Liebler (KL) divergence of the empirical PDF, and conducting a Kolmogorov-Sminorv (KS) test at 5% significance level. It is observed that simulation results fit measurement results. In Table 3.2, small KL-divergence values show a small divergence between PDFs obtained by simulation and measurement. Using the test statistic values of the KS test (D_{KS}) in this table, the obtained p-values are 0.61, 0.72 and 0.37 for power density, inter-arrival time and time occurrence respectively. As a result, the test does not reject the null hypothesis that simula-

tion and measurement results come from the same distributions at 95%. Therefore, simulation results are in agreement with experimental results in terms of first-order statistics.

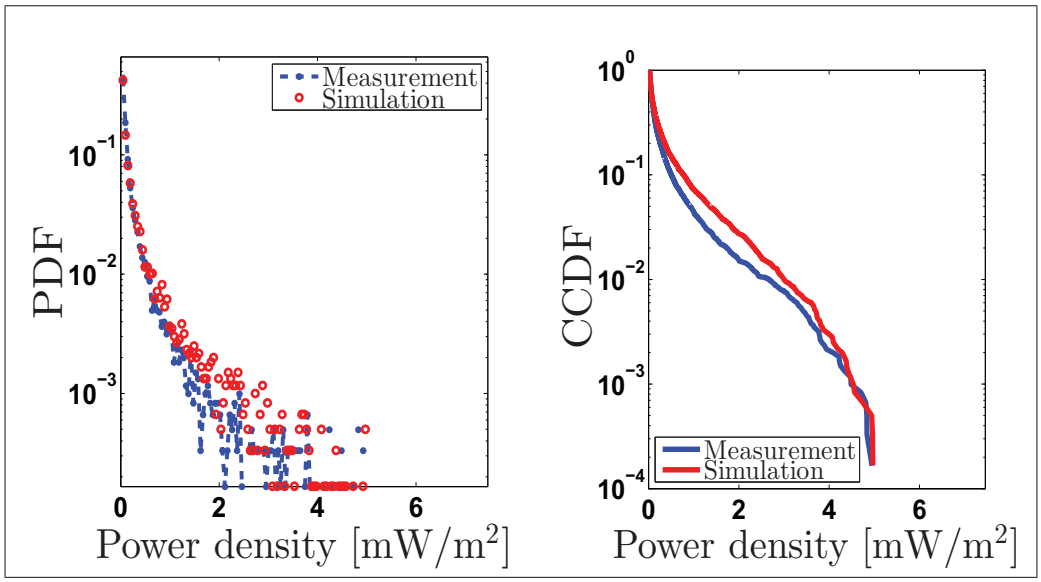

Figure 3.7 Power density distribution

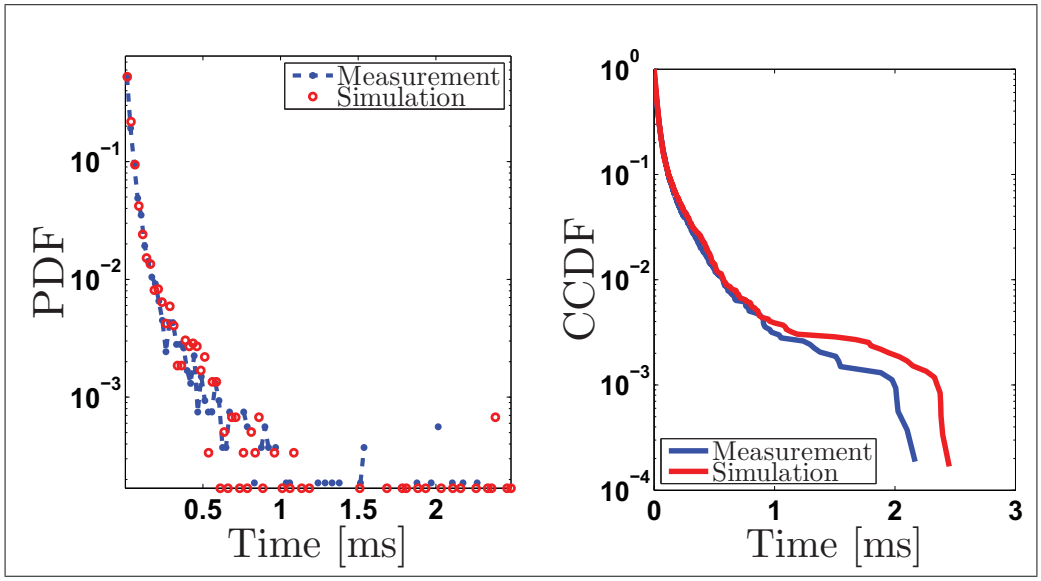

Figure 3.8 Inter-arrival time distribution

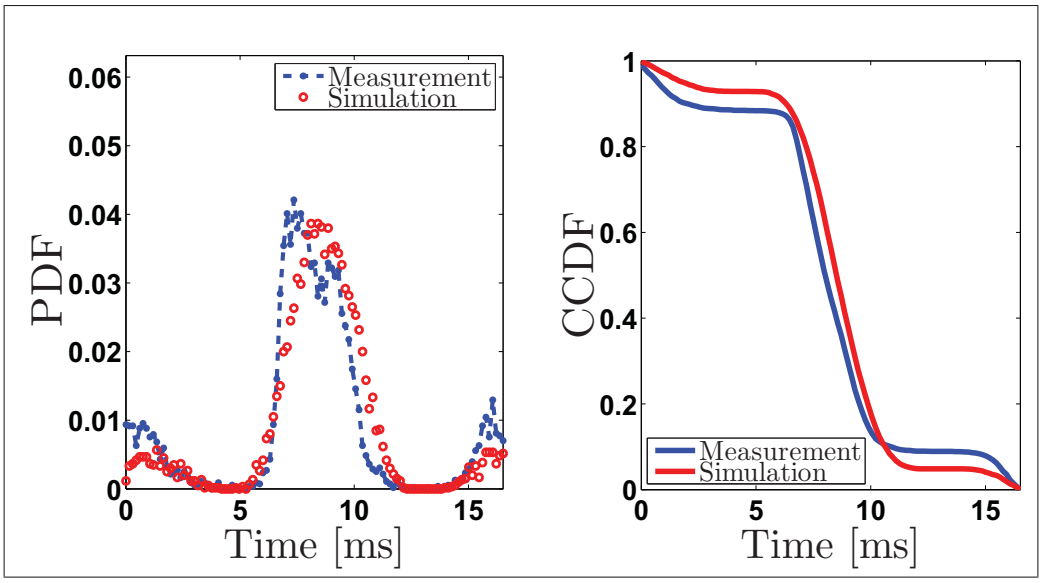

Figure 3.9 Time occurrence distribution

Table 3.2 The Goodness-of-fit: Measurement vs. simulation

Test Statistics	**Power density**	**Inter-arrival time**	**Time occurrence**
D_{KL}	0.1873	0.1706	0.2153
D_{KS}	0.0687	0.0077	0.127

3.6.3.3 PSD and waveforms of impulses

Simulation results validate the proposed model in terms of PSD and waveforms. The average PSD of measurement and simulation are presented in Figure 3.10. The ambient noise includes thermal noise, RF communications at 1.7 and 1.9 GHz and harmonics at 1.25, 2.5 and 3.75 GHz caused by interleaving artefacts and clock feedthrough from the oscilloscope. The PSD of impulses can be extracted from the ambient noise using a denoising process as depicted in Figure 3.10.(b). Low wavelet coefficient values have been removed via a hard threshold to extract the impulsive signal. However, the process can significantly modify the PSD of impulses mainly at frequencies at which the PSD of ambient noise is dominant.

PSD and waveforms can be provided by the proposed LTI model in Equation (3.30). We have considered the ambient noise by adding a Gaussian white noise. Parameters of the LTI filter have been set as follows: $\omega_0 = 0.5027$ (800 MHz) and $b_0 = 0.90$ (bandwidth of 273.2 MHz at -3 dB). By comparing the average PSDs, simulation results match experimentation results (see Figure 3.10). However, the proposed model cannot perform distortions of waveforms as depicted in Figure 3.11. This may due to multiple reflections of EM waves in the laboratory. In this example, the denoised waveforms and their induced PSDs are presented. Their average energies are approximately equal. It is seen that the measured waveform and the PSD are widely distorted.

The proposed LTI filter models the impulse response of RF-signals from PD activity on average. The filter can be improved by taking into account multiple delayed impulses. This can be done by using tapped delay line filters. The impulse response of the propagation channel should be estimated using measurements in the laboratory. Thus, a realistic impulsive RF signals model can be obtained under this condition.

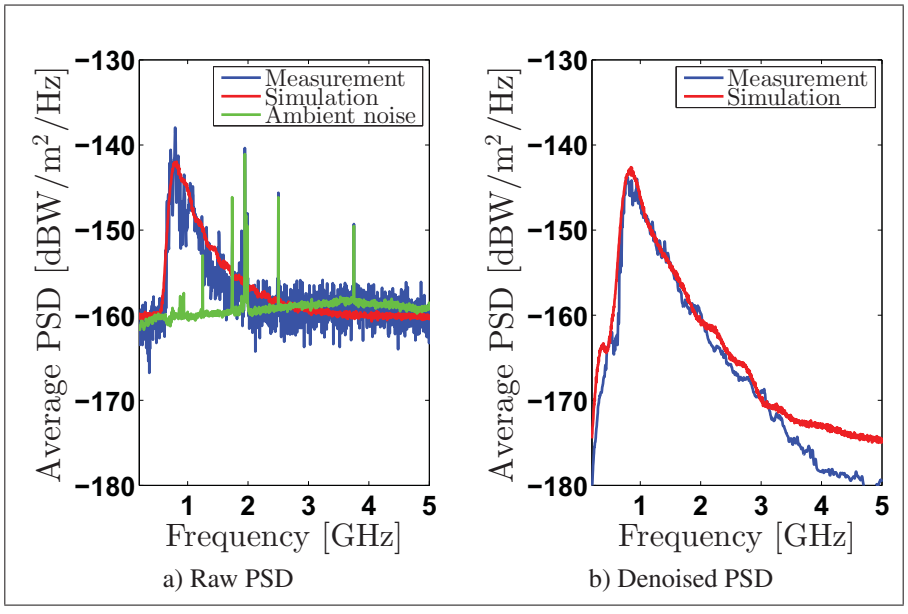

Figure 3.10 PSD Comparison: Measurement vs. simulation

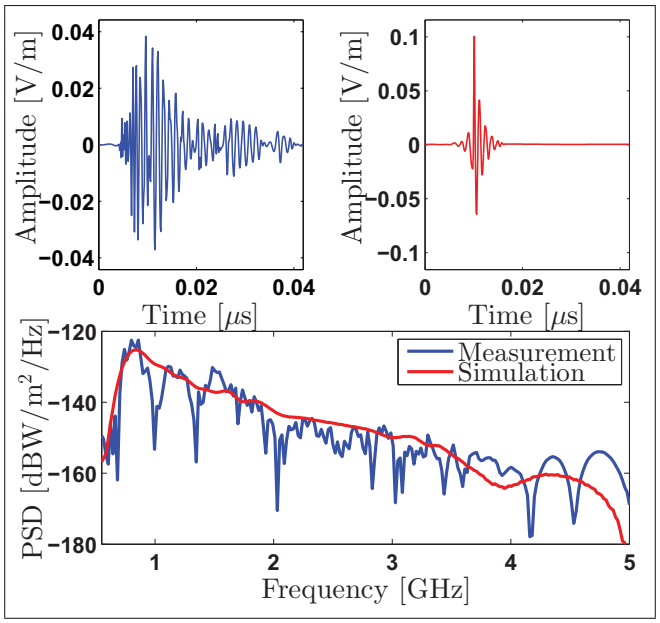

Figure 3.11 Waveforms and PSD of an impulse

3.7 Conclusion

A physical model of EMIs induced by corona discharges is presented in this chapter. A high stress field can produce an ionization process that leads to discharge. Charges and current densities induce electromagnetic radiations. The interference sources induced by PDs have particular behaviours that differ in terms of occurrences and amplitude from classical models of impulsive EMIs sources, (Shinde and Gupta, 1974; Middleton, 1977; Zimmermann and Dostert, 2002). Indeed, the AC voltages produce a cyclostationary behaviour of discharge events. Their amplitudes are induced by the local reduction of the electric field and charged particles during the discharge process.

The physical model allows for a coherent, detailed, and validated approach that links the discharge process to the induced far field wave propagation. As a result, we can link certain physical characteristics of high-voltage installations to the induced radio interference spectrum. We have shown the consistency of simulation results, provided by the proposed model, over experimental results. We have validated the model in terms of amplitude *i.e* power den-

sity, occurrences, and inter-arrival time of these impulsive radiations. We have also validated the induced spectrum and waveforms of these radiations received at the antenna.

Future work may focus on extending the proposed model to contexts in which there are many discharges with various parameters, such as electric field stress, where the insulation property of dielectrics can reproduce the environment of substations, or wherever else high-voltage installations and their induced discharged sources are randomly distributed in space. Moreover, based on the proposed LTI filter, modelling impulsive waveforms can be significantly improved by taking into account multiple delayed impulses.

In the next chapter, an analysis and modelling of wideband RF impulsive signals induced by partial discharges using second-order statistics is proposed. Based on an LTI filter, spectral characteristics of the PD can be captured.

CHAPTER 4

ANALYSIS AND MODELLING OF WIDEBAND RF IMPULSIVE SIGNALS INDUCED BY PARTIAL DISCHARGES USING SECOND-ORDER STATISTICS

4.1 Introduction

The recent advances in wireless sensor network (WSN) technologies in the last few years have allowed for the emergence of new smart grid applications in for use in substations (Gungor *et al.*, 2010, 2011). However, the reliability of these WSNs can be affected by the multiple presence of electromagnetic interferences (EMIs) from PD activity. Therefore, performance analyses have to be evaluated in the presence of these EMIs. To do so, an accurate and generic impulsive noise model is needed. At the same time, PD sources can cause mechanical failure or permanent damage to insulation materials in HV equipment. Their electromagnetic radiations can be detected by electronic devices for which significant improvements are possible for protection, control, automation and monitoring of HV equipment (Tenbohlen *et al.*, 2008; Judd *et al.*, 2005). An accurate model of RF signals induced by these impulsive EMIs is a valuable tool in the design of efficient signal processing methods for PD source detection, localisation and mitigation.

4.1.1 Motivation and prior related work

Au *et al.* (2013, 2015b) show that wideband impulsive noise waveforms emitted by partial discharges are transient, their samples are correlated and their power spectral densities have approximately a form of $\sim (f - f_0)^{-\gamma}$, where f_0 is the resonant frequency of the RF measurement setup and $\gamma > 0$ an arbitrary exponent. One of the most common impulsive noise models used are Middleton Class A and B (Middleton, 1977, 1999, 1979) and the α-stable noise models (Weron and Weron, 1995; Samarodnitsky and Taqqu, 2000; Chambers *et al.*, 1976). Although these models can approximate noise samples with impulsive noise based on first-order statistic, they are far from our observations. Indeed, an impulse is modelled by a single sample. Thus, second-order statistics are, most of the time, inaccurate in the sense that the autocorrelation

of an impulsive component yields a Dirac impulse function at zero so that the power spectral density is constant over all frequencies (*i.e* not proportional to $f^{-\gamma}$).

Alternatively, Zimmermann and Dostert (2002), and Sacuto *et al.* (2013) have found that transient impulsive noise can be modelled based on a partitioned Markov chain. The model can approximate second-order statistics from the measurements. However, the definition of a suitable number of states in the Markov chain can be challenging and the estimation procedure are complex, (Sacuto *et al.*, 2013; Ndo *et al.*, 2013). Using these models can also drastically increase computational complexity, (Sacuto *et al.*, 2013). On the other hand, impulsive noise can be modelled using Markov-Middleton or Gauss-Markov impulsive noise models as presented in Ndo *et al.* (2013), and Fertonani and Colavolpe (2009), which are used in order to account for the bursty nature of impulsive noises. However, the resulting impulsive waveforms are modelled by a group of uncorrelated samples. Therefore, the transient behaviour of the impulses is not taken into account and the modelled waveforms might be inaccurate. These impulsive noise models are physically limited because their parameters cannot provide any information linking the physical characteristics of HV installations to the induced radio interference spectrum.

A simpler way to model impulsive transient waveforms is to use LTI filters as developed by Au *et al.* (2015b), and Sadler (1996). Although these filters can capture spectral characteristics of the impulsive radio interference spectrum in substations, the resulting waveform is deterministic, which is not observed in practice. A study of propagation effects of wideband radiation signals from PD activity was investigated by Portugués and Moore (2006). It has been shown that measured impulsive waveforms are, in general, distorted by the effect of multipath in electromagnetic wave propagation. This is due to the presence of multiple reflectors in substations. Therefore, we may assume that PDs in HV equipment have spectral signatures whose resulting impulsive radio interference spectra are distorted by multipath propagation effects.

4.1.2 Main contribution and organization

In this chapter[1], we propose a novel approach to modelling impulsive noise for wireless channels. By this approach, modelled waveforms stochastically resemble the measurements, in that spectral characteristics of RF signals from PD sources can be captured, and the effect of multipath is taken into account. Compared to many approaches presented in the literature, such a model can reproduce transient effects of impulsive noise, and it fits accurately measurements in terms of second-order statistics. Moreover, a well-established validation procedure can be implemented for the estimation of the spectral characteristics and the selection of a suitable number of parameters in the LTI filter, (Dickey and Fuller, 1979; Phillips and Perron, 1988; Box *et al.*, 1994; Akaike, 1973; Schwarz, 1978). Our proposed impulsive noise model allows for the study of the spectrum of radio signals from PD activity and its relationships with physical characteristics of PD sites. This can be used to represent a generic environment of substations for performance analysis of wireless communication networks, as well as for PD detection methods.

The rest of this chapter is organized as follows: in Section 4.2, the measurement setup and two major pieces of HV equipment in a 735 kV substation are briefly presented. In Section 4.3, a review of measured impulsive noise is presented from this two HV equipment. We will show that HV equipment has a spectral signature due to the spectral characteristics of the emitted PD. In Section 4.4, we proposed a generalized model using an LTI filter approach, by which spectral characteristics of PD sources in HV equipment can be captured. In Section 4.5, the adequacy of the approach (the goodness-of-fit) can be measured by analysing the residuals of fitted ARMA models whose distributions are non-Gaussian and whose variances are time-dependent. The impulsiveness of the PD transient waveforms can be reproduced by assuming the conditional heteroskedasiticity of the residuals. Finally, in Section 4.6, computer simulations are provided

[1] This chapter is based on the submitted journal paper "Analysis and Modelling of Wideband RF Impulsive Signals Induced by Partial Discharges Using Second-Order Statistics" in IEEE Transaction on Electromagnetic Compatibility, January 2016.

to validate the effectiveness of the proposed model vis-a-vis impulsive waveforms measured in substations. The advantages and the limitations of our approach are also discussed.

4.2 Measurement setup

In the measurement campaigns, impulses are measured employing the measurement setup explained in Chapter 2. An antenna is positioned in the far field region of discharge sources. Measurements are made in a 735 kV outdoor substation, in which EMI produced by two typical HV installations: *i*) a power transformer tank (PTT) in which the applied voltage is 735 kV, and *ii*) a current transformer tank (CTT).

In this chapter, we characterize the electromagnetic interferences generated by discharge sources for any antenna or other RF component gain in our measurement setup. To do so, we consider real valued impulsive noise waveforms whose amplitudes are measured in terms of electric field strength in (V/m). This allows us to know the power densities of impulsive waves. We use Equation (4.1) to convert signals in voltage to electric field strength, according to (Au *et al.*, 2015b):

$$u(\theta,t) = u_m(\theta,t)\sqrt{\frac{Z_0 4\pi}{R_\ell G_r \lambda^2}} \tag{4.1}$$

where $u_m(\theta,t)$ is the measured waveform in voltage, $Z_0 = 120\pi\ \Omega$ is the impedance of the freespace, R_ℓ is the load resistance, G_r is the gain of the RF system including the antenna and λ is a given wavelength of the wideband antenna. Since the power densities of impulsive waveforms are mostly localized around $f_0 = 800$ MHz, we choose the wavelength at $\lambda = 0.375$ m. We can analyse the resulting signals in baseband by removing the resonant frequency f_0 via a local oscillator and a mixer. Significant impulsive radiations emitted by discharge sources are detected and captured by a given threshold slightly above the level of the background noise. The sample rate is 10 Gs/s for a given observation time according to the durations of impulses. From experimentations, significant impulses are captured above -33 dBW/m^2 for an observation time of approximately 50 ns in *i*) and -42 dBW/m^2 for an observation time of 50 ns in *ii*).

4.3 Conjectures and mathematical formulation of EM waves

This section provides a review of measured impulsive noises, a discussion of their properties, and a generalization of our observations. Radiations emitted by discharge sources are impulsive, have short durations and exhibit a damped effect which decays over time. We analyse measured waveforms by using a time-frequency representation and second-order statistics, using the autocorrelation function and power spectral density. The analysis will be helpful for the design of a general model of impulsive noise induced by electric arc discharges.

4.3.1 Second-order statistics

4.3.1.1 Time-frequency analysis

It may be useful to have a time-frequency representation of transient waveforms. Under this condition, we choose the spectrogram representation, which is based on the short-time Fourier transform (STFT), such that:

$$U(\theta, t_w, \omega) = \int_{-\infty}^{+\infty} u(\theta, t) w(t - t_w) e^{-j\omega t} dt \tag{4.2}$$

where $u(\theta, t)$ is the temporal waveform of impulsive noise and θ is a set of random variables denoting the local variation of amplitude in the time-frequency domain, as well as duration, time decay, etc. $w(t)$ is a given time window function, with t_w the length of the window. By computing the spectrogram as the squared magnitude of the STFT, we obtain the following expression:

$$S_{uu}(t_w, \omega) = \frac{1}{Z_0} |U(\theta, t_w, \omega)|^2 \tag{4.3}$$

where each segment $S_{uu}(t_w, \omega)$ is the power density of the process located in (t_w, ω). In order to have a suitable time-frequency resolution, we compute the spectrogram by considering $w(t)$ as a Hamming function with a window length of 32 samples. The overlap percentage between adjoining sections is 70% of 32 samples and the number of FFT is 512.

4.3.1.2 Autocorrelation function

Sample autocorrelation is used to estimate the theoretical autocorrelation function (ACF) given by:

$$r_k = \frac{\mathrm{Cov}\left[u(\theta,t), u(\theta,t-k)\right]}{\mathrm{Var}\left[u(\theta,t)\right]} \tag{4.4}$$

where $\mathrm{Cov}\left[\cdot,\cdot\right]$ is the estimated covariance function, $\mathrm{Var}\left[\cdot\right]$ is the estimated variance and $\bar{u}$ is the estimated mean value of the measured waveform. The lag is given by k, when one lag is chosen at the sampling interval of the oscilloscope, 0.1 ns. The 95%-confidence interval for the identification of time series models is given by the Barlett's formula as (Hamilton, 1994; Woodward *et al.*, 2012):

$$B = \pm 1.96 \sqrt{\frac{1}{M}\left(1 + 2\sum_{i=1}^{k} r_i^2\right)} \tag{4.5}$$

where M is the number of observations and $k > 0$. Although Gauss-Markov processes take into account the correlation, they are only one particular case of a first-order autoregressive process, AR(1). The ACF function of our measurements suggests that a high order of ARMA processes might be more accurate.

4.3.1.3 Results from the measurement campaigns

A typical example of waveforms captured in the measurement campaigns is depicted in Figures 4.1 and 4.2. Spectrograms and power spectral densities are also depicted. The spectrogram shows that the power of transient waveform is strong for a short duration with a large frequency bandwidth, but decreases over both time and frequency. Since the noise samples are correlated, the power spectral densities are non-constant over frequencies. Indeed, the power spectral density (PSD) decays proportionally as $\sim f^{-\gamma}$ where $\gamma > 0$. As shown in several studies (Portugués and Moore, 2006; Portugués *et al.*, 2003; Judd *et al.*, 2005, 1996b), local variations on PSD over frequency can be observed, which is characteristic of multipath effects. Moreover, due to their transient behaviour, there are significant correlations for high values of

lag. As a result, using Middleton Class A and B and α-stable models might not be reasonable because an impulse is modelled by a single sample. These waveforms can be seen as colored impulsive noise. The autocorrelation function shows that there are significant correlations for large values of lag. The ACFs decay slowly and go under the confidence interval.

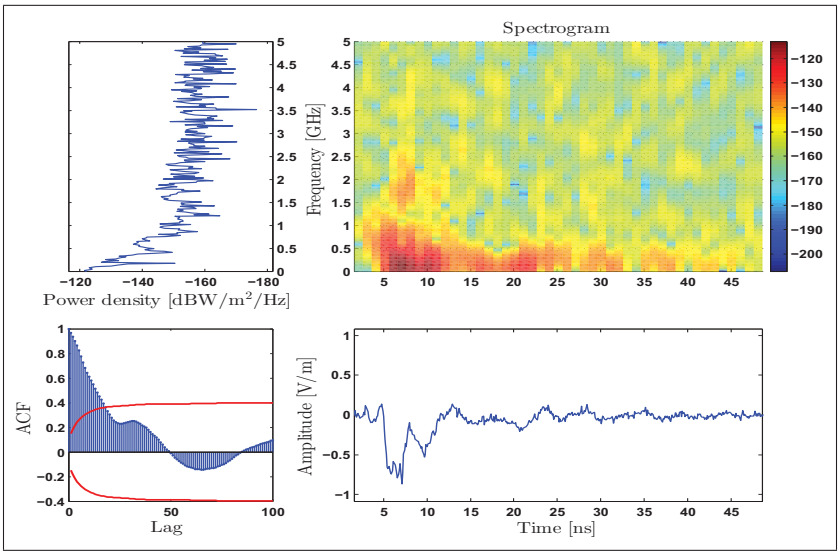

Figure 4.1 Waveform measured from PTT

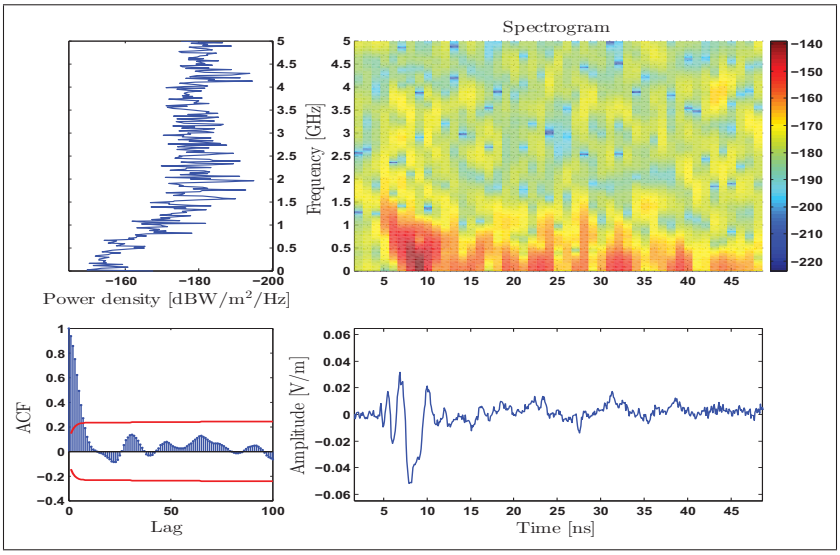

Figure 4.2 Waveform measured from CTT

4.3.2 A physical interpretation

When a discharge occurs, the emission of electromagnetic radiations propagate through the environment. Let $aD(\bar{\theta},t)$ be the original transient impulse induced by an elementary electric arc discharge where a is a random amplitude, $\bar{\theta}$ is a set of time-invariant random variables denoting the duration, time decay, phase shift, and other spectral characteristics. In freespace, the resulting measured impulsive noise $u(\theta,t)$ is the convolution product of $aD(\bar{\theta},t)$ and the measurement setup impulse response denoted by $h_m(t)$, such that:

$$u(\theta,t) = \alpha_0 aD(\bar{\theta},t) * h_m(t) \tag{4.6}$$

where α_0 is the signal freespace path loss coefficient and $*$ is the convolution product. The resulting waveform at the antenna is a simple transient impulse with a damped effect. However, the experimentations show that the amplitudes are distorted and attenuated. As a result, the received impulsive noise might be subject to fading. By denoting $W(\bar{\theta},t)$ as the convolution product of the original transient impulsive waveform and the impulse response of the measurement setup, the resulting impulsive waveform distorted and attenuated by multiple reflected waves can be written as:

$$u(\theta,t) = aW(\bar{\theta},t) * h(t) \tag{4.7}$$

where $h(t)$ is the impulse response of the multipath channel, which can be defined as:

$$h(t) = \sum_k \alpha_k e^{j\varphi_k} \delta(t-\tau_k) \tag{4.8}$$

where $\{\alpha_k\}$ is a real positive gain of the path k, $\{\varphi_k\}$ the associated phase shift and $\{\tau_k\}$ is the propagation delay. The equation (4.7) can be rewritten as a shot-noise process:

$$u(\theta,t) = \sum_k \alpha_k e^{j\varphi_k} aW(\bar{\theta},t-\tau_k) \tag{4.9}$$

The multiple reflected waves induced by the environment cause both destructive and constructive interferences that are received by the antenna. Therefore, the impulsive waveforms are distorted by multipath effects, as seen in Figures 4.1 and 4.2.

4.4 The proposed model

In this section, we propose a general model for impulsive noise induced by electric arc discharges when the waveforms are transient and their amplitudes are subject to multipath effect. Our research questions are: *i*) what is the appropriate model for impulsive noise waveforms induced by an electric arc discharge? and *ii*) How is the goodness-of-fit of the model, according to measurements?

4.4.1 Theory of filters and its relationship with time series models

Let $\{u_t\}_{t\in T\subset\mathbb{Z}}$ be the stochastic process modelling an impulsive noise waveform indexed by the discrete time set T, a subset of all integers $\mathbb{Z}$. In keeping with the model described by Au *et al.* (2015b), the random process u_t can be modelled as a discrete time linear filter in the z-domain, such that:

$$U(z) = H_d(z)\varepsilon(z) \tag{4.10}$$

where $U(z)$ is the output of the filter, $H_d(z)$ is the z-transform of an impulse response of the original impulse waveform received at the antenna, and $\varepsilon(z)$ is the input stress characterizing the electromagnetic disturbance in the environment. $H_d(z)$ can be written as:

$$H_d(z) = \frac{1+\sum_{k=1}^{q}\psi_k z^{-k}}{1-\sum_{i=1}^{p}\phi_i z^{-i}} \tag{4.11}$$

where all coefficients ϕ_i and ψ_k for any $i = \{1, \cdots, p\}$ and $k = \{1, \cdots, q\}$ lie outside the unit circle. By replacing $H_d(z)$ in Equation (4.11) into Equation (4.10), we have:

$$U(z)\left(1 - \sum_{i=1}^{p} \phi_i z^{-i}\right) = \left(1 + \sum_{k=1}^{q} \psi_k z^{-k}\right) \varepsilon(z) \tag{4.12}$$

By using the inverse z-transform, we have in the time domain a time series by writing Equation (4.12) as:

$$u_t = \sum_{i=1}^{p} \phi_i u_{t-i} + \varepsilon_t + \sum_{k=1}^{q} \psi_k \varepsilon_{t-k} \tag{4.13}$$

These terms within the equation induce correlated samples, since u_t depends on past samples. Furthermore, if the disturbance ε_t is a Dirac impulse, a deterministic transient impulse without any distortions is provided by the filter, as modelled in Au *et al.* (2015b), and Sadler (1996). This is not observed in our measurements. For ε_t to be modelled as a white Gaussian noise, its variance is constant over time, and the resulting waveform appears as a colored noise process spread indefinitely over time. Thas not been observed here, and it is not appropriate for impulsive noise modelling either. Measured impulsive noise can be seen as colored noise; however, its variance might be conditional, and therefore not constant over time.

4.4.2 Definition of the time series model

We define a lag operator L such that $L^i u_t = u_{t-i}$, where u_{t-i} is the instantaneous amplitude of the process at the discrete time $t-i$. We also define the differential operator Δ such that $\Delta^i u_t = (1 - L)^i u_t$ is the i-th degree differencing operator. From the measured waveforms, it is convenient to assume that impulsive noises do not express any seasonal effect. From the Box-Jenkins methodology (Box *et al.*, 1994), non-stationary random processes can be trend-stationary, as written in Equation (4.14a) or difference-stationary, as written in Equation (4.14b), such that:

$$u_t = m_t + \varepsilon_t \tag{4.14a}$$

$$\Delta^d u_t = m + \Psi(L)\varepsilon_t \tag{4.14b}$$

where m_t is a deterministic mean trend and m is a constant mean, ε_t is a zero-mean and uncorrelated stochastic process, $\Psi(L) = 1 + \psi_1 L + \psi_2 L^2 \cdots$ is an infinite degree polynomial operator in which coefficients are absolutely summable, and all roots lying outside the unit circle, Δ^d are d-th degree differencing operators. By assuming a finite degree polynomial operator, we can define u_t as a generalized autoregressive integrated moving average ARIMA(p,d,q), modelled as:

$$\Phi_p(L)\Delta^d u_t = m + \Psi_q(L)\varepsilon_t \tag{4.15}$$

where $\Phi_p(L) = 1 - \phi_1 L - \phi_2 L^2 \cdots - \phi_p L^p$ and $\Psi_q(L) = 1 + \psi_1 L + \psi_2 L^2 \cdots + \psi_q L^q$ are respectively the p-th and the q-th degree operator polynomials where all coefficients are absolutely summable and all roots lie outside the unit circle. The next task is to define the degrees (p,q) of the ARMA model and the d-th degree of differencing operator that fit our measurements. However, in ARIMA models, the process ε_t is assumed to be uncorrelated with a constant mean or a constant variance over time. In Section 4.3, measured impulsive noise may exhibit heteroskedasticity, *i.e* non-constant variance. When the variance of ε_t is not constant over time, we can include additional conditional heteroskedasticity models to the time series u_t, (Bollerslev, 1986; Engle, 1982; Nelson, 1991). Among these models, we can mention autoregressive conditional heteroskedascity (ARCH), generalized ARCH (GARCH) or exponential GARCH (EGARCH). We formally express ε_t by:

$$\varepsilon_t = \sigma_t \varepsilon_t \tag{4.16}$$

where ε_t is the white noise process and σ_t the time-dependent standard deviation of the process. The variance σ_t^2 can be seen as a time series. It can be modelled as an ARMA process for time-dependent effect of the disturbance ε_t (Bollerslev, 1986; Engle, 1982; Straumann, 2005). We will define a suitable model, which fits measurements based on our assumptions. The latter can be tested with various tests to be defined. In this chapter, the analysis of the time series is restricted to the measured waveforms presented in Figures 4.1 and 4.2. Similar conclusions with many measured impulsive noises can be drawn.

4.4.3 Tests for unit roots

Before estimating and selecting a model, it is necessary to test the "*stationarity*" (*i.e.* $d > 0$ (Phillips and Perron, 1988)) and unit roots of the measured impulsive noises to avoid the problem of spurious regression (Woodward *et al.*, 2012; Hamilton, 1994; Box *et al.*, 1994). To do so, we can treat the ARIMA(p,d,q) model as an ARMA($p+d$,q) model. As a result, we can write Equation (4.15) as follows:

$$\Phi_{p+d}(L)u_t = m + \Psi_q(L)\varepsilon_t \tag{4.17}$$

where $\Phi_{p+d}(L) = \Phi_p(L)(1-L)^d$. Since measured impulsive noise fluctuates around zero-mean, we assume that $m = 0$. Next, since all roots of the polynomial $\Psi_q(L)$ lie outside of the unit circle, the invertibility condition of the model is satisfied and thus we have:

$$\Psi_q(L)^{-1}\Phi_{p+d}(L)u_t = \varepsilon_t \tag{4.18}$$

We assume that a polynomial exists that is related $\Omega(L)$ related to the polynomial $\Psi_q(L)^{-1}\Phi_{p+d}(L)$ such that Equation (4.18) can be written as an AR process (Said and Dickey, 1984), defined by:

$$\begin{aligned} \Delta u_t &= (\Omega(L) - 1)u_{t-1} + \varepsilon_t \\ \Delta u_t &= \rho u_{t-1} + \sum_{i=1}^{k-1} \gamma_i \Delta u_{t-i} + \varepsilon_t \end{aligned} \tag{4.19}$$

where γ_i is a function of the ARMA process. If the time series u_t is suspected to be non-stationary in difference, then a unit root exists where $\rho = 0$. In this case, the ARIMA(p,1,q) model is recommended. The presence of unit roots may explain the non-stationary behaviour of our measurements. As a result, unit root tests can be used to determine whether impulsive noise contains a unit root.

The augmented Dickey-Fuller (ADF) (Dickey and Fuller, 1979) and the Phillips-Perron (PP) (Phillips and Perron, 1988) tests can be used to assess the presence of a unit root in the impulsive waveform. Based on the model defined in Equation (4.19), without any intercept or a drift terms, the null hypothesis of the unit root is $H_0 : \rho = 0$ against the alternative hypothesis, $H_1 : \rho < 0$. The estimation of $\hat{\rho}$ is based on ordinary least squares (OLS) and the test statistics for the null hypothesis is given by the t-statistic. However, the test statistics do not follow a standard distribution. Hence, the limiting distributions have been derived (Hamilton, 1994). The resulting value is compared to the interpolated Dickey-Fuller critical values, based on the tables in Fuller (1996) for the decision rule. An approximation of the p-values is given in (MacKinnon, 1994) on the basis of a regression surface. However, for the ADF test, the process ε_t should be stationary; in other words, ε_t does not exhibit conditional heteroskedasticity. Furthermore, the selected number of lags should be appropriate to keep the test unbiased or to decrease the power of the test.

At the same time, the PP test is a non-parametric test, based on the same model used in ADF tests, that modifies the ADF test statistics. It is made robust to serialize correlation and heteroskedasticity in ε_t (Phillips and Perron, 1988; Newey and West, 1987). The PP test procedure remains the same as the ADF test, and it uses the critical values based on the same tables in Fuller (1996). The tests need the number of autocovariance lags to include in the Newey-West estimator of the long-run variance, which depends on the number of observations M (Newey and West, 1987). This number is given by $\lfloor 4\,(\mathrm{M}/100)^{2/9} \rfloor$ where $\lfloor \cdot \rfloor$ is the floor function. Another advantage is that we do not need to specify the number of lags for the test. Hence, Equation (4.19) for the PP test is reduced to:

$$\Delta u_t = \rho u_{t-1} + \varepsilon_t \tag{4.20}$$

The samples in our measurements may exhibit heteroskedasticity. As a result, it is reasonable to choose the PP test. Table 4.1 depicts the results of the PP test. The waveforms, which are presented in Figures 4.1 and 4.2 are tested. The test is set for a significance level of 5%. The

test statistic values in the table are all below the interpolated Dickey-Fuller critical values and the estimated $\hat{\rho}$ is negative and the p-values are closed to zero. As a result, the test indicates the rejection of the unit root null in favor of the alternative model, at a 95% confidence interval. In other words, measured impulsive waveforms do not need to be differentiated. Thus, we should use ARMA(p,q) models with no integration for transient impulsive noise modelling.

Table 4.1 Results of PP test obtained from the measured impulsive noises

Waveforms	**Nb. obs**	**Test-stat.**	**Crit. val**	$\hat{\rho}$
PTT.	510	-2.68	-1.94	-0.027
CTT.	500	-4.27	-1.94	-0.062

4.4.4 Estimation and selection

Since data do not need to be differentiated, we can use the ARMA(p,q) models. The next task is to determine the degree (p,q) of the model at which coefficients ϕ_i and ψ_k can be estimated from the observed data u by using the maximum likelihood estimation (MLE). The model can be chosen based on the Akaike Information Criterion (AIC) (Akaike, 1973, 1974) or the Schwarz Bayesian Information Criterion (SBIC) (Schwarz, 1978), written respectively as:

$$\mathrm{AIC} = 2\kappa - 2\log(\mathfrak{L}(\theta_\kappa|u)) \tag{4.21a}$$

$$\mathrm{SBIC} = -2\log(\mathfrak{L}(\theta_\kappa|u)) + \kappa\log(M) \tag{4.21b}$$

where $\mathfrak{L}(\theta_\kappa|u)$ is the optimized likelihood objective function value of the proposed model parametrized by a vector θ_κ, to be estimated from the observed data u. The number of free parameters to be estimated is denoted by κ, and M, the number of observations. These values include a penalty for complex models with additional parameters. The SBIC is more severe than the AIC in terms of penalties, due to its relationship with the number of observations M.

Note that the model with the lowest AIC or SBIC has the best fit. It has been found that the ARMA(7,2) for PTT and the ARMA(4,1) for CTT are suitable models because AIC and SBIC values are small compared to the other values of p and q. The residuals of fitted ARMA models can be inferred to check the goodness-of-fit.

4.5 The goodness-of-fit

In this section, we study the models' goodness-of-fit. The residuals of fitted ARMA models are analysed to check the adequacy of the model. We will show that the residuals express conditional heteroskedasticities. Therefore, ARMA models need to be improved by adding ARCH effects.

4.5.1 Analysis of the residuals

Residuals are helpful for modelling the disturbance term ε_t so that u_t behaves like transient impulsive noise with correlated samples. Using the Box-Jenkins approach, the model is adequate if the residuals are white noise, *i.e* serially uncorrelated with zero mean and constant variance. It is necessary to determine if ARMA(p,q) models satisfy these conditions.

First of all, it is convenient to analyse the standardized residuals of fitted ARMA models by checking their whiteness. This can be showed by using the normal probability plot in which probability distributions of residuals can be graphically compared to the normal distribution (Wilk and Gnanadesikan, 1968). In addition, a Kolmogorov-Smirnov (KS) test can be used. These allow us to assess whether residuals could come from a normal distribution. Moreover, ACF and partial ACF (PACF) can be plotted to check whether residuals are uncorrelated. The bounds for autocorrelation set at 95% of confidence are given by:

$$B = \pm \frac{1.96}{\sqrt{M}} \tag{4.22}$$

The analysis of the autocorrelation can be refined by using the portmanteau test given by Ljung-Box Q-test for Residual Autocorrelation (Ljung and Box, 1978; Box and Pierce, 1970). It tests

for autocorrelation at multiple lags jointly. The null hypothesis is that the first K autocorrelations are jointly zero. For a number of observations M, the Ljung-Box Q-statistic is given by the portmanteau statistic written as:

$$Q_\varepsilon = M(M+2)\sum_{k=1}^{K}\frac{\hat{r}_k^2(\varepsilon)}{M-k} \tag{4.23}$$

where $\hat{r}_k^2(\varepsilon)$ is the estimated autocorrelation of residuals at lag k. Under the null hypothesis, Q_ε follows a chi-square distribution χ^2_{K-p-q} asymptotically with $K-p-q$ degrees of freedom, which depends on the (p,q) of the selected ARMA models. If a p-value is greater than a given significance level, then the test fails to reject the null hypothesis and proves that the residuals are not autocorrelated.

4.5.1.1 Residuals of fitted ARMA(7,2)

The distribution of the residuals is heavy-tailed since a deviation at the extreme values is observed in Figure 4.3. Since, the p-value of the KS test is below 0.05 the test rejects the null hypothesis of normal distribution at a 95% confidence interval. Therefore, the distribution could not come from a normal distribution since the curve is not linear, and the KS test rejects the null hypothesis. Furthermore, on the ACF and PACF, the correlation coefficients for different values of lags are, in general, below the limits for autocorrelation. Therefore, the residuals might be uncorrelated.

In order to check whether residuals are uncorrelated, we can use the Ljung-Box Q-test for residual autocorrelation. The test is set to a significance level of 5% with different values of K-first autocorrelations. Results of the test are depicted in Figure 4.4, in which the critical values are plotted in a red curve and the calculated Q-statistic values are plotted in a blue curve for the different values of K-first autocorrelations. The p-values are represented in this figure below. These values are compared to 0.05, since the test is set to a significance level of 5%.

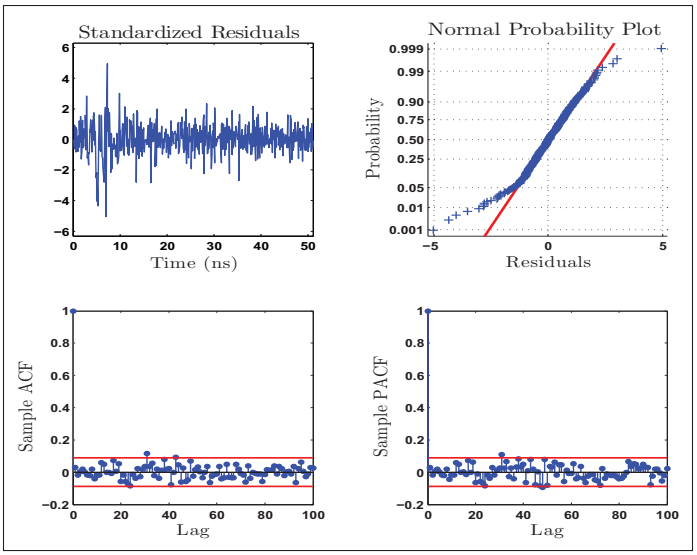

Figure 4.3 Analysis of the residuals of fitted ARMA(7,2) model

We can see that all values of the Q-statistic are below the critical values for different values of K. The p-values are all above 0.05. As a result, the test fails to reject the null hypothesis that the residuals are not autocorrelated at a confidence interval of 95% for different values of K-first autocorrelations tests.

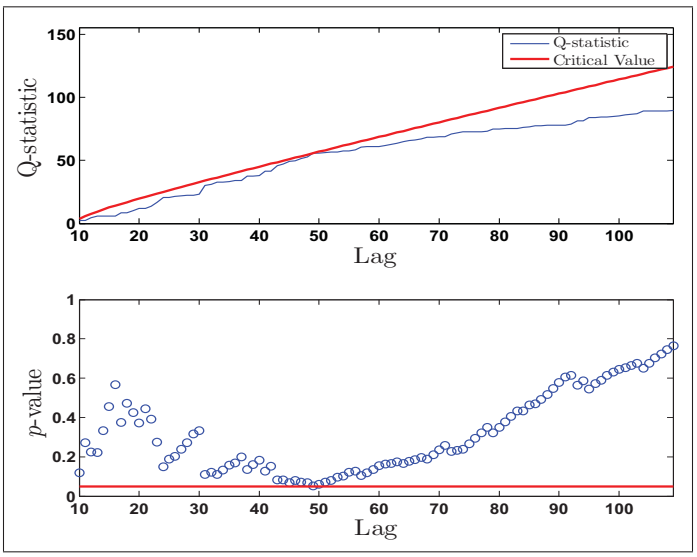

Figure 4.4 Results of Ljung-Box Q-test for residual autocorrelation of the ARMA(7,2)

4.5.1.2 Residuals of fitted ARMA(4,1)

The distribution of the residuals is less heavy-tailed. The KS test fails to reject the null that the distribution comes from the normal distribution. Nevertheless, a deviation at the negative values is observed, as in Figure 4.5. The distribution might be left-skewed. Moreover, some correlation coefficients are above the autocorrelation bounds in the ACF and the PACF. Hence, we may not conclude graphically whether the residuals are uncorrelated.

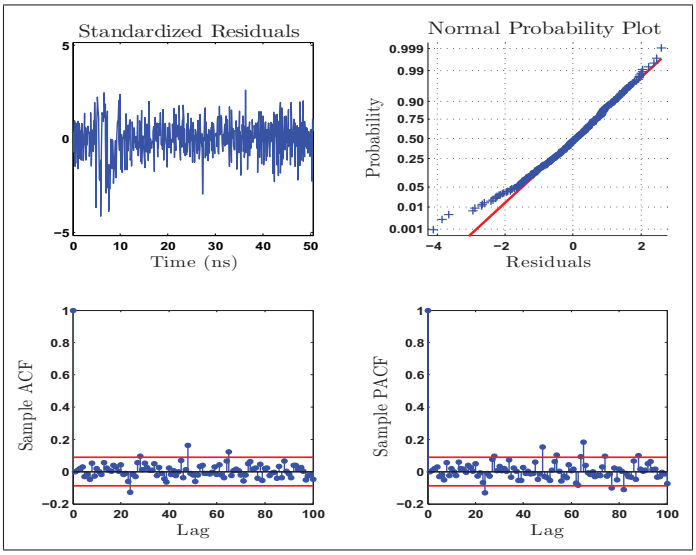

Figure 4.5 Analysis of the residuals of fitted ARMA(4,1) model

The Ljung-Box Q-test for residual autocorrelation is also set for a significance level of 5% with different values of K-first autocorrelations. The results of the test are depicted in Figure 4.6. We can see that there is no evidence to reject the null hypothesis that proves that the residuals are not autocorrelated at a 95% confidence interval, since all values of the Q-statistic are below the critical values and the p-values are all above 0.05 for different values of K-first autocorrelations.

In summary, for both models ARMA(7,2) and ARMA(4,1), the distributions of the residuals do not come from a normal distribution and the Ljung-Box Q-tests fail to reject the null hypothesis

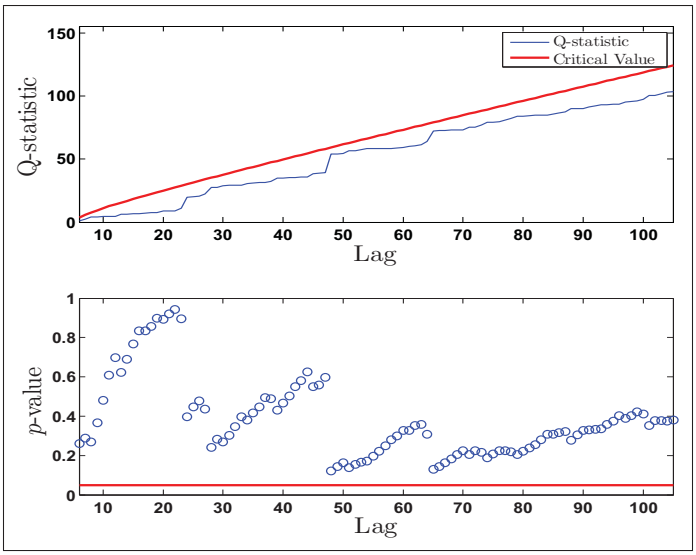

Figure 4.6 Results of Ljung-Box Q-test for residual autocorrelation of the ARMA(4,1)

that the residuals are not autocorrelated. We can conclude that the disturbance terms ε_t are uncorrelated non-Gaussian noise.

These proposed models need to be improved by adding additional parameters. Increasing the number of (p,q) can refine our models. However, the models would be more complex and over-fitting problems can occur (Hurvich and Tsai, 1988). Moreover, the heavy-tailed distributions of the residuals cannot be explained by increasing the number of (p,q). On the other hand, the proposed models can be refined by assuming that these residuals are the consequence of non-linear effects such as heteroskedasticities.

4.5.2 Tests for heteroskedasticity

The ARMA(p,q) process with unconditional variance of the disturbance process ε_t may not be a suitable assumption for modelling impulsive noises. When the process contains ARCH effects, we can write the variance σ_t^2 of the process ε_t given the information set available, which is denoted by $\mathscr{I}_{t-1} = \{\varepsilon_{t-1}, \varepsilon_{t-2}, \cdots\}$ at discrete time $t-1$ (Bollerslev, 1986; Engle,

1982; Straumann, 2005):

$$\begin{aligned}\sigma_t^2 &= \mathbb{E}[\varepsilon_t^2|\mathscr{I}_{t-1}] \\ &= \Upsilon_{q'}(L)\varepsilon_t^2 \\ &= \upsilon_0 + \sum_{i=1}^{q'} \upsilon_i \varepsilon_{t-i}^2\end{aligned} \tag{4.24}$$

where $\mathbb{E}[\cdot]$ denotes the expectation and υ_i are coefficients of the polynomial $\Upsilon_{q'}(L)$. We assume that ε_t is zero-mean. The assumption for conditional heteroskedasticity can be tested by the Ljung-Box Q-test of the squared residuals of fitted ARMA models (McLeod and Li, 1983). In addition, the Engle's ARCH test (Engle, 1982) for conditional heteroskedasticity can be set to ensure that our measurements contains ARCH effects.

Several authors (Granger and Andersen, 1978; McLeod and Li, 1983) have noted that the analyses of the squared residuals are useful for the detection of non-linear types of statistical dependence in the residuals of fitted ARMA models. Similarly to the Ljung-Box Q-statistic in Equation (4.21), the test statistic of squared residuals denoted by ε^2 is given by the following portmanteau statistic:

$$Q_{\varepsilon^2} = M(M+2)\sum_{k=1}^{K} \frac{\hat{r}_k^2(\varepsilon^2)}{M-k} \tag{4.25}$$

Under the null hypothesis, Q_{ε^2} asymptotically follows a chi-square distribution χ_K^2 with K degrees of freedom (McLeod and Li, 1983). The test rejects the null hypothesis of no autocorrelation in the squared residuals if $Q_{\varepsilon^2} > \chi_K^2$ where χ_K^2 is the chi-square distribution table value.

In addition, the Engle's ARCH test can be used. Following Equation (4.24), the null hypothesis is $H_0 : \upsilon_i = 0$ for all $i = 1 \cdots q'$. The test used is the Lagrange multiplier (LM) statistic MR^2, where M is the sample size and R^2 is the coefficient of determination from fitting the ARCH(q') model for a number of lags q'. The null hypothesis indicates the failure to reject the no ARCH effects (Engle, 1982). Under the null hypothesis, the asymptotic distribution of the test statistic

is χ^2 with q' degrees of freedom. Note that the test can be applied to GARCH models since a GARCH(p',q') model is locally equivalent to an ARCH($p'+q'$) model (Bollerslev, 1986).

As depicted in Figures 4.7 and 4.8, the Ljung-Box Q-test for squared residual autocorrelation rejects the null hypothesis that the squared residuals are not autocorrelated at 95% confidence for different values of K-first autocorrelations. As a result, a non-linear effect should be taken into account in our ARMA(p,q) models.

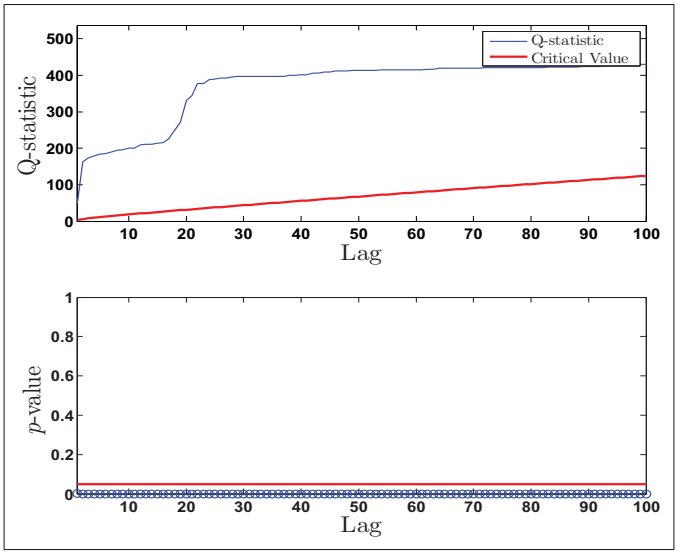

Figure 4.7 Results of Ljung-Box Q-test for squared residual autocorrelation of the ARMA(7,2)

Moreover, as seen in Figures 4.9 and 4.10, the null hypothesis is rejected for different values of lags q' at a confidence interval of 95%. Note that the test fails to reject the null hypothesis of no ARCH effects in the residuals of fitted ARMA(4,1) models at lags up to $q' = 75$. Due to its complexity, in practice we will not use an ARCH model with q' up to 75. As a result, we can argue that our measurements contain heteroskedasticities in conformity with results obtained from the Ljung-Box Q-tests for square residual autocorrelation.

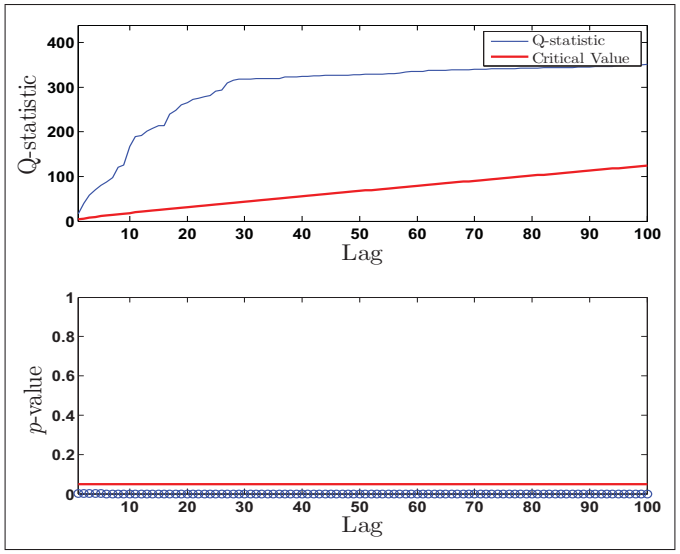

Figure 4.8 Results of Ljung-Box Q-test for squared residual autocorrelation of the ARMA(4,1)

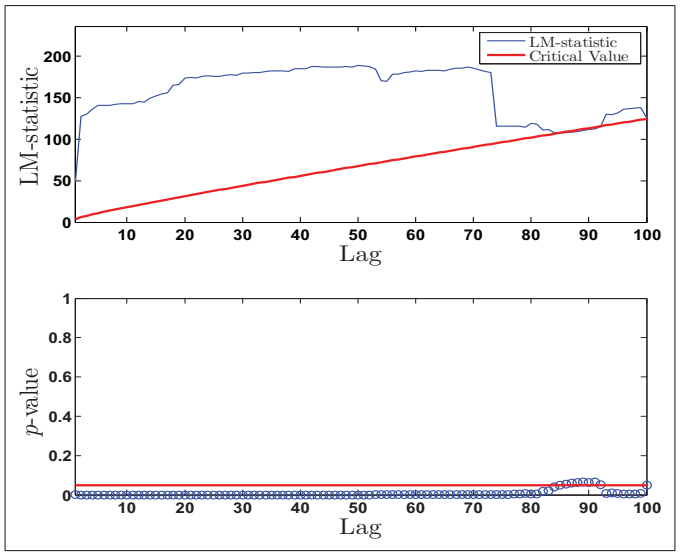

Figure 4.9 Results of Engle test for residual heteroskadasticity of the ARMA(7,2)

4.5.3 Analysis of the residuals of the improved models

Since the residuals of fitted ARMA(p,q) models contain conditional heteroskedasticities, the models can be refined by adding a non-constant variance in the disturbance term ε_t. It is

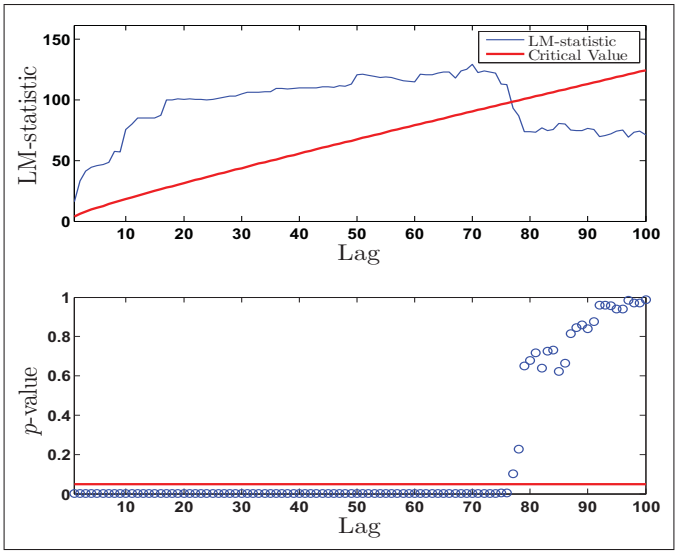

Figure 4.10 Results of Engle test for residual heteroskadasticity of the ARMA(4,1)

believed that the variance is a form of the power law decay function. Hence, the EGARCH models proposed by Nelson (1991) might be appropriate. According to the AIC and SBIC, we find that ARMA(7,2)-EGARCH(9,6), denoted by *Model* 1 and ARMA(4,1)-EGARCH(12,8), denoted by *Model* 2, are suitable models for our measurements. We can now analyse the standardized residuals of fitted models.

In Figures 4.11 and 4.12, the distribution of the residuals in each model are less heavy-tailed, not skewed and fit the red curve. In addition, the KS test's p-values are 0.9 and 0.48 for *Model* 1 and *Model* 2 respectively. Under such conditions, the residuals could come from a normal distribution. The ACF and the PACF show that many lags are far below the limits for autocorrelation. As a result, they might be uncorrelated, and we may conclude that the residuals might be white Gaussian noise.

By using the Ljung-Box Q-test for residual and squared residual autocorrelations, the results of the tests are resumed for a few values of K-first correlations in this chapter. As depicted in Tables 4.2 and 4.3, all p-values are above the significance level of 5%. Hence, the Ljung-Box Q-test fails to reject the null hypothesis that proves that the residuals are not autocorrelated at

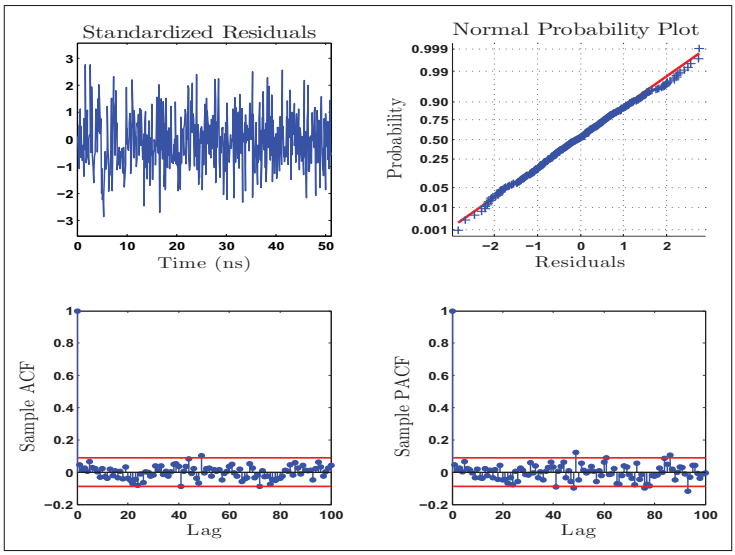

Figure 4.11 Analysis of the residuals of fitted *Model* 1

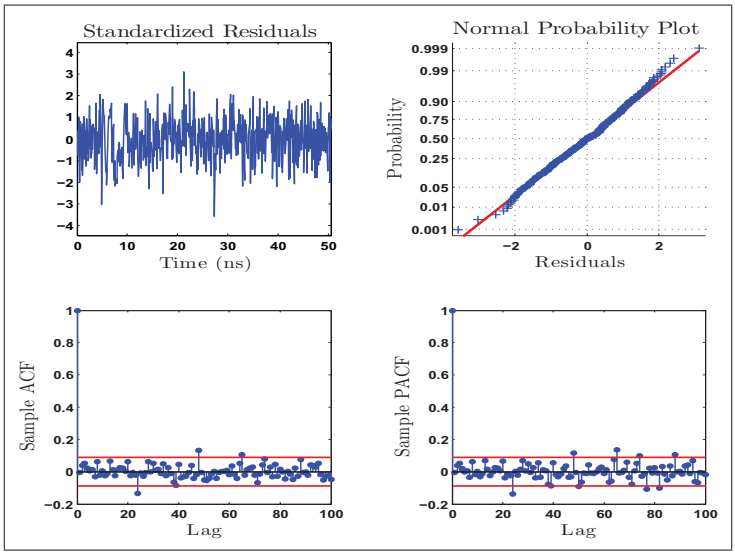

Figure 4.12 Analysis of the residuals of fitted *Model* 2

95% of confidence for different values of K-first autocorrelations. Since we want a generic model, it is reasonable to approximate the residuals from fitted ARMA-EGARCH models as white Gaussian noise.

Table 4.2 Results of Ljung-Box Q-test for residual autocorrelation

p-value of Q statistic	**K = 10**	**K = 25**	**K = 60**	**K = 80**
Model 1	0.83	0.93	0.87	0.82
Model 2	0.96	0.96	0.98	0.98

Table 4.3 Results of Ljung-Box Q-test for squared residual autocorrelation

p-value of Q statistic	**K = 10**	**K = 25**	**K = 60**	**K = 80**
Model 1	0.81	0.52	0.57	0.68
Model 2	0.47	0.24	0.28	0.2

4.5.4 Summary

Impulsive noise with correlated samples can be analysed and modelled using an LTI filters approach. Their relationship with discrete time series can help us to choose a suitable filter, such as the number of parameters, and the input time series is given by ε_t. From this analysis, we can retain that:

- impulsive noise that is obtained by measurements can be fitted by ARMA(p,q) models where all coefficients may lie outside the unit circle. Thus, the stationarity and the invertibility conditions are satisfied;
- the impulsiveness of the data comes from conditional errors. Indeed, the residuals from fitted ARMA models contain ARCH effects as shown with the Ljung-Box Q-test for squared residual autocorrelation and the Engle test for residual heteroskedasticity;
- the ARMA models can be improved by adding ARCH effects such as EGARCH models. Thus, the standardized disturbance term $\varepsilon_t = \varepsilon_t/\sigma_t$ can be approximated by a white Gaussian noise. This suitable approximation can reproduce distortions induced by the multipath propagation effects.

4.6 Simulation and results

4.6.1 Simulation parameters

In order to demonstrate the efficiency of the proposed model, we can simulate the resulting waveforms obtained at the output of the LTI filters. They can be compared to measured impulsive waveforms to determine the goodness-of-fit. The analysis of the obtained results is provided.

By using the ARMA(p,q) models fitted from our measurements, we define a disturbance term $\varepsilon_t = \sigma_t \varepsilon_t$, as defined in Equation (4.16) where ε_t is a white noise with normal distribution $\sim \mathcal{N}(0,1)$ and σ_t is the time-dependent standard deviation. We choose to define the time-dependent function given by:

$$\sigma_t = \frac{\sigma_0}{t\nu\sqrt{2\pi}} \exp\left(-\frac{(\log t - \mu)^2}{2\nu^2}\right) \tag{4.26}$$

where ν and μ are parameters related to the rise and decay time and σ_0 is a normalized scale parameter. These parameters are adjusted to compare measurement and simulation results.

4.6.2 A comparison of measurement vs. simulation results

By using the ARMA(p,q) models fitted from our measurements, and by considering the disturbance term ε_t as a white Gaussian noise whose variance is a time-dependent function, we can plot the results obtained by a simulation. Simulated waveforms and spectral densities can be compared to measured impulsive noise.

We use the ARMA(7,2) model with conditional heteroskedasticity. It is denoted by *Model* 1. In Figure 4.13, the resulting waveform obtained by the model is an impulsive waveform. Its power spectral density, in red curve, accurately fits the PSD of measurements, which are in blue curve. The frequency response of the LTI filter is represented by the black curve. The

PSDs are decaying as a form of $\sim f^{-\gamma}$ where $\gamma > 0$. The effect of the disturbance term induces local variations of the PSD.

For *Model* 2, we use the ARMA(4,1) model, with conditional heteroskedasticity. The obtained waveform and the PSD are depicted in Figure 4.14. The waveform is impulsive and randomly distorted. By comparing the PSDs, the simulation fits the measurement accurately.

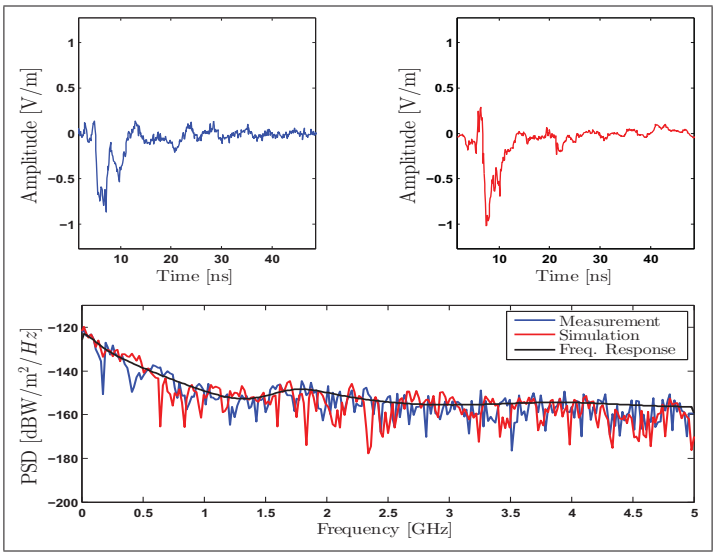

Figure 4.13 Comparison of waveforms : PTT vs. *Model* 1

4.6.3 Analysis of simulated impulsive waveforms

A more detailed analysis of simulated waveforms can be provided by studying their spectrograms and their autocorrelation functions. As depicted in Figures 4.15 and 4.16, the obtained results are quite similar to the measured impulsive noises presented in Figures 4.1 and 4.2. The samples of these impulsive waveforms are correlated. Indeed, slow decays, quite similar to our measurements, are observed in the autocorrelation functions. Hence, there are significant correlations at different values of lags. Moreover, the effect of the disturbance term, modelled as a white noise with conditional variance, can reproduce the impulsiveness of the process. The

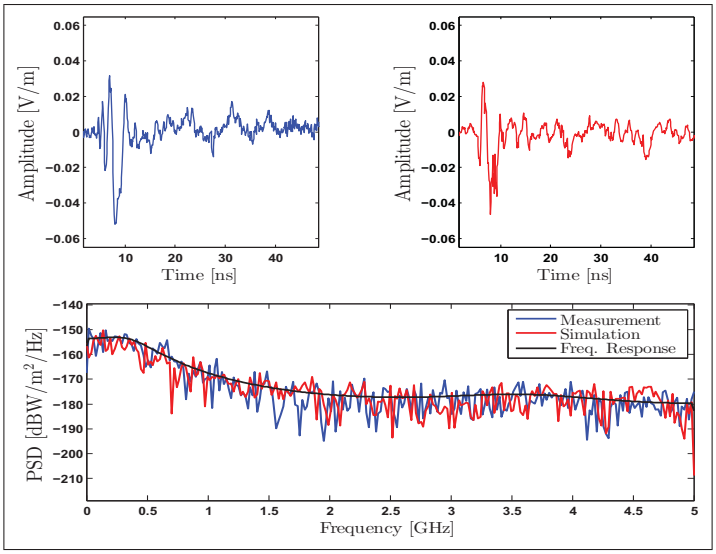

Figure 4.14 Comparison of waveforms : CTT vs. *Model* 2

spectrograms show that the power density of the simulated impulsive waveforms are strong for a short duration with a large frequency bandwidth, and it decreases over time and frequency. Note that the proposed model is based on the modelling of second-order statistics of the measurements. The model can be validated using second-order statistics such as PSD, spectrogram and ACF. This approach is accurate for modelling these impulsive noises.

4.6.4 Advantages and limitations of the proposed model

Compared to partitioned Markov chain based-model, the proposed approach allows for an accurate estimation of the spectral characteristics of PD from data via a simple and straightforward estimation procedure (Dickey and Fuller, 1979; Phillips and Perron, 1988; Box *et al.*, 1994; Akaike, 1973; Schwarz, 1978). In addition, the measure of the goodness-of-fit allows us to assess the adequacy and the accuracy of time series models.

The main issue of such approaches is the selection of the time series model and the number of parameters to be estimated. The complexity of the model increases as the number of parameters increases and overfitting problems can occur (Hurvich and Tsai, 1988). There is a

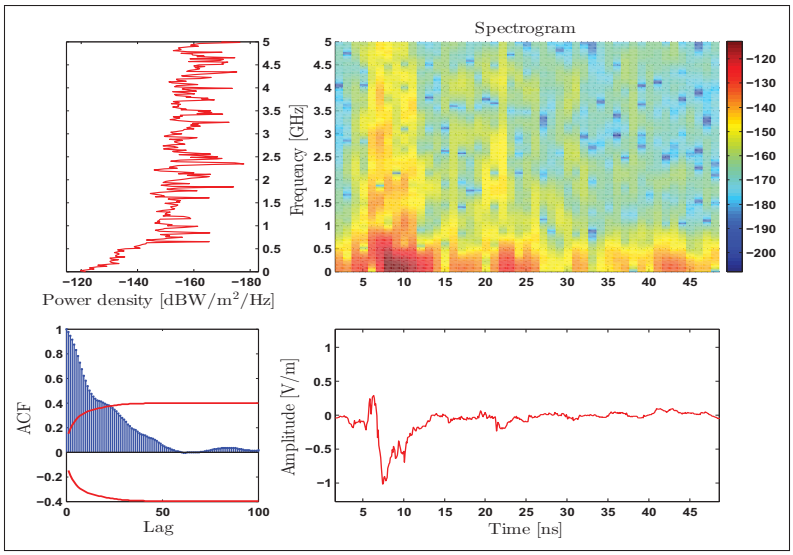

Figure 4.15 Waveform obtained with the *Model* 1

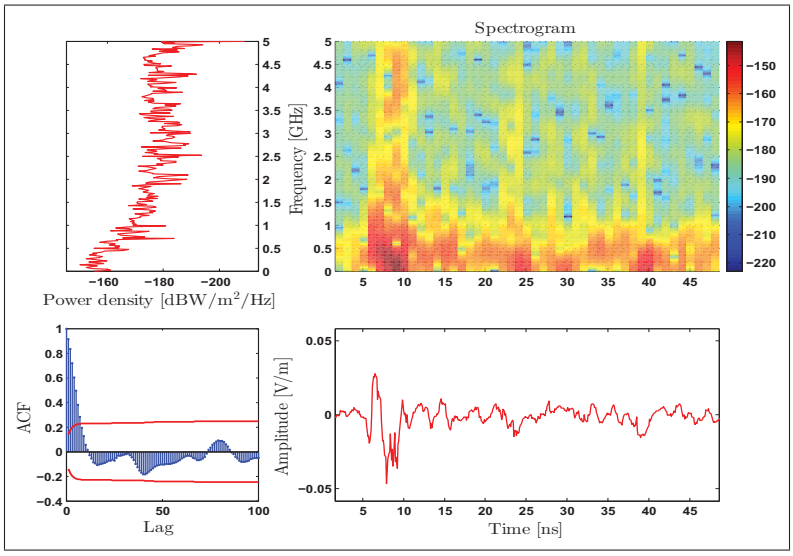

Figure 4.16 Waveform obtained with the *Model* 2

clear trade-off between the accuracy and the complexity of such models. Fortunately, this can be resolved by using the Akaike information criterion (Akaike, 1973, 1974) or the Schwarz bayesian information criterion (Schwarz, 1978).

4.7 Conclusion

In this chapter, we propose a new approach to capturing spectral characteristics of EMIs induced by PD activity, based on second-order statistics EMIs from PD activity. Experimentations and measurement campaigns show that the wideband impulsive noise waveforms emitted by electric arc discharges are transient when samples are correlated. Moreover, their power spectral densities have a form of approximately $\sim f^{-\gamma}$ where $\gamma > 0$ is an arbitrary exponent.

These impulsive noises can be modelled by an LTI filter in which correlated samples are induced by the autoregressive and/or the moving average terms. We can analyse the filter in a time domain by using a time series in which all coefficients, the AR(p) and the MA(q) terms, can be estimated by using the maximum-likelihood function.

From the analysis of the time series fitted from our measurements, all coefficients of the ARMA(p,q) models lie outside the unit circle in which the stationarity condition is ensured. The residuals of fitted ARMA models contain ARCH effects in which the variance could be seen as a time dependent function, *i.e.* not constant over time. As a result, the models can be refined by adding heteroskedasticity in the disturbance term. The standardized residuals from fitted ARMA models with heteroskedasticity can be approximated by a white noise. Consequently, the disturbance terms can be modelled as white noise with a time dependent variance. It allows for the reproduction of distortions induced by the multipath propagation effects. The efficiency of our approach is demonstrated by comparing the waveforms obtained by simulation to those seen in measurements. Their second-order statistics fits our measurements accurately.

In future work, the proposed model can be extended to vector ARMA models with heteroskedasticity in which the vector is a collection of many measured impulsive noise waveforms. The estimation and the analysis follow the same procedure as described in this chapter exactly. Under this condition, the ARMA(p,q) models and the parameters defining the heteroskedasticity can be estimated empirically from any discharge sources generated by any HV equipment in substation environments such as power transformers, overhead power lines, or circuit breakers.

In the next chapter, a statistical analysis of impulsive RF signals from PD activity in a Poisson field of interferers in substations is provided. Based on the work hitherto described, a generic impulsive noise model is proposed by using a Poisson field of interferers. Based on practical assumptions, statistical properties of our proposed model can be derived from which signal processing algorithms can be implemented for a rapid PD identification and localisation in HV equipment. Impulsive noise mitigation techniques can be implemented for wireless communications in substations.

CHAPTER 5

A STATISTICAL ANALYSIS OF IMPULSIVE NOISE IN A POISSON FIELD OF INTERFERERS IN SUBSTATION ENVIRONMENTS

5.1 Introduction

The deployment of recent and advanced wireless communication technologies in substations offers significant improvement in terms of the efficiency, reliability and safety of the electric power grid (Yan *et al.*, 2013; Gungor *et al.*, 2011, 2010; Gungor and Lambert, 2006; Amin and Wollenberg, 2005). Unfortunately, high-voltage (HV) environments are harsh and hostile to such an extent as to render wireless communication performances severely degraded (Shan *et al.*, 2007; Madi *et al.*, 2010, 2011; Ndo *et al.*, 2013). Accordingly, the development of rapid and online methods of detection, identification and/or localization of partial discharge (PD) sources using wireless intelligent electronic devices (WIED) is an area of growing interest (Montanari and Cavallini, 2015; Wu *et al.*, 2015; Ma *et al.*, 2015; Au *et al.*, 2015e). The design of more accurate, rapid and efficient signal processing algorithms can be achieved with tractable and reasonable assumptions underlying the physics of such radio frequency (RF) signals/noise in substations. This chapter deals with statistical characterization and analysis of impulsive noise in situations in which RF impulsive signals are caused by electromagnetic radiations from PD sources.

5.1.1 Prior and related work

The fields of PD measurement, diagnostics, and communications all offer overviews of prior and related work pertaining to EMIs from PD sources.

5.1.1.1 EMIs in substation environments

The noise process typical of substation environments consists of impulsive discharges from PD activity and background noise induced by the overall interferences in substations. The

impulsive component is characterized by a strong amplitude with short durations, which makes such a noise process non-Gaussian (Madi *et al.*, 2010, 2011; Shan *et al.*, 2007). Over a long time observation, the rare events of these discharges produce heavy-tailed behaviour in the probability distribution.

Over the last four decades, several measurement campaigns have been conducted in substations using antennas in order to measure the EM radiations from PD activity (Pakala and Chartier, 1971; Arai *et al.*, 1985; CISPR, 2010; Portugués *et al.*, 2003; Sacuto *et al.*, 2012; Au *et al.*, 2013). Based on measurement results, the radio noise emitted by PDs consists of very short transient impulsive discharges of a duration of 10 to 200 ns, on average. The spectra have a form of $1/f^{\gamma}$, where γ is the exponent characterizing the decay over frequency (Au *et al.*, 2015b,d). The measurement of PD sources by their EM radiations has become increasingly important to researchers because RF measurement systems are non-invasive to HV equipment, they ensure a better signal-to-noise ratio, and their use allows failure location (Tenbohlen *et al.*, 2008; Judd *et al.*, 2005; Portugués *et al.*, 2003).

5.1.1.2 Partial discharge diagnostics

The presence of significant PD sources causes permanent damage to and possible failure of HV equipment (Hudon and Bélec, 2005; Bartnikas, 2002; Kuffel *et al.*, 2000). As a result, researchers have proposed valuable diagnostic tools for the assessment of aging and lifespan of power equipment. Over the last decade, PD diagnostic tools based on PD's EM radiations have been emphasized due to the ease of deployment, cost-effectiveness, speed, and the potential for online remote monitoring of HV equipment (Tenbohlen *et al.*, 2008; Judd *et al.*, 2005; Portugués *et al.*, 2003; Pearson *et al.*, 1991).

Moore *et al.* (2005), Markalous *et al.* (2008), Tang *et al.* (2009) and Sinaga *et al.* (2012) have proposed several methods for identifying and localizing PD sources using ultra-high frequency sensors (UHF) and/or acoustic sensors. Although the effectiveness of their proposed approaches have been shown experimentally, the performance analysis of signal-processing

methods underlying the identification and localisation of sources cannot be compared with various real-life situations, especially in terms of computational complexity. Therefore, it might be useful to provide a generalized and physically-complete model that can be used for performing analyses of such signal processing methods, and designing and optimizing PD diagnostic tool systems.

5.1.1.3 Communication in substation environments

Over the last few years, smart-grid has emerged as the next generation of electric grids. In particular, the design of more robust wireless communication systems in substation environments is a growing interest (Madi *et al.*, 2011; Shan *et al.*, 2007; Ndo *et al.*, 2013; Ali *et al.*, 2015; Ali, 2015). In the literature, researchers have used computer methods to simulate random variables that reproduce EMIs which are typical of substations, based on related work in statistical impulsive-noise modelling (Middleton, 1999; Shao and Nikias, 1993a; Llow and Hatzinakos, 1998). Using the empirical probability distributions (first-order statistics) of experimental data, the estimation procedure is well-established and straightforward (Zabin and Poor, 1989; Tsihrintzis and Nikias, 1995; Weron and Weron, 1995; Middleton, 1999). However, this is not a satisfying condition when impulsive noise exhibits transient behaviour, because second-order statistics are largely ignored.

Samarodnitsky and Taqqu (2000), Nikias and Shao (1995), Madi *et al.* (2011), and Ndo *et al.* (2013) have provided performance communication analyses, and the design of more robust communication systems have been built upon the assumption that such noise processes are independent and identically distributed (*idd*). When EMIs from PD produce transient impulsive waveforms, the *idd* assumption does not hold because impulsive noise samples are correlated (Au *et al.*, 2015b,d; Sacuto *et al.*, 2013). Recently, Ali (2015) has shown that communication systems that are robust against *idd* impulsive noise perform poorly when the receiver is corrupted by transient impulsive noise.

5.1.2 Contribution and organization

This chapter provides a statistical analysis of transient impulsive noise in substation environments. A new and generalized impulsive noise model will be implemented using the Poisson field of interferers, from which first- and second-order statistics can be derived analytically based on the physics of the noise process. The statistical analysis allows for the identification of some interesting statistical properties of moments, cumulants and probability distributions. These can, in turn, be utilized in signal processing algorithms for rapid PD identification, localization, and impulsive noise mitigation techniques in wireless communications in substations.

The chapter is structured as follows: in Section 5.2, a mathematical formulation of multiple PD interference sources is presented, based on tractable and reasonable assumptions regarding the physical process of PD and the propagation of EM waves. By assuming that PD sources are randomly distributed over space-time, the Poisson-field of interferers allows for the generalization of an impulsive noise model in the presence of multiple PD sources in substations. In Section 5.3, probability distributions and first- and higher-order moments of such noice processes are derived by taking advantage of the Poisson field of interferers. In Section 5.4, experimental and simulation results are presented to assess the goodness-of-fit of the proposed filtered Poisson process and existing impulsive noise models used by Shan *et al.* (2007), Shan *et al.* (2011), Bhatti *et al.* (2009) and Madi *et al.* (2011) for substation environments. An estimation procedure is proposed in order to compare first- and second-order statistics. Results show that it is more appropriate to use the filtered Poisson process rather than memoryless impulsive noise models when the impulsive component has transient effects. Section 5.5 is an application of the generalized model, by which a new technique for a rapid and online identification of PD sources is proposed using a blind-source separation technique. An estimation of a number of PD sources can help to evaluate the insulation performance and lifespan of HV equipment.

5.2 A mathematical formulation of multiple PD interference sources

In this section, we define a mathematical formulation of a noise process in the presence of multiple PD interference sources based on tractable and reasonable physical assumptions, thereby establishing a generalized impulsive noise model for substation environments.

5.2.1 Electromagnetic radiations of multiple PD sources

Assuming a given receiver is surrounded by an arbitrary number of HV equipment under normal operation in a spatial region, $\Upsilon \in \mathbb{R}^d$ where d is the dimension of the space. For simplicity, the spatial region is restricted to a sphere in the three-dimensional Euclidean space where the receiver is located at the origin.

5.2.1.1 The emission of the PD impulses

Inside this spatial region Υ, each HV installation generates an arbitrary number of PD sources in which the induced electromagnetic radiations produce transient impulsive waveforms. PD impulses are characterized by a rapid impulse whose durations, rise-time, fall-time and amplitude are linked to the physical characteristics of PD, such as over-voltages, ionization processes, and/or free-electron rates (Bartnikas and Novak, 1993; Brunt, 1991). In such circumstances, it is reasonable to assume that all of the PD sources share a common random mechanism in which the original transient impulses induced by PD sources have the same type of waveform. This is denoted by $aD(\bar{\theta},t)$, where a is a real positive random amplitude, and $\bar{\theta}$ is a set of time-invariant random variables denoting the duration, rise-time, and spectral characteristics.

5.2.1.2 Basic assumptions of spatial and temporal PD events

Inside the spatial region Υ, we assume that the number of HV equipment is countable when their positions are randomly distributed over space. Moreover, each HV installation has an arbitrary and countable number of PD sources where their positions are denoted by $\mathbf{r}_1, \mathbf{r}_2, \cdots$

and $\mathbf{r}_k \in \Upsilon$ is a random variable. As a result, the distance between the k^{th} PD source and the receiver is written as $r_k = \|\mathbf{r}_k\|$, since the receiver is located at the origin of the spatial region.

In Chapters 2 and 3, we described that the emission of a single PD is linked to both the local electric field and the number of free-electrons, which depend on the physical characteristics of PD sites as well as the applied voltage, thermal aging, and electrical insulation of an HV installation. Under such conditions, the amplitude and the time occurrence of the PD can be described as time-dependent random variables. In particular, the time occurrence follows a cyclostationary process due to the AC voltages. However, since the three-phase AC voltage is used in substations, the cyclostationary condition might not hold due to the superposition of all impulses from multiple PD sources. As a result, it is reasonable to assume that an impulse $a_k D(\bar{\theta}_k, t)$ occurs independently at random time $t_1, t_2, \cdots \in \mathbb{R}^+$. In addition, we shall assume that the random amplitude a_k and the random parameter characterizing the impulse $\bar{\theta}_k$ are independent and identically distributed (*iid*) whose statistical distributions are respectively given by $p_a(a)$ and $p_{\bar{\theta}}(\bar{\theta})$. PD sources are also assumed to be independent; in other words, the location $\mathbf{r}_k$, the temporal event of the impulse t_k, the random amplitude a_k and the random parameter $\bar{\theta}_k$ of the k^{th} are independent for all PD sources $k = 1, 2 \cdots$.

The resulting noise process observed by the receiver is a superposition of all transient PD impulses activated in the spatial region Υ. Since the receiver and PD sources are located in distinct positions, a transient impulse will be attenuated and distorted by the propagation channel and the receiver. With reasonable assumptions of the propagation conditions of EM waves, and the spatial and temporal distribution of PD sources, the statistical properties of the received noise process can be derived.

5.2.2 Propagation of EM waves induced by PD sources

Statistical properties of the received noise process can be derived with suitable assumptions of the basic impulsive waveform of interferences sources. Middleton (1974, 1973) has specified a very general waveform when the physical process of source emission is taken into consid-

eration for major classes of noise processes. Unlike his expression, which requires some restrictions on the bandwidth of the receiver, we may simplify the expression by assuming that all of the PD sources inside the spatial region have the same isotropic radiation pattern and the receiver has an omni-directional antenna. This assumption is applicable for both narrowband and wideband noise processes.

5.2.2.1 The noise process observed by the receiver

An emitted PD impulse observed by the receiver is distorted and attenuated by both a propagation channel and the receiver itself. These distortions can be determined by the beam patterns of the PD source and the antenna, source location, and the impulse response of the receiver, including RF and IF stages of linear filters. As conjectured in Chapter 4, a PD transient impulse might be attenuated and distorted by the multipath effects induced by the presence of multiple reflected EM waves of the emitted impulse and the impulse response of the receiver by which the resulting impulsive signal has a transient effect. In such instances, the distortion is produced by the convolution product of an original transient PD impulse $aD(\bar{\theta},t)$ located at $\mathbf{r}$ and the impulse response of the receiver, such that:

$$\begin{aligned} au(\theta,t,\mathbf{r}) &= c(\mathbf{r})aD(\bar{\theta},t) * h(t) \\ &= c(\mathbf{r})au(\theta,t) \end{aligned} \tag{5.1}$$

where $h(t)$ is the impulse response of both the propagation channel and the receiver. $c(\mathbf{r})$ is the attenuation factor function related to the distance between the PD source and the receiver. This can be determined by the beam patterns of sources and the receiver. θ is a set of random variables characterizing the distorted PD impulse observed by the receiver after any RF and IF stages of linear filtering.

In the presence of multiple PD sources, the resulting noise process is given by the superposition of all PD impulses, such that the instantaneous amplitude observed by the receiver is written

as:

$$X = \sum_{k=1}^{N_I} a_k u(\theta_k, t_k, \mathbf{r}_k) \tag{5.2}$$

where N_I is the total number of PD impulses arriving at the receiver within a given time observation. This will be defined from assumptions with respect to the spatial and temporal distribution of the PD sources. Next, the definition and emulation of the attenuated and distorted transient impulse $u(\theta_k, t_k, \mathbf{r}_k)$ are examined in detail.

5.2.2.2 A generic temporal impulsive waveform from PD

According to measurements in substations and laboratories, a generic transient impulsive waveform from PD activity can be simulated the model proposed and developed in Chapter 4 whose spectral characteristics of transient impulses have been gleaned from data. Our proposed time series models are able to reproduce the transient behaviour of PD impulses that are randomly distorted by the impulse response of both the propagation channel and the receiver. Following our proposed model, a generalized PD impulse waveform is modelled numerically with an LTI filter, which is given by:

$$u_t = \sum_{i=1}^{p_u} \phi_i u_{t-i} + \varepsilon_t + \sum_{k=1}^{q_u} \psi_k \varepsilon_{t-k} \tag{5.3}$$

where u_t is the real-valued discrete-time impulse waveform from PD activity, u_{t-i} is the sample at discrete-time $t-i$. ϕ_i and ψ_k for any $i = \{1, \cdots, p_u\}$ and $k = \{1, \cdots, q_u\}$ are spectral characteristics of the impulse whose coefficients lie outside the unit circle. ε_t is the disturbance term which controls the impulsiveness and the duration of the distorted impulsive noise. This is modelled as a heteroskedastic Gaussian noise. In the presence of multiple PD sources, we assume that these parameters are *iid* random variables. These values are summarized in the set θ. The random parameter a and all of the random variables in θ are independent.

5.2.2.3 The attenuation factor

We assume that the antenna and PD sources are positioned to yield far-field conditions; in other words, PD sources must be positioned so that the distance source-receiver is, at least,

greater than the wavelength of the antenna's receiver. As a result, the attenuation factor $c(\mathbf{r})$ in Equation (5.1) is a decreasing function of the distance from the source and the receiver. For simplicity, $c(\mathbf{r})$ is approximated by the inverse of the distance source-receiver with an attenuation coefficient p, such that:

$$c(\mathbf{r}) = \frac{c_0}{r^p} \tag{5.4}$$

where $r = \|\mathbf{r}\|$ is the distance source-receiver and c_0 is a real positive random value induced by multipath effects. These parameters can be obtained by measuring the propagation channels in substations or any other environments where PD sources are observed.

5.2.3 Spatial and temporal distribution of PD sources

The spatial and temporal distributions of PD sources are intrinsically linked to the number of pieces of HV equipment, their aging and the intensity of the electric field within PD sites. Let Ξ be a finite space-time region in which the receiver observes such electromagnetic radiations emitted by PD sources inside the spatial region $\Upsilon(R_1, R_2)$ and within a finite time interval $[0,T]$ where $\Xi = \Upsilon(R_1,R_2) \times [0,T] \subset \Upsilon \times [0,+\infty]$. In such instances, we shall approximate the noise process as follows: we assume that two PD sources cannot be located in the exact same position and that their emissions could not occur at the same exact time. In addition, it is also assumed that the number of PD events in the future is identically distributed over space and, independent of past events. From this approximation, we claim that the spatial and temporal distribution of PD sources follows a space-time Poisson point process (Parzen, 1962; Girault, 1966; Snyder and Miller, 1991). Thus, the total number of impulses arriving at the receiver N_I inside the space-time region Ξ is a random number following a space-time Poisson point process whose the intensity is given by $\lambda(\mathbf{r},t)$ where:

$$\begin{aligned} N_s &= \int_{\Xi} \lambda(t,\mathbf{r}) dt d\mathbf{r} \\ &= \int_0^T \int_{\Upsilon(R_1,R_2)} \lambda(t,\mathbf{r}) dt d\mathbf{r} \end{aligned} \tag{5.5}$$

where N_s is the associated parameter of the Poisson distribution of PD sources inside Ξ, which is the average number of PD sources radiating transient impulses. The probability mass function of N_I is written as:

$$Pr(N_I = k) = \frac{N_s^k}{k!} e^{-N_s} \tag{5.6}$$

for all $k = 0, 1, 2, 3, \cdots$. To yield mathematically tractable results, we assume the homogeneity of the space-time Poisson point process whose intensity $\lambda(t, \mathbf{r}) = \lambda$ is constant. Physically, the intensity λ is proportional to the number of pieces of HV equipment, their aging, the degradation of the electrical insulation systems, and the average intensity of the electric field within PD sites. Under such conditions, if the observation period is short, then the physical characteristics of HV installations does not vary over space and time.

From the homogeneity of the space-time Poisson point process, the average number of PD sources radiating transient impulses from Equation (5.5) is written as:

$$N_s = \lambda S \tag{5.7}$$

where S includes the volume of the spatial region and the time observation. We have restricted the spatial region to a finite sphere in the three-dimensional Euclidean space within a time observation $[0, T]$, $S = \frac{4}{3}\pi R^3 T$ where R is the radius of the finite sphere. Therefore, the parameter λ is the density of PD sources radiating impulses. Note that if the cyclostationary assumption must hold, then the density is a time-dependent function with respect to the periods of AC voltages. For simplicity, we assume that λ is constant.

The Poisson field of interferers allows us to formulate a generalized and physically complete noise model for substation environments, in which the physical characteristics of HV installations are grouped into a few statistical quantities. The proposed impulsive model is a filtered Poisson process whose typical response function $u(\theta, t, \mathbf{r})$ is a transient impulse induced by PD activity in substations. The spectral characteristics, amplitude, and durations can be captured from data (see Chapter 4). Moreover, the number of PD sources and their emissions can be controlled by the density parameter $\lambda(t, \mathbf{r})$ of the spatial and temporal Poisson point process.

5.3 Statistical analysis

In this section, interesting statistical properties of the noise process can be derived based on practical assumptions. Eventually, they could be used to design a more robust receiver in impulsive noise environments, or in the development of new PD identification and detection methods for rapid diagnostics of electrical insulation systems in HV equipment via WIEDs. To do so, it is necessary to derive the first-order statistics of the instantaneous amplitude of the resulting noise.

5.3.1 Probability density function of the instantaneous amplitude

Taking advantage of the Poisson field of interferers, we derive the probability density function (PDF) of the instantaneous amplitude of Equation (5.2) via its characteristic function (*c.f*). Inside the space-time region Ξ, the *c.f* of the overall noise process X is given by:

$$\mathscr{M}_X(j\xi) = \sum_{k=0}^{\infty} \mathbb{E}\left[\exp(j\xi X)\right] P(k) \tag{5.8}$$

where $\mathbb{E}[\cdot]$ denotes the expectation and $P(k)$ is the probability of getting k PD impulses observed by the receiver in Ξ. Since we have assumed a homogeneous Poisson point process whose density parameter is constant λ, the average number of PD sources radiating transient impulses N_s is constant. Since X is filtered by a basic PD impulse waveform $u(\theta,t,\mathbf{r})$ with a real positive random amplitude a whose $\{a_i,\theta_i,t_i,\mathbf{r}_i\}$ is an *iid* random sequence for all $i = 0,1,2,\cdots$, and the positions of PD sources and their occurrences are uniformly distributed on any interval of space and time inside Ξ, the characteristic function is written as:

$$\mathscr{M}_X(j\xi) = \sum_{k=0}^{\infty} \left(\frac{1}{S} \int_{\Xi} \mathbb{E}\left[\exp(j\xi a u(\theta,t,\mathbf{r}))\right] dt d\mathbf{r} \right)^k \frac{N_s^k}{k!} e^{-N_s} \tag{5.9}$$

From the Taylor series expansion of an exponential function, Equation (5.9) is written as:

$$\begin{aligned}\mathscr{M}_X(j\xi) &= \exp\left(\lambda \int_{\Xi} \left(\mathbb{E}\left[\exp(j\xi a u(\theta,t,\mathbf{r}))\right]-1\right) dt d\mathbf{r}\right) \\ &= \exp\left(\lambda \int_{\Xi} \left(\mathscr{Q}_{a,u}(j\xi)-1\right) dt d\mathbf{r}\right)\end{aligned} \tag{5.10}$$

Note that $S = \int_{\Xi} dt d\mathbf{r}$. From Section 5.2, we have assumed that $\{a,\theta\}$ and $\{t,\mathbf{r}\}$ are independent and, therefore, all of these parameters are also independent. The PDFs of the real positive amplitude a and the set of random variables θ are denoted by $p_a(a)$ and $p_\theta(\theta)$ respectively. Using the attenuation factor in Equation (5.4) and since $\{a,\theta\}$ and $\{t,\mathbf{r}\}$ are independent, we write $\mathscr{Q}_{a,u}(j\xi)$ as follows (Rice, 1944, 1945):

$$\mathscr{Q}_{a,u}(j\xi) = \int_{\mathbb{R}^+} p_a(a) \int_{\Theta} p_\theta(\theta) \exp\left(j\xi \frac{c_0}{r^p} a u(\theta,t)\right) d\theta \; da \tag{5.11}$$

Assuming that c_0 is a positive random value with a PDF $p_{c_0}(c_0)$, for which the variable and all mentioned random variables are independent. Thus, $\mathscr{Q}_{a,u}(j\xi)$ can be written as:

$$\mathscr{Q}_{a,u}(j\xi) = \int_{\mathbb{R}^+} p_a(a) \int_{\Theta} p_\theta(\theta) \int_{\mathbb{R}^+} p_{c_0}(c_0) \exp\left(j\xi \frac{c_0}{r^p} a u(\theta,t)\right) dc_0 \; d\theta \; da \tag{5.12}$$

As an approximation, let the space-time region Ξ go to infinity. Now, by taking the logarithm of the characteristic function of X in Equation (5.10), and using the Fubini's theorem, we have (Rice, 1944, 1945):

$$\begin{aligned}\log \mathscr{M}_X(j\xi) &= \lambda \int_{\mathbb{R}^+} p_a(a) \int_{\Theta} p_\theta(\theta) \int_{\mathbb{R}^+} p_{c_0}(c_0) \int_{\Xi} \left[\exp\left(j\xi \frac{c_0}{r^p} a u(\theta,t)\right) - 1\right] d\mathbf{r} \; dt \; da \; d\theta \; dc_0 \\ &= \lambda \int_{\mathbb{R}^+} p_a(a) \int_{\Theta} p_\theta(\theta) \int_{\mathbb{R}^+} p_{c_0}(c_0) \int_0^{\infty} \\ &\quad \cdot \int_{\Upsilon} \left[\exp\left(j\xi \frac{c_0}{r^p} a u(\theta,t)\right) - 1\right] d\mathbf{r} \; dt \; dc_0 \; d\theta \; da\end{aligned} \tag{5.13}$$

where $R_1 \to 0$, R_2 and $T \to \infty$. Since the spatial region is restricted to a sphere with a radius $R \to \infty$, Equation (5.13) is can be written in spherical coordinates as:

$$\begin{aligned}\log \mathscr{M}_X(j\xi) = 4\pi\lambda \int_{\mathbb{R}^+} p_a(a) \int_\Theta p_\theta(\theta) \int_{\mathbb{R}^+} p_{c_0}(c_0) \int_0^\infty \\ \cdot \int_0^\infty \left[\exp\left(j\xi \frac{c_0}{r^p} a u(\theta,t)\right) - 1\right] r^2 dr\, dt\, dc_0\, d\theta\, da\end{aligned} \tag{5.14}$$

replacing g with $c_0 a r^{-p}$, the integration-by-substitution gives the following equation:

$$\begin{aligned}\log \mathscr{M}_X(j\xi) = \frac{4\pi\lambda}{p} \int_{\mathbb{R}^+} a^{3/p} p_a(a) \int_\Theta p_\theta(\theta) \int_{\mathbb{R}^+} c_0^{3/p} p_{c_0}(c_0) \int_0^\infty \\ \cdot \int_0^\infty \left[\exp\left(j\xi g u(\theta,t)\right) - 1\right] g^{-3/p-1} dg\, dt\, dc_0\, d\theta\, da\end{aligned} \tag{5.15}$$

Hence, Equation (5.15) is simplified as:

$$\log \mathscr{M}_X(j\xi) = \frac{4\pi\lambda}{p} \mathbb{E}[a^\alpha]\, \mathbb{E}[c_0^\alpha] \int_\Theta p_\theta(\theta) \int_0^\infty \int_0^\infty \mathscr{F}(\theta,t,g) dg\, dt\, d\theta \tag{5.16}$$

where $\alpha = 3/p$ is the stability index of the noise process and $\mathscr{F}(\theta,t,g)$ is given by:

$$\mathscr{F}(\theta,t,g) = \left[\exp\left(j\xi g u(\theta,t)\right) - 1\right] g^{-\alpha-1} \tag{5.17}$$

Note that Equation (5.16) is valid if and only if $\mathbb{E}[a^\alpha]$ and $\mathbb{E}\left[c_0^\alpha\right]$ are finite and the integrand $\mathscr{F}(\theta,t,g)$ is absolutely integrable. Using Euler's formula, the integral over space is given by:

$$\begin{aligned}\int_0^\infty \mathscr{F}(\theta,t,g) dg &= \int_0^\infty (\cos(bg) - 1) g^{-\alpha-1} dg + j \int_0^\infty \sin(bg) g^{-\alpha-1} dg \\ &= \int_0^\infty -2\sin^2(bg/2) g^{-\alpha-1} dg + j \int_0^\infty \sin(bg) g^{-\alpha-1} dg\end{aligned} \tag{5.18}$$

where $b = \xi u(\theta,t)$. In such instances, the integral on the left-hand side is absolutely integrable if $0 < \alpha < 2$, and the right-hand side is absolutely integrable if $0 < \alpha < 1$ (Gradshteyn and Ryzhik, 2007). In this case, the integral is absolutely integrable if the attenuation coefficient is $p > 3$ since $\alpha = 3/p$. If we assume that the noise process X has a symmetric probability distribution, then the characteristic function is real-valued. As a result, the integral

is absolutely integrable if $p > 3/2$.

$$\int_0^{\infty} \mathscr{F}(\theta,t,g)dg = -\frac{\Gamma(1-\alpha)}{\alpha}|b|^{\alpha}\left(\cos\left(\frac{\pi}{2}\alpha\right) - j\,\mathrm{sign}(b)\sin\left(\frac{\pi}{2}\alpha\right)\right) \tag{5.19}$$

where $\Gamma(\cdot)$ is the gamma function, such that:

$$\Gamma(x) = \int_{\mathbb{R}^+} t^{x-1}e^{-t}dt \tag{5.20}$$

Finally, the logarithm of the characteristic function of X in Equation (5.16) is given by:

$$\log \mathscr{M}_X(j\xi) = -\sigma|\xi|^{\alpha}\left(1 - j\beta\,\mathrm{sign}(\xi)\tan(\pi\alpha/2)\right) \tag{5.21}$$

where

$$\sigma = \frac{4\pi\lambda\Gamma(1-\alpha)\cos(\pi\alpha/2)}{p\alpha}\mathbb{E}\left[a^{\alpha}\right]\mathbb{E}\left[c_0^{\alpha}\right]\int_{\Theta} p_{\theta}(\theta)\int_0^{\infty}|u(\theta,t)|^{\alpha}dt\,d\theta \tag{5.22a}$$

$$\beta = \mathrm{sign}(u(\theta,t)) \tag{5.22b}$$

where $\sigma > 0$ and $\beta \in [-1,1]$. The characteristic function of X has the form of the *c.f* of the α-stable, if $\mathbb{E}[a^{\alpha}]$, $\mathbb{E}\left[c_0^{\alpha}\right]$ and $\int_0^{\infty}|u(\theta,t)|^{\alpha}dt$ are finite. Therefore, the PDF of the instantaneous amplitude of X can be approximated as an α-stable distribution. Note that if X has a symmetric distribution, then the logarithm of the *c.f* in Equation (5.21) is simply:

$$\log \mathscr{M}_X(j\xi) = -\sigma|\xi|^{\alpha} \tag{5.23}$$

By using the Poisson field of interferers in which PD sources radiate transient impulsive waveforms in a realistic scenario, we have demonstrated that the PDF of X can be approximated as an α-stable distribution, under certain conditions. This is characterized by a heavy-tailed behaviour induced by the stability index $0 < \alpha < 2$ and a possible skewness (*i.e.* the probability distribution is asymmetric) induced by β. However, in practice, the noise process consists

of impulsive noise and an additive background noise, including thermal noise, in the receiver. Hence, the resulting noise process is given by:

$$X = \sum_{k=1}^{N_I} a_k u(\theta_k, t_k, \mathbf{r}_k) + n(t) \tag{5.24}$$

where $n(t)$ is background noise, which is a spatially isotropic noise process. Assuming that the central limit theorem holds for the background noise (*i.e.* non-impulsive noise), we consider this to be a Gaussian noise. Under this condition, the logarithm of the *c.f* of the overall noise process is written as:

$$\log \mathscr{M}_X(j\xi) = -\sigma|\xi|^\alpha (1 - j\beta \,\mathrm{sign}(\xi) \tan(\pi\alpha/2)) - \sigma_n^2 \xi^2 \tag{5.25}$$

where σ_n^2 is the variance of the background noise. Note that the impulsive noise process and the background noise are independent. As a result, the PDF of X is given by:

$$f_X(x) = \frac{1}{2\pi} \int_{\mathbb{R}} \mathscr{M}_X(j\xi) e^{-j\xi x} d\xi \tag{5.26}$$

The $f_X(x)$ of the noise process might be difficult to derive in closed-form because α-stable cannot be written analytically except when $\alpha = 2, 1$, and $1/2$, which are Gaussian, Cauchy and Levy distributions respectively. When the background noise is negligible $\sigma_n^2 \ll \sigma$, the PDF might be approximated by an α-stable distribution, but the PDF might be approximated by a Gaussian distribution when $\sigma_n^2 \gg \sigma$. Assuming that the PDF of the noise process is α-stable, the statistical analysis of the amplitude probability distribution, as well as its tails and moments, is well-established. Extensive research covering the characterization and implementation of α-stable noise processes has been provided in the literature (Chambers *et al.*, 1976; Koutrouvelis, 1981; Samarodnitsky and Taqqu, 2000; Weron and Weron, 1995; Lévy, 1925). This analysis is summarized in the following paragraphs. We will show that the high-order moments of the α-stable distributions are not finite. In particular, the second-order moment is infinite. Unless fractional lower-order moments are used, it is inappropriate to use an infinite variance in signal processing problems (Shao and Nikias, 1993b). Fortunately, since the noise process is based

on the Poisson field of interferers, Campbell's theorem allows for the derivation of high-order moments of the noise process, which are finite under certain conditions.

5.3.2 Amplitude probability distribution

The probability distribution is the cumulative distribution function (CDF) of the instantaneous amplitude of the noise. This is characterized by the PDF of the noise, such that:

$$F_X(x) = P(X \leq x) = \int_{-\infty}^{x} f_X(\xi) d\xi \tag{5.27}$$

However, since we have demonstrated that the PDF is an α-stable distribution, a closed-form is not available when $0 < \alpha < 2$ and particularly when $\alpha \neq 0.5, 1$ and 2. Nevertheless, the CDF is determined by α and β namely; if $\beta = 0$, then the CDF is symmetric around $x = 0$. When $\beta > 0$, the CDF is right-skewed, *i.e.* the right-tail of the distribution is heavier than the left-tail and $P(X > x) > P(X < -x)$. On the other hand, the CDF is left-skewed, which means that the left-tail of the distribution is heavier than the right-tail and $P(X > x) < P(X < -x)$ when $\beta < 0$. If α decreases, then the tail probabilities increase.

5.3.3 Tails and moments

The tail distribution is the complementary cumulative distribution function (CCDF) of the noise process. This is defined as:

$$\bar{F}_X(x) = P(X > x) = 1 - F_X(x) \tag{5.28}$$

Samarodnitsky and Taqqu (2000) have shown that tail behaviour is determined by α and β. When $0 < \alpha < 2$ and $-1 < \beta \leq 1$, then as $x \to \infty$ the tail approximation is given by:

$$P(X > x) \sim \sigma^{\alpha} \sin(\pi\alpha/2) \frac{\Gamma(\alpha)}{\pi} (1 + \beta) x^{-\alpha} \tag{5.29}$$

However, when $0 < \alpha < 2$ and $-1 \leq \beta < 1$, then as $x \to \infty$ the lower tail approximation is given by:

$$P(X < -x) \sim \sigma^{\alpha} \sin(\pi\alpha/2) \frac{\Gamma(\alpha)}{\pi} (1-\beta) x^{-\alpha} \tag{5.30}$$

For any value of $\alpha < 2$ and $-1 < \beta < 1$, the PDF and the CCDF are asymptotically power laws. However, when $\beta = -1$ or 1, the tails of the distributions are not asymptotically power laws.

5.3.3.1 Moments of α-stable distributions

The moments of the probability distribution is given by:

$$\begin{aligned} \mu_k &= \mathbb{E}\left[X^k\right] \\ &= \int_{\mathbb{R}} x^k f_X(x) dx \end{aligned} \tag{5.31}$$

where μ_m is the k^{th} moment of the probability distribution. Note that if the moments are finite $\forall k < \infty$, then the mean, the variance and the kurtosis can be measured. Unfortunately, Shao and Nikias (1993b) and Samarodnitsky and Taqqu (2000) have indicated that all moments do not exist (*i.e.* μ_k is not finite) when the distribution is α-stable. In particular if $0 < \alpha < 2$, then:

$$\mathbb{E}\left[X^k\right] = \begin{cases} \infty, & \text{if } k \geq \alpha. \\ \mu_k < \infty, & \text{if } 0 < k < \alpha. \end{cases} \tag{5.32}$$

In other words, for $0 < \alpha \leq 1$, first- or higher-order moments are not finite; for $1 < \alpha < 2$, the first and all of the k^{th} moments are finite when $k < \alpha$. In particular, α-stable distributions have infinite variance (*i.e.* $\mu_2 - \mu_1^2 = \infty$). Under such conditions, higher-order moments such as the second-order and/or the fourth-order moment cannot be exploited in practice. Shao and Nikias (1993b) have derived fractional lower-order moments (*i.e.* $\mu_k < \infty$ when $0 < k < \alpha$) for prac-

tical engineering applications. Unfortunately, the authors have stated that these lower-order moments are much harder to work with than second- and higher-order moments because they introduce non-linearity to even linear problems.

5.3.3.2 Moments of shot-noise processes

Fortunately, since the proposed model is based on the Poisson field of interferers and the noise process X is a shot-noise process filtered by a basic transient impulsive waveform, Campbell's theorem allows for the derivation of first- or higher-order moments (Rice, 1944). Assuming that the impulsive noise process and the background noise are independent, statistical moments are written as:

$$\mathbb{E}\left[X^k\right] = \lambda \mathbb{E}\left[(au(\theta,t,\mathbf{r}))^k\right] + \mathbb{E}\left[n^k(t)\right] \tag{5.33}$$

Using our proposed basic waveform $au(\theta,t,\mathbf{r})$ and assuming that $\{a_i,\theta_i,t_i,\mathbf{r}_i\}$ is an *iid* random sequence for all $i = 0,1,2,\cdots$, we write the statistical moments as:

$$\begin{aligned}\mathbb{E}\left[X^k\right] &= \lambda \mathbb{E}\left[a^k\right]\mathbb{E}\left[u^k(\theta,t,\mathbf{r})\right] + \mathbb{E}\left[n^k(t)\right] \\ &= \lambda \mathbb{E}\left[a^k\right]\mathbb{E}\left[c_0^k\right]\int_0^T \mathbb{E}\left[u^k(\theta,t)\right]\int_{\Upsilon(R_1,R_2)} r^{-pk}d\mathbf{r}\,dt + \mathbb{E}\left[n^k(t)\right]\end{aligned} \tag{5.34}$$

The noise process X has finite first- or higher-order moments if and only if $\mathbb{E}\left[a^k\right]$, $\mathbb{E}\left[c_0^k\right]$ and $\mathbb{E}\left[n^k(t)\right]$ have finite moments and the integrands $\mathbb{E}\left[u^k(\theta,t)\right]$ and r^{-pk} are integrable over time and space respectively. In particular, by examining the integral over space in spherical coordinates, we have:

$$\int_{\Upsilon} r^{-pk}d\mathbf{r} = 4\pi\int_{R_1}^{R_2} r^{-(p-2)k}dr \tag{5.35}$$

Therefore, the noise process X has no finite first- or higher-order moments if and only if $R_1 = 0$ and $p-2 \geq 1/k$ or if $R_2 = \infty$ and $p-2 \leq 1/k$ (Lowen and Teich, 1990). In practice, the receiver does not detect PD sources when $R_2 = \infty$ and since we have assumed that the receiver

is located at the origin of the sphere, there are no PD sources located at this position. Note that R_1 needs to be much greater than the wavelength of the antenna, thereby establishing far-field conditions, which renders the attenuation factor in Equation (5.4) valid. If far-field conditions hold, then the integrand r^{-pk} is integrable over space $\forall k < \infty$. Moreover, since the waveform $u(\theta,t)$ observed by the receiver is a transient impulse with a finite energy and duration, then the integrand $\mathbb{E}\left[u^k(\theta,t)\right]$ is integrable over time $\forall k < \infty$.

5.3.4 A summary of important findings

We have proposed a generalized, complete, and physically-coherent radio-noise model for substation environments with respect to the induced EMIs created by the presence of multiple PD sources in HV equipment. Based on practical assumptions, we have assumed that PD sources are distributed according to a space-time Poisson point process (the Poisson field of interferers). Accordingly, the basic transient impulsive waveform, $au(\theta,t,\mathbf{r})$, which is generated by these sources, has been specified according to the far-field wave propagation and physical characteristics of impulses such as amplitude, durations, and spectra.

This proposed model is a filtered Poisson point process, in which the number of PD sources per unit volume or unit area, as well as the number of emissions per unit time per source, can be set by a single density parameter λ. Although the cyclostationary process has been neglected in this work, one could add a time-dependent function into the parameter λ to conduct such processes. The relative intensity of the impulses can be derived using the far-field wave propagation and the intensity of radiations.

Taking advantage of the Poisson field of interferers, the PDF of the instantaneous amplitude of the resulting noise X has been derived from the characteristic function $\mathscr{M}_X(j\xi)$. Under practical and realistic assumptions, we have demonstrated that the PDF can be approximated by an α-stable distribution. However, all moments of these distributions do not exist. In particular, the noise power level (second-order moment) and the degree of impulsiveness (fourth-order moment) are not finite. As a result, signal processing methods based on these statistical mo-

ments cannot be used for detection, estimation or identification. Fortunately, the Campbell's theorem allows for the derivation of first- or higher-order moments in closed-form. These moments are finite if and only if first- and higher-order moments of the basic transient impulsive waveform and its random parameters are finite. In particular, by examining the integral obtained in the spatial domain, we have found that first- and higher-order moments do not exist when PD sources are located closed to the antenna position. Theoretically, such conditions do not hold, because the attenuation factor used in Equation (5.4) is valid, if and only if the far-field conditions are established.

The noise generation of our proposed model is physically coherent compared to other statistical models using first-order statistics. This is because the spectra, occurrences and durations of the impulsive component, as well as background noise, are taken into account. Moreover, the first-order statistics, such as probability distributions and moments, can be linked to the physical process of the noise, which can, in turn, be utilized for performing communications analyses and designing and optimizing communication systems in substations.

5.4 Experimental and simulation results

In this section, a simple procedure for estimation is presented in order to reproduce such noise processes in substations. Then, the estimated parameters will be used, by which the effectiveness of the proposed approach will be shown by comparing measurement and simulation results in terms of first- and second-order statistics. In addition, since α-stable and Middleton Class A impulsive noise models are commonly utilized in substations environments, they will be used for comparison (Shan *et al.*, 2007, 2011; Bhatti *et al.*, 2009; Madi *et al.*, 2011).

5.4.1 Measurements in substations

Using the measurement setup that has been employed in Chapters 2, 3 and 4, the antenna is surrounded by HV equipment, by which multiple PD sources can be detected. By setting a time observation of $T = 5\ \mu$s, many impulses from PD activity are captured via an oscilloscope.

400 temporal waveforms have been recorded in the frequency range of 800 MHz to 5 GHz. PD sources are characterized by any RF gain in the measurement setup by removing the antenna factor. We have used a frequency mixer with a local oscillator of $f_0 = 800$ MHz in order to yield a baseband representation of RF signals. The EM radiations are measured in terms of electric strength (V/m).

Since the antenna is positioned in a specific position within a substation and we do not have any information on the location of PD sources, the noise process X is written as a temporal function, such that:

$$X = \sum_{k=1}^{N_I} a_k u(\theta_k, t_k) + n(t) \tag{5.36}$$

where N_I is the number of observed impulses and a_k is a random amplitude including the attenuation induced by wave propagation and the amplitude generated by a PD source. $n(t)$ is the background noise.

5.4.2 A procedure for estimation

Based on the proposed characterization process in Chapter 2, a simple estimation procedure of the noise process can be proposed, in which the estimated parameters can be utilized in our proposed generalized impulsive noise model. The estimation procedure can be presented as follows:

- assuming $n(t)$ is a Gaussian noise, record waveforms when PD impulses have not occurred. Then, estimate the level of the background noise, such that:

$$\hat{\sigma}_n^2 = \mathrm{Var}[n(t)] \tag{5.37}$$

  where $\mathrm{Var}[\cdot]$ is the estimated variance;

- in the presence of PD impulses, count the number of impulses that have occurred. Hence, the parameter density λ can be estimated by the average number of impulses occurring

over time observation:

$$\hat{\lambda} = \frac{\bar{N}_I}{T} \tag{5.38}$$

where $\hat{\lambda}$ is the estimated density parameter and $\bar{N}_s$ is the average number of impulses.

- detect each impulse and estimate the spectral characteristics via our proposed time series models with heteroskedasticity. Note that the duration of an impulse can be estimated using ARCH or EGARCH models. Next, check the goodness-of-fit of these models via the estimation procedure detailed in Chapter 4;

- the amplitude a can be provided by measuring the variance of each PD impulse, such that:

$$\begin{aligned} \hat{a}_k^2 &= \mathrm{Var}\left[a_k u(\theta_k, t_k)\right] \\ &= \mathrm{Var}\left[a_k\right] \int_0^{T_u} |u^2(\theta_k, t_k)| dt \end{aligned} \tag{5.39}$$

where $\hat{a}_k^2$ is the estimated square of the amplitude and T_u is the duration of an impulse. Therefore, $\hat{a}_k$ is obtained via the square-root of $\hat{a}_k^2$. Next, plot the histogram of $\hat{a}_k$ or $\hat{a}_k^2$ and estimate the probability density.

In the measurement campaign, the estimated background noise level is $\hat{\sigma}_n^2 = -65.35$ dBW/m^2, the average number of PD emissions is $\bar{N}_s = 2.46$ (*i.e.* the density is $\hat{\lambda} = 4.92 \times 10^{-5}$ s^{-1}), and the power density of PD impulses $\hat{a}_k^2$ follows an exponential distribution whose average power density is $\bar{a}_k^2 = -51.96$ dBW/m^2.

5.4.3 Measurement-simulation comparison

Measurement and simulation results are presented for comparison. The goodness-of-fit is measured to assess the effectiveness of the approach.

5.4.3.1 First-order statistics

Using our proposed generalized model, the estimated parameters have been utilized in order to reproduce the impulsive noise process in substations. The adequacy of the model is discussed via fist-order statistics from simulation and measurement results. α-stable and Middleton Class A distributions are also provided. The empirical probability distributions (PDFs, CDFs, and CCDFs) are presented to assess the goodness-of-fit of these models.

In Figure 5.1, a typical waveform is obtained by simulation using a second-order of autoregressive time series model with heteroskedasticity. The LTI filter reproduces the spectrum of an impulse. Distortions and the duration are generated by the disturbance term. Using the estimated parameters, the noise process X via the proposed impulsive noise model is depicted in Figure 5.2.

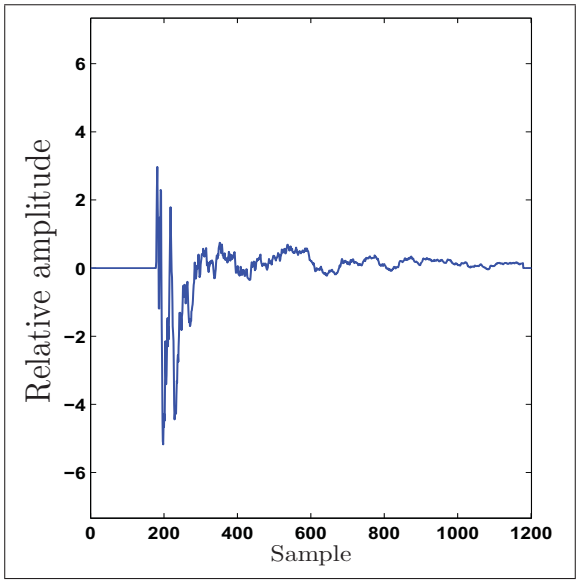

Figure 5.1 Impulsive waveform obtained by simulation

As a comparison, 400 waveforms have been simulated to yield the overall empirical PDFs, CDFs, and CCDFs. In addition, parameters of α-stable and Middleton Class A have been esti-

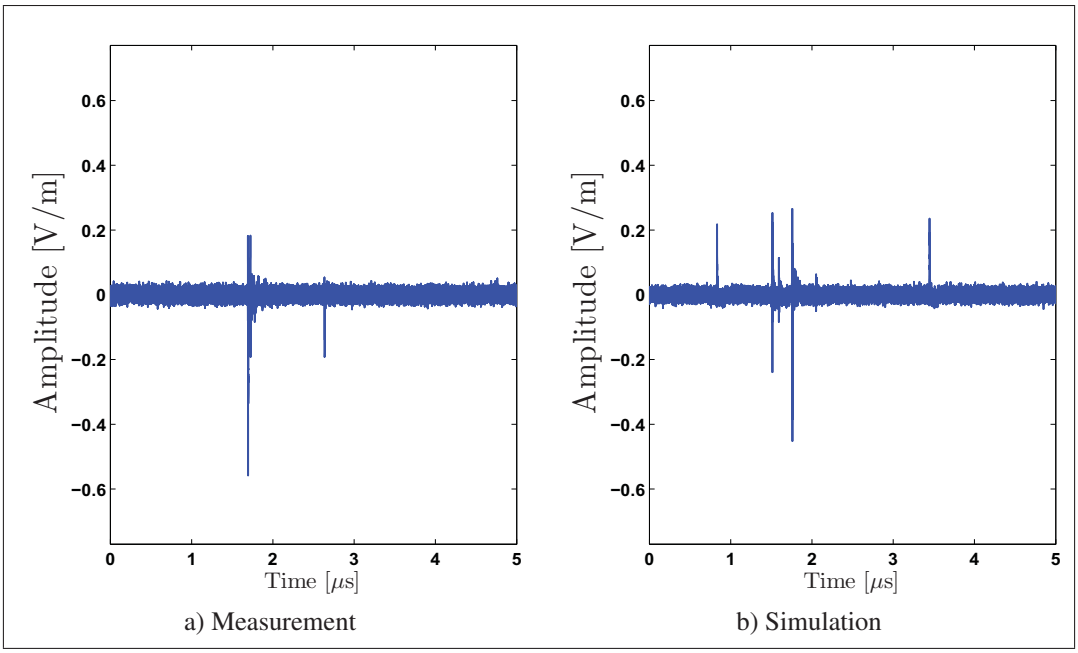

Figure 5.2 Physical shot-noise process X

mated using statistical methods as developed by Middleton (1979), Zabin and Poor (1991), McCulloch (1986), and Tsihrintzis and Nikias (1996). Then, probability distributions are plotted and the goodness-of-fit of the impulsive noise model are measured using the Kullback-Leibler (KL) divergence, and the Kolmogorov-Smirnov (KS) test.

The empirical PDFs and CCDFs of measurements and impulsive noise models are depicted in Figure 5.3. In the presence of impulsive noise, the PDF's behaviours are heavy-tailed, and the probability of having a strong amplitude ($X > |0.05|$ V/m) represents to the impulsive component. The probability densities are symmetric (*i.e.* $f_X(x) = f_X(-x)$), and the tail can be described approximately as a power-law, such that $\bar{F}_X(x) \sim |x|^{-\nu}$ as $x > 0.05$ V/m, where ν is an exponent characterizing the decay. An accurate impulsive noise model can be defined by its ability to reproduce the decay in the probability distribution. By comparing PDFs, however, these impulsive noise models can reproduce the heavy-tailed behaviour; our generalized impulsive noise model is therefore more accurate compared to the α-stable and the Middleton Class A distribution. Indeed, the proposed model has the smallest value in terms of KL-divergence (see Table 5.1). The KS-test value in our model has again the smallest value; the p-values

are 0.622, 0.5181, and 2.0×10^{-4} for the proposed model, α-stable, and Middleton Class A respectively. As a result, the KS-test rejects the null hypothesis that measurement results and Middleton Class A noise model come from the same distribution at a 95% confidence interval. The test does not reject the null hypothesis for the other impulsive noise models. In addition, by comparing CCDFs, the tail of our proposed model is closer than other impulsive noise models.

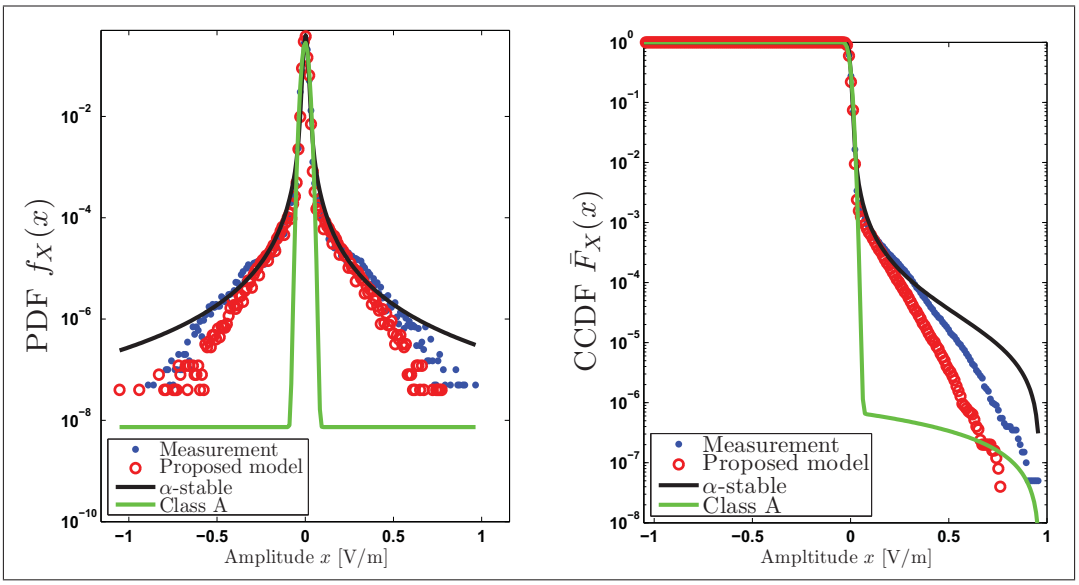

Figure 5.3 Probability distributions of the noise process

Table 5.1 The Goodness-of-fit: Measurement vs. impulsive noise models

Test Statistics	**Proposed model**	**α-stable**	**Middleton Class A**
D_{KL}	0.0140	0.0437	0.0756
D_{KS}	0.0306	0.0547	0.1294

5.4.3.2 Second-order statistics

Although α-stable and Middleton Class A noise models might be adequate for noise processes in substations, computer methods for reproducing noise samples are limited because the resulting random process X is independent and identically distributed so that the impulsive component is modelled as a single-noise sample. As the noise process X is a collection of independent random variables, the resulting autocorrelation function $R_X(\tau)$ is defined as:

$$R_X(\tau) = \mathbb{E}\left[X^2\right]\delta(\tau) \tag{5.40}$$

where $\delta(\tau)$ is the Dirac impulse function. Under such a condition, the power spectral density (PSD) of such noise processes is constant over all frequencies. In particular, an α-stable noise process does not have a PSD because $R_X(0) = \mathbb{E}\left[X^2\right]$, and we have shown that its second-order moment does not exist. In practice, impulsive noise components are characterized by transient effects whose spectra have a form of $\sim (f - f_0)^{-\gamma}$. From Equation (5.36), Campbell's theorem allows us to define the autocorrelation function and the power spectral density of the noise process X, such that:

$$\begin{aligned} R_X(\tau) &= \lambda R_u(\tau) + R_n(\tau) \\ &= \lambda \mathbb{E}\left[a^2\right] \mathbb{E}\left[u(\theta,t)u(\theta,t+\tau)\right] + \mathbb{E}\left[n(t)n(t+\tau)\right] \end{aligned} \tag{5.41}$$

where τ is a temporal lag. If $R_u(\tau)$ exists for all value of τ, then the PSD of X is defined by the Fourier transform of $R_X(\tau)$ (Carson, 1931):

$$\begin{aligned} S_{xx}(f) &= \int_{\mathbb{R}} R_X(\tau) e^{-j2\pi f\tau} d\tau \\ &= \lambda \mathbb{E}\left[a^2\right] \int_{\mathbb{R}} (R_u(\tau) + R_n(\tau)) e^{-j2\pi f\tau} d\tau \\ &= \lambda \mathbb{E}\left[a^2\right] S_{uu}(f) + S_{nn}(f) \end{aligned} \tag{5.42}$$

where $S_{uu}(f)$ and $S_{nn}(f)$ are PSDs of the transient PD impulse and background noise respectively. Since $S_{uu}(f)$ has a form of $\sim (f-f_0)^{-\gamma}$, the PSD $S_{xx}(f)$ has a form of:

$$S_{xx}(f) \sim (f-f_0)^{-\gamma} + S_{nn}(f) \tag{5.43}$$

The behaviour of such PSDs can be emulated via LTI filters. By using the periodogram, the average PSD of the noise process has been estimated, as depicted in Figure 5.4. The measured noise process contains transient PD impulses and background noise. Since we have used a frequency mixer with a local oscillator at f_0, the average PSD has a form of $\sim f^{-\gamma}$. On average, the background noise consists of thermal noise, RF communications and harmonics caused by interleaving artefacts and clock feedthrough from the oscilloscope. The average PSD of the emulated noise process matches experimentation. A more accurate noise model can be achieved by modelling RF communications and harmonics from the oscilloscope. This case is beyond the scope of this work. The PSD of impulses has been extracted from the ambient noise using a denoising process, as depicted in Figure 5.4.(b). Again, by comparing the average PSDs, simulation results match experimentation.

Using filtered Poisson processes may be appropriate when impulsive noise has a spectrum of $\sim f^{-\gamma}$ rather than using memoryless impulsive noise models that generate *idd* random noise. Based on our proposed estimation methods, the effectiveness of our approach has been shown for substation environments when impulses are generated by PD sources. Practical applications can be implemented based on advanced signal processing methods for detecting, estimating, and identifying any desired RF signals from RF communications and/or PD sources.

5.5 A rapid identification of PD sources using blind source separation

In this section[1], we proposed a practical application for a rapid identification of PD sources by using blind-source separation and calculating the fourth-order moment. Spatial second-

[1] This work is based on the published journal paper "A Fast Identification of Partial Discharge Sources Using Blind Source Separation and Kurtosis" in Electronic Letters IET. 2015

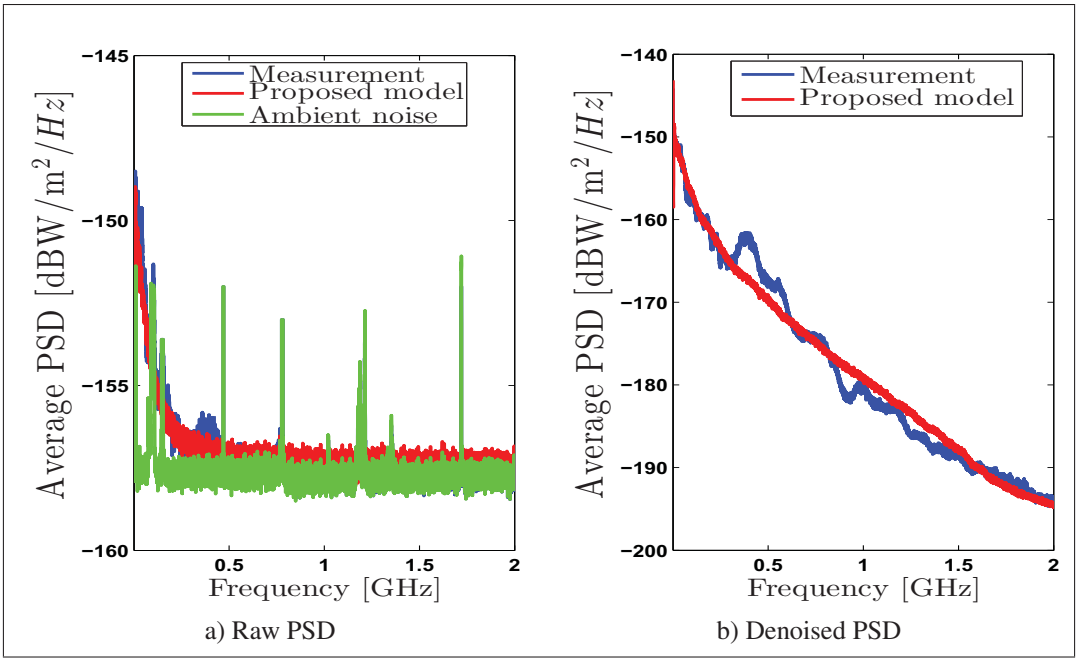

Figure 5.4 Second-order statistics: average PSD

and higher order statistics have been exploited through multiple antennas (array of antennas) combined by a measure of the degree of impulsiveness at each antenna to estimate the number of PD sources in HV equipment.

5.5.1 Motivation and contribution

Recent advances in wireless sensor networks in substations can provide significant improvements for protection, control, automation and monitoring. One example of remote monitoring applications is a rapid insulation diagnosis in power equipment using WIEDs. PD activities can cause irreversible damage and possible failure of electrical insulation systems. Insulation performances and lifespan can be evaluated by measuring the number of PD sources in power equipment. Electromagnetic radiations can be detected by wireless devices for remote monitoring applications. The resulting signal is highly impulsive when the spectrum can cover very large frequency bands (above few GHz) (Au *et al.*, 2013, 2015b).

A technique for a rapid identification of PD sources is proposed. This can be implemented in a low cost WIED for remote monitoring applications. By using multiple antennas, PD sources can be separated based on BSS techniques via generalized eigenvalue decomposition presented in Parra and Sajda (2003). Furthermore, the presence of significant impulsive events produces heavy-tailed distribution when the excess kurtosis is greater than zero. Therefore, the number of PD sources can be estimated by measuring the excess kurtosis of the demixed signals at each antenna. To demonstrate the efficiency and the performance of the proposed method, we use a generic and realistic impulsive noise model developed in Au *et al.* (2015c), where impulsive waveforms are generated by autoregressive (AR) models and their parameters can be estimated from various measurement campaigns in substations. Discharge sources are modelled as a spatial PPP. One can control physical parameters such as the density of PD sources and the average intensity of impulsive component over background noise.

5.5.2 System model

We consider N unknown PD sources written as a $N \times 1$ vector $\mathbf{u}$ of a collection of impulsive waveforms as:

$$\mathbf{u} = [u_1(t)u_2(t)\cdots u_N(t)]^T \tag{5.44}$$

where $u_i(t)$ are complex-valued signals emitted by the i^{th} PD sources. The receiver has M dimensional observations $\mathbf{x}$ into a $M \times N$ complex-valued mixing channel $\mathbf{H}$, such that:

$$\mathbf{x} = \mathbf{H}\mathbf{u} \tag{5.45}$$

$$\mathbf{y} = \mathbf{x} + \mathbf{n} \tag{5.46}$$

where $\mathbf{n}$ is an additive background noise generated by thermal noise and ambient noise in a substation. Note that no precise knowledge is available regarding either the mixing channel or the sources. To recover discharge sources from observation, we need to find $\mathbf{G}$, an inverse matrix, such that:

$$\hat{\mathbf{u}} = \mathbf{G}^*\mathbf{y} \tag{5.47}$$

where $\mathbf{G}^*\mathbf{H} = \mathbf{I}$ and $\mathbf{G}^*$ is the conjugate transpose of $\mathbf{G}$. The number of PD sources can be estimated from the demixed signals by measuring the excess kurtosis given by the fourth moment about the mean minus three:

$$\kappa_i = \frac{\mathbb{E}\left[(\hat{u}_i(t) - \mu_i)^4\right]}{(\mathbb{E}\left[(\hat{u}_i(t) - \mu_i)^2\right])^2} - 3 \tag{5.48}$$

where μ_i is the mean of the i^{th} demixed signals. In the presence of significant impulsive signals, the instantaneous amplitude distribution is heavy-tailed where $\kappa_i > 0$. Thus, the estimated number of PD sources $\hat{N}$ is given by summing κ_i greater than a given threshold $T_h > 0$ to be defined later:

$$\hat{N} = \sum_i (\kappa_i > T_h) \tag{5.49}$$

An overview of the system model is depicted in Figure 5.5, where the receiver estimates the number of PD sources in power equipment for remote monitoring applications.

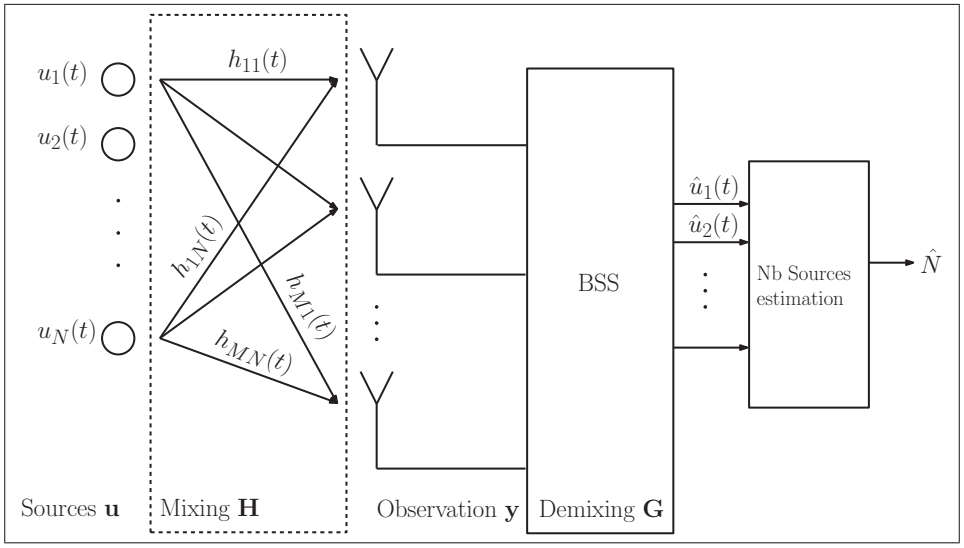

Figure 5.5 Overview of the system model

5.5.3 Blind source separation via generalized eigenvalue decomposition

Partial discharge phenomena are stochastic processes where the pulse height, event and spectrum depend on various physical parameters such as electric field intensity, free electron rate, and ageing mechanism (Brunt, 1991). Hence, in the presence of multiple PD sources, it is reasonable to consider that sources are independent, or at least decorrelated. Moreover, according to the physical characteristics of radiated radio frequency (RF) signals from PD activity measured by Au *et al.* (2013), and Au *et al.* (2015b), one can assume that PD are non-Gaussian. During measurement campaigns in substations, these impulsive signals have transient behaviour with damped oscillation. Therefore, sources may be non-white and/or non-stationary processes.

According to Parra and Sajda (2003), two conditions are sufficient for source separation via generalized eigenvalue decomposition: *i*) if sources are independent or decorrelated, the covariance matrix $\mathbf{R_y}$ can be written as:

$$\begin{aligned} \mathbf{R_y} &= \mathbb{E}\left[\mathbf{y}\mathbf{y}^*\right] \\ &= \mathbf{R_x} + \mathbf{R_n} \\ &= \mathbf{H}\mathbf{R_u}\mathbf{H}^* + \mathbf{R_n} \end{aligned} \tag{5.50}$$

where $\mathbf{R_u}$ and $\mathbf{R_n}$ are diagonal. Therefore, $\mathbf{R_x}$ is also diagonal. Assuming the background noise is modelled as a circular complex Gaussian noise, $\mathbf{R_n} = \sigma^2\mathbf{I}$. *ii*) if PD sources are non-Gaussian, non-stationary, or non-white, there exists $\mathbf{Q_u}$ which has the same diagonalization property such that:

$$\mathbf{Q_x} = \mathbf{H}\mathbf{Q_u}\mathbf{H}^* \tag{5.51}$$

From equations (5.46) and (5.51), we write:

$$\mathbf{Q_y} = \mathbf{Q_x} + \mathbf{Q_n} \tag{5.52}$$

where $\mathbf{Q_n}$ is also diagonalizable. From these two conditions, generalized eigenvalue decomposition can be used for source separation (Parra and Sajda, 2003). Indeed, in Equation (5.50) and Equation (5.52), by multiplying them by $\mathbf{G}$ and Equation (5.52) by $\Lambda = \mathbf{R_x}\mathbf{Q_x}^{-1} + \mathbf{R_n}\mathbf{Q_n}^{-1}$, we have:

$$\mathbf{R_y}\mathbf{G} = \mathbf{Q_y}\mathbf{G}\Lambda \tag{5.53}$$

From statistical assumptions, $\mathbf{Q}$ can have various forms. By assuming that sources are:

- non-stationary and decorrelated (Parra and Spence, 2000); we have:

$$\mathbf{Q}_{\mathbf{y},1} = \mathbf{R_y} = \mathbb{E}[\mathbf{y}\mathbf{y}^*] \tag{5.54}$$

- non-white and decorrelated (Weinstein *et al.*, 1993); we have:

$$\mathbf{Q}_{\mathbf{y},2} = \mathbf{R_y}(\tau) = \mathbb{E}[\mathbf{y}(t)\mathbf{y}^*(t+\tau)] \tag{5.55}$$

  where τ is a time delay. In this work, we consider that $\tau = 1$ sample.

- non-Gaussian and independent (Cardoso and Souloumiac, 1993); we have :

$$\mathbf{Q}_{\mathbf{y},3} = \mathbb{E}[\mathbf{y}^*\mathbf{y}\mathbf{y}\mathbf{y}^*] - \mathbf{R_y}\mathrm{Tr}(\mathbf{R_y}) - \mathbb{E}\left[\mathbf{y}\mathbf{y}^T\right]\mathbb{E}[\bar{\mathbf{y}}\mathbf{y}^*] - \mathbf{R_y}\mathbf{R_y} \tag{5.56}$$

  where $\bar{\mathbf{y}}$ is the conjugate of $\mathbf{y}$ and $\mathrm{Tr}(\mathbf{R_y})$ is the trace of $\mathbf{R_y}$.

The inverse matrix $\mathbf{G}$ is given by the generalized eigenvalue of the matrices $\mathbf{R_y}$ and $\mathbf{Q_y}$.

5.5.4 Simulation and results

Performance of the proposed technique is provided using a Monte Carlo simulation, in which PD sources are simulated based on spatial PPP and the number of sources is a random variable unknown to the receiver. The average number of sources per unit volume or surface is given by

λ_s. Over a long observation time, sources emit impulsive discharges when their events follow a temporal PPP. The average number of emissions per unit time per sources is given by λ_e.

Transient impulsive signals from discharge activity are simulated by using autoregressive (AR) models, such that a single discrete-time impulse u_t is written as:

$$u_t = \sum_{i=1}^{p_u} \phi_i u_{t-i} + \varepsilon_t \tag{5.57}$$

where coefficients $\{\phi_i\}$ are parameters of the model which can be obtained from measurements in various substations. ε_t is a Gaussian noise process in which the variance is unconditional (*i.e.* non-constant over time) in order to take into account the impulse duration (Au *et al.*, 2015b,c). The pulse height is an exponential random variable for which the average intensity of impulsive component over background noise is given by $\Gamma = \sigma_u^2/\sigma_n^2$.

In this work, the receiver operates at an average rate of $\lambda_s = 4$ PD sources per unit volume or surface. For an observation time of 5×10^4 samples, the average number of emissions is $\lambda_s = 5$ discharges per unit time per source. We use the second order of the AR model where $p_u = 2$ in Equation (5.57). Parameters are obtained from measurements in various substations.

For BSS, we use these three forms of $\mathbf{Q}_\mathbf{y}$ to recover PD sources. Their potential to estimate the correct number of sources is compared via their probability of error P_e (the estimated number of PD sources is not correct). To limit the probability of a false alarm, the estimated number of sources $\hat{N}$ is determined when the threshold $T_h = 1$ according to Equation (5.49). Under this condition, the excess kurtosis is zero because the background noise is modelled as a Gaussian noise. Hence, the probability of a false alarm is $P_{\text{fa}} = 0$. The mixing channel $\mathbf{H}$ is a $M \times N$ symmetric circular complex Gaussian noise. The probability of error P_e, is obtained from a Monte Carlo simulation of 15000 simulations.

The performance of the receiver is plotted in Figure 5.6 where the probability of error P_e is given for different values of Γ and different forms of $\mathbf{Q}_\mathbf{y}$. The number of PD sources is a random variable which is not known and not available to the receiver. The number of observations is

$M = 20$, and thus always greater than the number of sources ($M > N$). By applying $\mathbf{Q}_{\mathbf{y},2}$ and $\mathbf{Q}_{\mathbf{y},3}$ for BSS, the probability of error P_e decreases when the average intensity of the impulsive component is higher than the background noise. However, P_e is high and nearly constant when $\mathbf{Q}_{\mathbf{y},1}$ is applied. As a result, the number of PD sources can be determined with low probability of error if we assume that the sources are non-white and decorrelated, or non-Gaussian and independent. For high values of Γ, where discharges are more significant, the receiver can estimate the exact number of PD sources when $\mathbf{Q}_{\mathbf{y},2}$ is applied.

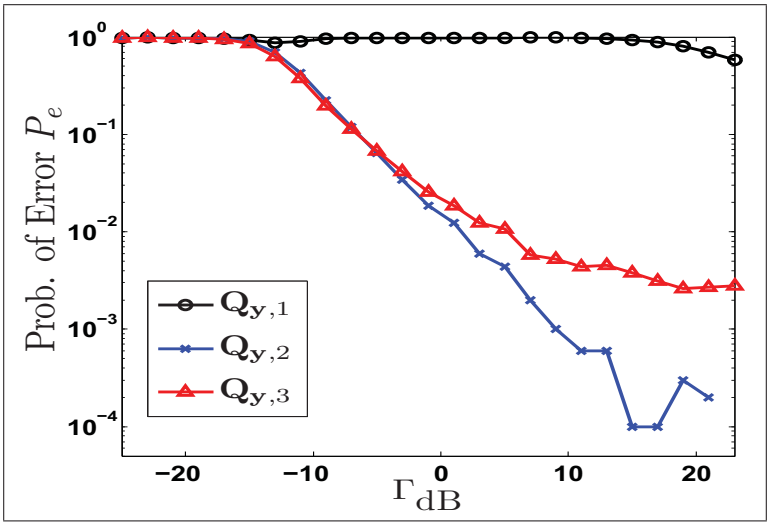

Figure 5.6 Probability of error vs. Γ_{dB}. Based on PPP model: Avg. PD source density $\lambda_s = 4$ sources per unit volume or surface, avg. emission density $\lambda_e = 5$ discharges per unit time per sources, NB. obs. $M = 20 > N$

Figure 5.7 shows the performance of the receiver for a given number of observations where only $\mathbf{Q}_{\mathbf{y},2}$ is applied. The probability of error P_e is high when the number of observations is lower than the number of PD sources ($M < N$). The system is said to be underdetermined because BSS cannot recover more than M sources. Nevertheless, there are at least M PD sources. When the number of observations is greater than the number of PD sources ($M > N$), the system is said to be overdetermined and the probability of error P_e decreases drastically

because BSS can recover the exact number of PD sources. However, a very large number of observations does not provide a better performance.

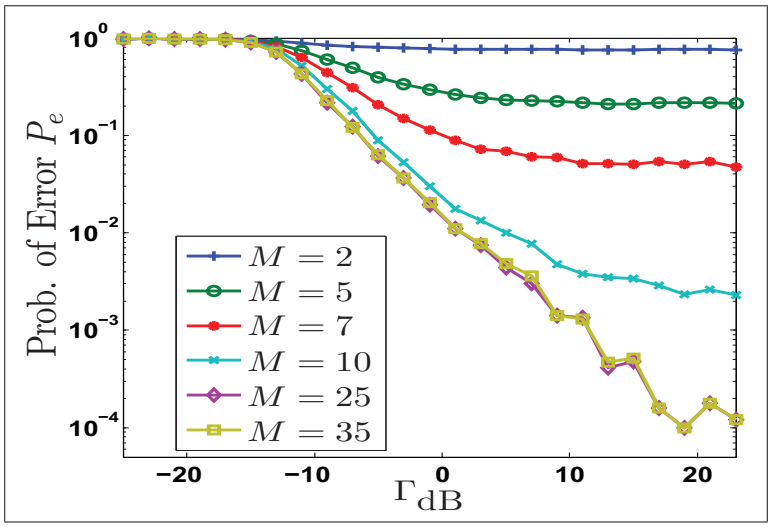

Figure 5.7 Probability of error vs. Γ_{dB} with various Nb. obs. M. Based on PPP model: Avg. PD source density $\lambda_s = 4$ sources per unit volume or surface, avg. emission density $\lambda_e = 5$ discharges per unit time per sources

A rapid identification of PD sources is proposed by which the number of sources can be estimated in power equipments for remote monitoring applications using a low cost WIED. The technique is based on BSS via a generalized eigenvalue decomposition and the number of sources can be estimated by measuring the excess kurtosis. If we assume that the sources are non-white and decorrelated, or non-Gaussian and independent, the exact number of PD sources can be identified with a low probability of error, especially when discharges are significant. Performances can be affected by an underdetermined problem in BSS.

5.6 Conclusion

When EMIs from PD activity generate transient RF signals, it is not reasonable to reproduce such impulsive noise processes in substations via memoryless impulsive noise models because

the resulting noise processes are *idd*, which implies that the PSD is constant over all frequencies. However, experimentation shows that, on average, the PSD of RF signals from PDs decays over frequency.

In this chapter, we have proposed a novel generalized impulsive noise model for substations. We have used a filtered Poisson process so that first- and second-order statistics can be derived based on practical and reasonable assumptions. The radio-noise process has been mathematically formulated based on the physics of PDs and the induced wave propagation. Taking advantage of the Poisson field of interferers model, some interesting statistical properties of moments, cumulants and probability distributions have been identified. These properties can be used for characterizing interference phenomena, performing communications analyses, and designing and optimizing communication systems or electronic intelligent devices for PD diagnostics in HV equipment.

The efficiency of our approach has been shown by comparing first- and second-order statistics of measurement and simulation results. The transient RF signals induced by PD sources are emulated by the time series models developed by Au *et al.* (2015d) with first-order statistics of PDs obtained from data via a simple estimation procedure.

A practical application has been presented using our generalized impulsive noise model. We have developed a method for rapid identification of PD sources in HV equipment. It has been found that the number of PD sources can be estimated in arbitrary HV equipment via blind source separation using a generalized eigenvalue decomposition and the fourth-moment of the noise process.

Future work may focus on the comparison of impulsive noise models recently proposed by Sacuto *et al.* (2013) using partitioned Markov chain models and/or any other existing impulsive noise models whose second-order statistics are taken into account as developed by Zimmermann and Dostert (2002), Gilbert (1960), and Elliot (1963). The proposed rapid identification of PD sources can be tested experimentally in a laboratory with a definite number of PD sources. We believe that signal processing algorithms using the fourth-order moment as pro-

posed by Moulines and Cardoso (1995) can be implemented for PD localization together with our proposed PD identification methods.

CONCLUSION

As mentioned in many publications, the deployment of recent and advanced communications technology in substation environments is an area of growing interest (Yan *et al.*, 2013; Gungor *et al.*, 2011, 2010; Gungor and Lambert, 2006; Amin and Wollenberg, 2005). This research has contributed to investigating the reliability of wireless sensor networks in substations by analysing, characterizing and modelling EMIs caused by PD sources. This allows for the design of more rapid and on-line PD diagnostic tools when EM radiations are generated by PD sources in HV equipment, as well as the deployment of more robust wireless communication systems against man-made noise in the environment typical of substations. We have successfully characterized EMIs induced by PD sources, and formalized a radio-noise model that links the discharge process to the induced far-field wave propagation. To our knowledge, we have first proposed a complete and coherent approach that the links physical characteristics of high-voltage installations to the induced radio-interference spectrum. The last chapter reviews the main highlights of the research, possible extensions, and the possible impact on research in the field of both PD diagnostic in HV equipment and communication in the presence of impulsive noise.

Measurement and characterization of EMIs from PD

Chapter 2 consists of the characterization of EMIs induced by PDs in substations. Using an RF measurement setup with a wideband antenna, we have captured signals from PD. A characterization procedure has been proposed for which first- and second-order statistics of PDs have been measured and characterized experimentally via advanced signal-processing tools. Our approach allows for the evaluation of the electromagnetic compatibility of PD interference sources with any electronic communication devices in the range of 800 MHz to 5 GHz. This work has been published in *Progress in Electromagnetics Research Symposiums* (Au *et al.*, 2013).

It has been found that such spectral interferences can cover the frequency range of 800 MHz to 2 GHz on average. The RF signals from PD activity are characterized by very short rise

times so that the spectra can reach 3 GHz. Thus, PDs are a major source of interferences for conventional wireless communications in ISM bands, in particular for the IEEE 802.15.4 standard which uses 915 MHz, 868 MHz and 2.4 GHz bands in the Americas, Europe and worldwide. Experimentations have demonstrated that IEEE 802.15.4 standard performs poorly in the presence of PDs and even worst when IEEE 802.11 standards are used in the 2.4 GHz bands (Sacuto *et al.*, 2012; Madi *et al.*, 2011; Bhatti *et al.*, 2009, 2012; Shan *et al.*, 2008b). As a result, substation environments can pose challenges to the reliability of wireless sensor networks due to PD phenomena.

One possible solution is to provide an accurate and efficient wireless network plan by positioning sensors in strategic locations to avoid EM radiations from PD activity. Our RF measurement setup can be used to assess the RF interference in substations. The level of the amplitude, number of impulses, and duration might be excellent criteria for assessing electromagnetic interference. Another possible solution is to use some communication systems that operate at higher frequency. For example, IEEE 802.11a/n/ac use 5 GHz bands, and in Canada, IEEE 802.16 standards use 3.5 or 5.8 GHz bands. To our knowledge, there is no research that investigates the impact of PD on the performance of such wireless communications. Our RF measurement setup can be extended for higher frequency bands by using an RF amplifier and a bandpass filter that operates over a large frequency range (*i.e*. 2 to 10 GHz).

At the same time, the frequency range of 800 MHz to 2 GHz can be used for PD measurement, detection, identification and localization, thereby allowing the development of rapid on-line remote monitoring and diagnostic tools in HV equipment. PD phenomena are a category of stochastic processes whose characteristics can be described as time-dependent random variables. With AC voltages, the PD process is especially cyclostationary as the PD occurs at every half-cycle of the applied voltage.

A physical model of EMIs from PD activity in substations

Chapters 3, 4, and 5 have contributed to modelling EMIs from PD activity for the deployment of wireless communication systems in substations. They have also contributed to the development of rapid and on-line PD diagnostic tools in HV equipment.

The literature has investigated impulsive radio-noise modelling for wireless communications in substations. Most of the time, researchers use statistical impulsive noise models that are mathematically tractable and well-established. One of the major drawbacks of such models is that the noise samples are generated from random variables that are *idd*. Therefore, the PSD is constant over all frequencies. Several experimentations reveal that impulses are transient so that spectra have a form of $1/f^{\gamma}$. As a result, it is not appropriate to use these statistical impulsive noise models because they do not consider the physics underlying the radio-noise in substations. Recently, Ali (2015) has shown that communication systems that are robust against *idd* impulsive noise perform poorly when the receiver is corrupted by transient impulsive noise.

Physical models of PDs have been investigated in the literature as in (Niemeyer, 1995; Gutfleisch and Niemeyer, 1995; Fruth and Niemeyer, 1992; Levesque *et al.*, 2013). Unfortunately, they have not been adapted because the electromagnetic radiation of PD is not taken into account.

Physical model of EMI induced by a PD source: In Chapter 3, we proposed a coherent, detailed, and validated EMI model that links the discharge process to the induced far-field wave propagation. Assuming a PD source to be an electric dipole, the induced currents and charges have been linked to a magnetic potential vector source and an electric scalar potential source in which potentials can be expressed by solving Lorenz gauge condition equations in the far-field region. This allows for the derivation of derive the electromagnetic radiation of PD while keeping the cyclostationary process induced by AC voltages.

Using our proposed characterization process, we have successfully fulfilled validated the effectiveness of our approach. This work has been published in *IEEE Transaction in Electro-*

magnetic Compatibility (Au *et al.*, 2015b). The major concern raised by the reviewers of this journal paper pertained to the methodology that was employed to model transient impulsive waveforms. We used an LTI filter to reproduce the transient behaviour, and spectral characteristics were then estimated from data. Even though the LTI filter fits in terms of second-order statistics, the approach needs to be refined because distortions induced by multipath effects are not considered.

Modelling transient impulsive noise induced by PDs: In Chapter 4, we generalized the approach by which spectral characteristics of PD and distortions can be estimated from data via a simple procedure. We have shown that time-series models are a natural generalization of LTI filter models, from which the estimation procedure and a measure of the goodness-of-fit are well-established in the literature (Dickey and Fuller, 1979; Phillips and Perron, 1988; Box *et al.*, 1994; Akaike, 1973; Schwarz, 1978). The main issue is the selection of the time series model and the number of parameters to be estimated. There is a clear trade-off between the accuracy and the complexity of such models. Fortunately, this can be resolved by using the Akaike Information Criterion (Akaike, 1973, 1974) or the Schwarz Bayesian Information Criterion (Schwarz, 1978).

The goodness-of-fit has been measured by an analysis of the residuals from the fitted filters. We have shown that the effect of distortion can be modelled as a time-dependent Gaussian noise (*i.e.* heteroskedasticities in the residuals). These effects can be estimated via time series models with conditional heteroskedasticity such as ARCH, GARCH, or EGARCH. The analysis of the goodness-of-fit and a comparison between measurement and simulation results show the adequacy of the approach. This work has been submitted to *IEEE Transaction on Electromagnetic Compatibility* (Au *et al.*, 2015d).

A generalized radio-noise model for substations: Chapter 5 focuses on extending the radio-noise model to contexts in which there are many PD sources that are randomly distributed in space. The Poisson field of interferers has been used because it allows for the identification of some interesting statistical properties of moments, cumulants and probability distributions that

are linked by the physics of RF noise in substations. These can, in turn, be utilized in signal processing algorithms for rapid PD identification, localization, and impulsive noise mitigation techniques in wireless communications in substations.

Based on tractable and reasonable assumptions regarding the physical process of PD and the propagation of EM waves in the far-field region, first- and second-order statistics have been derived analytically by taking advantage of the Poisson field of interferers. We have demonstrated that the probability distribution of the noise process can be approximated by an α-stable distribution. However, the main drawback of such an approximation is that first- and higher-order moments do not exist. In particular, the variance is infinite, which is not physically relevant because the power of an impulsive signal is finite. Under such conditions, Shao and Nikias (1993b) have suggested using fractional lower-order moments for practical engineering applications. However, the authors have stated that these lower-order moments are much harder to work with than second- or higher-order moments because they introduce non-linearity to even linear problems. Fortunately, Campbell's theorem allows for the derivation of first- or higher-order moments in closed-form. These moments are finite if and only if first- and higher-order moments of the basic transient impulsive waveform and its random parameters are finite.

The effectiveness of the proposed model has been shown by comparing first- and second-order statistics of measurement and simulation results. The simulation parameters have been estimated from data using a simple estimation procedure.

On the practical use of the proposed EMI model

The main research objective has been fulfilled in terms of characterizing EMIs induced by PD sources and formalizing radio-noise model that links the discharge process to the induced far-field wave propagation. We anticipate that, several practical applications can be implemented for performance analyses, and the design and optimization of both PD diagnostic tools and wireless communication systems.

PD diagnostic tools in HV equipment: A new rapid identification of PD sources in HV equipment has been presented. This work has been published in *Electronic Letters IET* (Au *et al.*, 2015e). Through an array of antennas, second-order statistics (the spatial covariance matrix) have been exploited in order to estimate the number of PD sources in arbitrary HV equipment. The generalized eigenvalue decomposition allows for the separation of PD sources. The latter can be counted by measuring the kurtosis (*i.e*. fourth-order of moment) at each antenna.

A performance analysis has been provided when the number of PD sources is not known by the receiver. It has been shown that the performance can be affected when the number of antennas is lower than the PD sources. The algorithm might be improved by estimating the number of strong PD sources in HV equipment. This can be done by measuring the kurtosis because a high value of the kurtosis suggests that the impulsive component is greater than the level of the background noise.

The literature has largely investigated PD localization problems in assessing insulation condition in aged HV equipment. Several publications show that this is an area of intensive research (Sinaga *et al.*, 2012; Tenbohlen *et al.*, 2008; Moore *et al.*, 2005; Markalous *et al.*, 2008; Wu *et al.*, 2015; Montanari and Cavallini, 2015; Kawada, 2003). PD localization methods use the time difference of arrival (TDOA) between signals that is captured by an array of sensors or antennas. Although such methods show high accuracy, their effectiveness is based on: first, the assumption that there is a temporal correlation between signals captured by different sensors, which actually depends on the position of sensors (Sinaga *et al.*, 2012); second, that an expensive fast digital oscilloscope is needed to visualize a TDOA (Tang *et al.*, 2006; Tenbohlen *et al.*, 2008); and third, that the arrival time between sensors is determined based on human judgement (Moore *et al.*, 2005; Markalous *et al.*, 2008). We believe that more rapid, cost-effective and automated PD localization algorithms can be developed based on spatial second- or higher-order statistics as summarized by Trees (2004), and Gonen and Mendel (2010). One of the most interesting methods is the use of spatial fourth-order moment, as proposed by Moulines and Cardoso (1995), since background noise can be suppressed regardless of its

coloring (Gonen and Mendel, 2010). Such approaches are only based on spatial statistical assumptions of PD sources regardless of either temporal correlation or arrival time of impulses between sensors. However, they need a suitable temporal synchronization between sensors.

Wireless communication in substation environments: Performing communications analyses and designing and optimizing communication systems in such harsh and hostile environments can be done through our proposed generalized radio-noise model. Recently, we have proposed a novel impulsive noise mitigation technique with multi-antenna systems (Ali *et al.*, 2015). When PD sources are located in a specific region, those transient impulses arrive via the array of antennas with an arbitrary arrival angle. In narrowband, the interference signals received at each antenna differ only by amplitude and phase shifts. Taking a reference signal measured by a given sensor, the phase shift of the strongest impulse is estimated. This allows for impulsive noise mitigation, in which interference signals are cancelled successively. In addition, a new decision rule has been proposed to manage the effects of both background noise and impulsive noise components for decoding the transmitted message.

Simulation results show that the proposed receiver outperforms conventional receivers that are robust against Gaussian noise; this effect is amplified even more when the number of antennas is increased. However, the decision rule for impulsive noise mitigation is based on a heuristic weighting factor. This factor should be increased as the relative intensity of impulsive interferences is high; in other words, the degree of impulsiveness (the fourth-order of moment) is one important feature in the decision rule (Ali *et al.*, 2015).

The generalized radio-noise model can be used to plan and optimize wireless networks in substations via some interesting signal processing methods for impulsive noise mitigation techniques. In addition, new optimal and/or sub-optimal decision rules for decoding messages in harsh and hostile environments can by developed.

BIBLIOGRAPHY

Akaike, H. 1973. "Information Theory and an Extension of the Maximum likelihood Principle". In *Second International Symposium on Information Theory*. p. 267-281.

Akaike, H. 1974. "A New look at the Statistical Model Identification". *IEEE Transaction on Automatic Control*, vol. 19 No. 6, p. 716-723.

Ali, I. B. S. 2015. "Traitement du Bruit Impulsionnel dans des Postes Électriques pour les Systèmes de Communication Sans-Fil". Master's thesis, École de Technologie Supérieure.

Ali, I. B. S., M. Au, B. L. Agba, and F. Gagnon. 2015. "Mitigation of Impulsive Interference in Power Substation with Multi-Antenna Systems". In *IEEE ICUWB*.

Ambike, S. and J. J. L. Hatzinakos. 1994. "Detection for Binary Transmission in a Mixture of Gaussian Noise and Impulsive Noise Modeled as an Alpha-Stable Process". *IEEE Signal Processing Letters*, vol. 1 no 3, p. 55-57.

Amin, S. M. and B. F. Wollenberg. 2005. "Toward a Smart Grid: Power Delivery for the 21st Century". *IEEE Power and Energy Magazine*, vol. 3 no 5, p. 34-41.

Arai, K., W. Janischewskyj, and N. Miguchi. 1985. "Micro-Gap Discharge Phenomena and Television Interference". *IEEE Transactions on Power Apparatus and Systems*, vol. PAS-104 No 1, p. 221-232.

Au, M., F. Gagnon, and B. L. Agba. 2013. "An Experimental Characterization of Substation Impulsive Noise for a RF Channel Model". *Progress In Electromagnetics Research Symposium, PIERS Proceedings*, vol. 1, p. 1371-1376.

Au, M., B. L. Agba, and F. Gagnon. 2015a. "An Analysis of Transient Impulsive Noise in a Poisson Field of Interferers for Wireless Channel in Substation Environments". *IEEE tansactions on Signal Processing*, vol. 1, p. 1-13.

Au, M., B. L. Agba, and F. Gagnon. 2015b. "A Model of Electromagnetic Interferences Induced by Corona Discharges for Wireless Channels in Substation Environments". *IEEE Transactions on Electromagnetic Compatibility*, vol. 57, no 3, p. 522-531.

Au, M., B. L. Agba, and F. Gagnon. 2015c. Analysis of transient impulsive noise in a poisson field of interferers for wireless channel in substation environements. arxiv. <http://arxiv.org/abs/1504.06880>.

Au, M., B. L. Agba, and F. Gagnon. 2015d. "Analysis and Modelling of Wideband RF Impulsive Signals Induced by Partial Discharges Using Second-Order Statistics". *IEEE Transaction on Electromagnetic Compatibility*, vol. 1, p. 1-11.

Au, M., B. L. Agba, and F. Gagnon. 2015e. "A Fast Identification of Partial Discharge Sources Using Blind Source Separation and Kurtosis". *Electronic Letters IET*, vol. 1, n° 1, p. 1-2.

Babnik, T., R. K. Aggarwal, P. J. Moore, and Z. D. Wang. 2003. "Radio Frequency Measurement of Different Discharges". *Power Tech. Conference Proceedings IEEE Bologna*, vol. 3, p. 1-5.

Bartlett, E. J., M. Vaughan, and P. J. Moore. 1999. "Investigations into Electromagnetic Emissions from Power System Arcs". In *Electromagnetic Compatibility. EMC York. International Conference and Exhibition on (Conf. Publ. No 464)*. p. 47-52.

Bartnikas, R. 2002. "Partial Discharges their Mechanism, Detection and Measurement". *IEEE Transactions on Dielectrics and Electrical Insulation*, vol. 9 No 5, p. 763-808.

Bartnikas, R. and E. J. McMahon, 1979. *Engineering Dielectrics volume I Corona Measurement and Interpretation*.

Bartnikas, R. and J. P. Novak. 1993. "On the Character of Different Forms of PD and their Related terminologies". *IEEE Transactions on Electrical Insulation*, vol. 28, p. 956-968.

Bhatti, S. A., Q. Shan, I. A. Glover, R. Atkinson, I. E. Portugues, P. J. Moore, and R. Rutherford. 2009. "Impulsive Noise Modelling and Prediction of its Impact on the Performance of WLAN Receiver". In *17th European Signal Processing Conference*. p. 1680-1684.

Bhatti, S. A., Q. Shan, I. A. Glover, and R. Atkinson. 2012. "Performance Simulation of WLAN and Zigbee in Electricity Substation Impulsive Noise Environments". In *IEEE SmartGridComm Workshop*.

Bollerslev, T. 1986. "Generalized Autoregressive Conditional Heteroscedasticity". *Journal of Econometrics*, vol. 31, p. 307-327.

Box, G. E. P. and D. A. Pierce. 1970. "Distribution of Residual Autocorrelations in Autoregressive-Integrated Moving Average Time Series Models". *Journal of the American Statistical Association*, vol. 65 No 332, p. 1509-1526.

Box, G. E. P., G. M. Jenkins, and G. C. Reinsel, 1994. *Time Series Analysis: Forecasting and Control 3rd Ed.*

Brunt, R. J. V. 1991. "Stochastic Properties of Partial-Discharge Phenomena". *IEEE Transactions on Electrical Insulation*, vol. 26 No 5, p. 902-947.

Brunt, R. J. V. and S. V. Kulkarni. 1990. "Stochastic Properties of Trichel-Pulse Corona: A Non-Markovian Random Point Process". *Physical Review. A, General Physics*, vol. 42 No 8, p. 4908-4932.

Cardoso, J. F. and A. Souloumiac. 1993. "Blind Beamforming for Non-Gaussian Signals". *IEE Proceedings F (Radar and Signal Processing)*, vol. 140 no 6, p. 362-370.

Carson, J. R. 1931. "The Statistical Energy-Frequency Spectrum of Random Disturbances". *Bell Syst. tech. Journal*, vol. 10 No 3, p. 374-381.

Chambers, J. M., C. L. Mallows, and B. W. Stuck. 1976. "A Method for Simulating Stable Random Variables". *Journal of the American Statistical Association*, vol. 71 No 354, p. 340-344.

Chang, J. S., P. A. Lawless, and T. Yamamoto. 1991. "Corona Discharge Processes". *IEEE Transactions on Plasma Science*, vol. 19 No 6, p. 1152-1166.

Chartier, V. L., R. Sheridan, J. N. DiPlacido, and M. O. Loftness. 1986. "Electromagnetic Interference Measurements at 900 MHz on 230 kV and 500 kV Transmission Lines". *IEEE Transactions on Power Delivery*, vol. 1 Issue:2, p. 140-149.

CIGRÉ, 1974. *Perturbations Engendrées Par l'effet de Couronne des Réseaux de Transport : Description des Phénomènes Guide Practique de Calcul*.

CISPR. 2010. *Radio interference characteristics of overhead power lines and high-voltage equipement. part 1 description of phenomena*. Technical report.

David, E. and L. Lamarre. 2006. "Low-Frequency Dielectric Response of Epoxy-Mica Insulated Generator Bars during Multi-Stress Aging". *IEEE Transactions on Dielectrics and Electrical Insulation*, vol. 14 no 1, p. 212-226.

Degardin, V., M. Lienard, A. Zeddam, F. Gauthier., and P. Degauquel. 2002. "Classification and Characterization of Impulsive Noise on Indoor Power-line Used for Data Communications". *IEEE Transactions on Consumer Electronics*, vol. 48 Issue:4, p. 913-918.

Dickey, D. A. and W. A. Fuller. 1979. "Distribution of the Estimators for Autoregressive Time Series with a Unit Root". *Journal of the American Statistical Association*, vol. 74, No. 366, p. 427-431.

Donoho, D. and I. M. Johnstone. 1994. "Ideal Spatial Adaptation by Wavelet Shrinkage". *Biometrika*, vol. 81 No 3, p. 425-455.

Elliot, E. O. 1963. "Estimates of Error Rates for CCode on Burst-Noise Channels". *Bell Syst. Tech. Journal*, vol. 42, p. 1977-1997.

Engle, R. F. 1982. "Autoregressive Conditional Heteroscedasticity with Estimates of the Variance of United Kingdom Inflation". *Journal of Econometrics*, vol. 50 No 4, p. 987-1007.

Farhangi, H. 2010. "The Path of the Smart Grid". *IEEE Power and Energy Magazine*, vol. 8 no 1, p. 18-29.

Fertonani, D. and G. Colavolpe. 2009. "On Reliable Communications over Channels Impaired by Bursty Impulse noise". *IEEE tansactions on Communications*, vol. 57 No 7, p. 2024-2030.

Florkowska, B. and R. Wlodek. 1993. "Pulse Height Analysis of Partial Discharges in Air". *IEEE Transactions on Electrical Insulation*, vol. 28 No 6, p. 932-940.

Fruth, B. and L. Niemeyer. 1992. "The Importance of Statistical Characteristics of Partial Discharge Data". *IEEE Transactions on Electrical Insulation*, vol. 27 No 1, p. 60-69.

Fuller, W. A., 1996. *Introduction to Statistical Time Series. 2nd Ed.*

Gallimberti, I., G. Marchesi, and R. turri. 1985. "Corona Formation and Propagation in Weakly and Strongly Attaching Gases". *Proc. 8th InT. Conf. on Gas Discharges*, vol. 1 No 1, p. 587-594.

Gary, C. 1998. "Effet Couronne sur les Reseaux Electriques Aeriens". *Techniques de l'ingénieur. Génie électrique*, vol. D9, p. D4440.1-D4440.25.

Ghosh, M. 1996. "Analysis of the Effect of Impulse Noise on Multicarrier and Single Carrier QAM Systems". *IEEE Transaction on Communications*, vol. 44 no 2, p. 145-147.

Gilbert, E. N. 1960. "Capacity of Burst-Noise Channels". *Bell Syst. Tech. Journal*, vol. 39, p. 1253-1266.

Girault, M., 1966. *Stochastic Processes*.

Goldsmith, A., 2005. *Wireless Communications*.

Gonen, E. and J. M. Mendel, 2010. *The Digital Signal Processing Handbook: Second Edition Wireless, NetNetwork, Sensor Array PProcessing and Nonlinear Signal Processing*.

Gradshteyn, I. and I. Ryzhik, 2007. *Tables of Integrals, Series and Products: Seventh Edition*.

Granger, C. and A. Andersen, 1978. *An Introduction of Bilinear Time Series Models*.

Gungor, V. C., D. Sahin, T. Kocak, S. Ergut, C. Bucella, C. Cecatti, and G. P. Hancke. 2011. "Smart Grid Technologies : Communication Technologies and Standards". *IEEE Transactions on Industrial Informatics*, vol. 7 no 4, p. 529-539.

Gungor, V. and F. Lambert. 2006. "A Survey on Communication Networks for Electric System Automation". *Computer Networks Elsevier*, vol. 50 no 7, p. 877-897.

Gungor, V., B. Lu, and G. P. Hancke. 2010. "Opportunities and Challenges of Wireless Sensor Networks in Smart Grid". *IEEE Transactions on Industrial Electronics*, vol. 57 no 10, p. 3557-3564.

Gutfleisch, F. and L. Niemeyer. 1995. "Measurement and Simulation of PD in Epoxy Voids". *IEEE Transactions on Dielectrics and Electrical Insulation*, vol. 2 No 5, p. 729-743.

Hamilton, J. D., 1994. *Time Series Analysis*.

Hammond, J. and P. White. 1996. "The Analysis of Non-Stationary Signals Using Time-Frequency Methods". *Journal of Sound and Vibration Elsevier*, vol. 190, Issue 3, p. 419-447.

Haring, J. and H. Vinck. 2000. "OFDM Transmission Corrupted by Impulsive Noise". In *International Symposium on Power-Line Communications and its Applications*. p. 5-7.

Hikita, M., H. Yamashita, T. Hoshino, T. Kato, N. Hayakawa, T.Ueda, and H.Okubo. 1998. "Electromagnetic Noise Spectrum Caused by Partial Discharges in Air at High Voltage Substations". *IEEE Transactions on Power Delivery*, vol. 13, No 2, p. 434-439.

Hoek, S., M. Koch, A. Kraetge, P. WInter, and M. HeInd. 2012. "Emission and Propagation Mechanisms of PD Pulses for UHF and Traditional Electrical Measurements". In *IEEE International Symposium on Electrical Insulation (ISEI), Conference Record*.

Hudon, C., M. Bélec, and M. Lévesque. 2008. "Study of Slot Partial DIscharges in Air-Cooled Generators". *IEEE Transactions on Dielectrics and Electrical Insulation*, vol. 15 No 6, p. 1675-1690.

Hudon, C. and M. Bélec. 2005. "Partial Discharge Signal Interpretation for Generator Diagnostics". *IEEE Transactions on Dielectrics and Electrical Insulation*, vol. 12 No 2, p. 297-319.

Hurvich, C. and C. Tsai. 1988. "Regression and Time Series Model Selection in Small Samples". *Biometrika*, vol. 76, n° 2, p. 297-307.

IEC-60270. 2000. *High-voltage test techniques - partial discharge measurements*. Technical report.

Judd, M. D., L. Yang, and I. B. Frut. 2005. "Partial Discharge Monitoring of Power Transformers Using UHF Sensors. Part I: Sensors and Signal Interpretation". *Electrical Insulation Magazine, IEEE*, vol. 21 Issue:2, p. 5-14.

Judd, M., O. Farish, and B. Hampton. 1996a. "The Excitation of UHF Signals by Partial Discharges in GIS". *IEEE Transactions on Dielectrics and Electrical Insulation*, vol. 3 No 2, p. 213-228.

Judd, M., B. Hampton, and O. Farish. 1996b. "Modelling Partial Discharge Excitation of UHF Signals in Waveguide Structures Using Green's Functions". *IEE Procedings Science, Measurement and Technology*, vol. 143 No 1, p. 63-70.

Kaiser, K. L., 2005. *Electromagnetic Compatibility Handbook*.

Kawada, M. 2003. "Fundamental Study on Location of a Partial Discharge Source with a VHF-UHF Radio Interferometer System". *Electrical Engineering in Japan*, vol. 144, p. p 32?41.

Kogan, V., F. Dawson, G. Gao, and B. NIndra. 1995. "Surface Corona Suppression in High Voltage Stator winding end Turns". *Electrical Electronics Insulation Conference and Electrical Manufacturing & Coil WInding Conference. Proceedings*, vol. 1. No 1, p. 411-415.

Koutrouvelis, I. A. 1981. "An Iterative Procedure for the Estimation of the Parameters of Stable Laws". *Communications in Statistics-Simulation and Computation*, vol. 10 No 1, p. 17-28.

Krim, H., D. Tucker, S. Mallat, and D. Donoho. 1999. "On Denoising and the Best Signal Representation". *IEEE Transactions on Information Theory*, vol. 45 No 7, p. 2225-2238.

Kuffel, E., W. Zaengl, and J. Kuffel, 2000. *High Voltage Engineering : Fundamentals Second Edition*.

Kullback, S. and R. A. Leiber. 1951. "On Information and Sufficiency". *The annals of Mathematical Statistics*, vol. 22 No 1, p. 79-86.

Lemke, E. 2008. *Guide for partial discharge measurements in compliance to iec 60270*. Technical report.

Levesque, M., E. David, C. Hudon, and M. Belec. 2010. "Effect of Surface Degradation on Slot Partial Discharge Activity". *IEEE Transactions on Dielectrics and Electrical Insulation*, vol. 17 No 5, p. 1428-1440.

Levesque, M., E. David, and C. Hudon. 2013. "Effect of Surface Conditions on the Electric Field in Air Cavities". *IEEE Transactions on Electrical Insulation*, vol. 20 No 1, p. 71-81.

Lévy, P., 1925. *Calcul des Probabilités*.

Ling, J., M. Nassar, and B. L. Evans. 2013. "Impulsive Noise Mitigation in Power Line Communications Using Sparse Bayesian Learning". *IEEE Journal Selected Areas in Communications*, vol. 31 no 7, p. 1172-1183.

Ljung, G. M. and G. E. P. Box. 1978. "On a Measure of a Lack of Fit in Time Series Models". *Biometrika*, vol. 65, issue 2, p. 297-303.

Llow, J. and D. Hatzinakos. 1998. "Analytic Alpha-Stable Noise Modeling in a Poisson Field of Interferers or Scatterers". *IEEE Transactions on Signal Processing*, vol. 46 No 6, p. 1601-1611.

Loeb, L. B., 1965. *Electrical Coronas: Their Basic Physical Mechanisms*.

Loeb, L. B. and J. M. Meek. 1940. "The Mechanism of Spark Discharge in Air at Atmospheric Pressure". *Journal of Applied Physics*, vol. 11, p. 438-447.

Lowen, S. B. and M. C. Teich. 1990. "Power-Law Shot Noise". *IEEE Transactions on Information Theory*, vol. 36 No 6, p. 1302-1317.

Ma, H., K. Saha, C. Ekanayake, and D. Martin. 2015. "Smart Transformer for Smart Grid-Intelligent Framework and Techniques for Power Transformer Asset Management". *IEEE Transaction on Smart Grid*, vol. 6, n° 2, p. 1026-1034.

Ma, X., C. Zhou, and I. J. Kemp. 2002. "Interpretation of Wavelet Analysis and its Application in Partial Discharge Detection". *IEEE Transactions on Dielectrics and Electrical Insulation*, vol. 9 No 3, p. 446-457.

Ma, Y., P. So, and E. Gunawan. 2005. "Performance AnaLysis of OFDM Systems for Broadband Power Line Communications Under Impulsive Noise and Multipath Effects". *IEEE Transaction on Power Delivery*, vol. 20 no 2, p. 674-682.

MacKinnon, J. G. 1994. "Approximate Asymptotic Distribution Functions for Unit-Root and Co-Integration Tests". *Journal of Business & Economic Statistics*, vol. 12, No. 2, p. 167-176.

Madi, G., B. Vrigneau, Y. Pousset, R. Vauzelle, and B. L. Agba. 2010. "Impulsive Noise of Partial Discharge and its Impact on a Minumum Distance-Based Precoder of MIMO System". In *18th European Signal Processing Conference (EUSIPCO-2010)*. p. 1602-1606.

Madi, G., F. Sacuto, B. Vrigneau, B. L. Agba, Y. Pousset, R. Vauzelle, and F. Gagnon. 2011. "Impacts of Impulsive Noise from Partial Discharges on Wireless Systems performance: Application to MIMO Precoders". *EURASIP Journal on Wireless Communications and Networking*, vol. 186, p. 1-12.

Mallat, S., 1998. *A Wavelet tour of Signal Processing*.

Markalous, S., S. Tenbohlen, and K. Feser. 2008. "Detection and Location of Partial Discharges in Power Transformers Using Acoustic and Electromagnetic Signals". *IEEE Transaction on Dielectrics and Electrical Insulation*, vol. 15, n° 6, p. 1576-1583.

Massey, F. J. 1951. "The Kolmogorov-Smirnov Test for Goodness of Fit". *Journal of the American Statistical Association*, vol. 46, n° 253, p. 68-78.

McCulloch, J. 1986. "Simple Consistent Estimators of Stable Distribution Parameters". *Communications in Statistics - Simulation and Computation*, vol. 15, n° 4, p. 1109-1136.

McLeod, A. I. and W. K. Li. 1983. "Diagnostic Checking ARMA Time Series Models Using Squared-Residual Autocorrelations". *Journal of Time Series Analysis*, vol. 4. No. 4, p. 269-273.

Meek, J. M. and J. D. Craggs, 1953. *Electric Breakdown of Gases*.

Meng, H., Y. L. Guan, and S. Chen. 2005. "Modelling and Analysis of Noise Effects on Broadband Power-Line Communications". *IEEE Transactions on Power Delivery*, vol. 20 No 2, p. 630-637.

Middleton, D. 1973. "Man-made Noise in Urban Environments and Transportation System : Models and Measurements". *IEEE Transactions on Communications*, vol. 21, No 11, p. 1232-1241.

Middleton, D. 1974. *Statistical-physical model of man-made radio noise, part I : First-order probability models of the instantaneous amplitude*. Technical report. 1-59 p.

Middleton, D. 1977. "Statistical-Physical Models of Electromagnetic Interference". *IEEE Transactions on Electromagnetic Compatibility*, vol. 19 Issue 3, p. 106-127.

Middleton, D. 1979. "Procedures for Determining the Parameters of the First-Order Canonical Models of Class A and Class B Electromagnetic Interference". *IEEE Transactions on Electromagnetic Compatibility*, vol. 21 Issue 3, p. 190-208.

Middleton, D. 1983. "Canonical and Quasi-Canonical Probability Models of Class A Interference". *IEEE Transactions on Electromagnetic Compatibility*, vol. 25 Issue 2, p. 76-106.

Middleton, D. 1999. "Non-Gaussian Noise Models in Signal Processing for Telecommunications : New Methods and Results for Class A and Class B Noise Models". *IEEE Transaction on Information Theory*, vol. 45 No 4, p. 1129-1149.

Minegishi, S., H. Echigo, and R. Sato. 1989. "Frequency Spectra of the Arc Current Due to Opening Electric Contacts in Air". *IEEE Transactions on Electromagnetic Compatibility*, vol. 31, No 4, p. 342-345.

Montanari, G. C. and A. Cavallini. 2015. "Partial Discharge Diagnostics: From Apparatus Monitoring to Smart Grid Assessment". *IEEE Electrical Insulation Magazine*, vol. 29, n° 3, p. 8-17.

Moore, P. J., I. E. Portugués, and I. A. Glover. 2005. "Radiometric Location of Partial Discharges Sources on Energized High-Voltage Plant". *IEEE Transaction on Power Delivery*, vol. 20 no. 3, p. 2264-2272.

Moore, P. J., I. E. Portugués, and I. A. Glover. 2006. "Partial Discharge investigation of a Power Transformer Using wireless Wideband Radio-Frequency Measurements". *IEEE Transactions on Power Delivery*, vol. 21 No 1, p. 528-530.

Moose, P. H. and J. M. O'dwyer. 1986. "A Model for Impulsive Power-Line Radio Disturbance Due to Gap-type Discharges". *IEEE Transactions on Electromagnetic Compatibility*, vol. 28 Issue:4, p. 185-192.

Moulines, E. and J.-F. Cardoso. 1995. "Asymptotic Performance Analysis of Direction-Finding Algorithms based on Fourth-Order Cumulant". *IEEE Transaction on Signal Processing*, vol. 57, n° 8, p. 214-224.

Ndo, G., F. Labeau, and M. Kassouf. 2013. "A Markov-Middleton Model for Bursty Impulsive Noise : Modelling and Receiver Design". *IEEE Transactions on Power Delivery*, vol. 28 No 4, p. 2317-2325.

Nelson, D. 1991. "Conditional Heteroskedasticity in Asset Returns: A New Approach". *Econometrica*, vol. 59, No. 2, p. 347-370.

Newey, W. K. and K. D. West. 1987. "A Simple, Positive Semi-definite, Heteroskedasticity and Autocorrelation consistent Covariance Matrix". *Econometrica*, vol. 55 No. 3, p. 703-708.

Niemeyer, L. 1995. "A generalized Approach to Partial Discharge Modelling". *IEEE Transactions on Dielectrics and Electrical Insulation*, vol. 2 No 4, p. 510-528.

Nikias, C. and M. Shao, 1995. *Signal Processing with Alpha-Stablet Distributions and Applications*.

Okazaki, T., Z. Kawasaki, and A. Hirata. 2005. "Wideband Characteristics of Impulsive EM Noise Emitted from Discharges and Development of Mathematical Noise Model". In *EMC, International Symposium on Electromagnetic Compatibility*. p. p 469-472.

Pakala, W. E., E. R. taylor, Jr., and R. T. Harrold. 1968. "Radio Noise Measurements on High Voltage Lines from 2.4 to 345 kV". In *IEEE Electromagnetic Compatibility Symposium Record*. p. 96-107.

Pakala, W. and V. Chartier. 1971. "Radio Noise Measurements on Overhead Power Lines from 2.4 to 800 kV". *IEEE Transactions on Power Apparatus and Systems*, vol. PAS-90, issue 3, p. 1155-1165.

Parra, L. and P. Sajda. 2003. "Blind Source Separation via Generalized Eigenvalue Decomposition". *Journal of Machine Learning Research*, vol. 4, p. 1261-1269.

Parra, L. and C. Spence. 2000. "Convolutive Blind Separation of non-Stationary Sources". *IEEE Transaction on Speech and Audio Processing*, vol. 8 no 3, p. 320-327.

Parzen, E., 1962. *Stochastic Processes*.

Pater, R. 2009. *Télégestion réseaux intelligents aperçu de quelques approches*. Technical report.

Pearson, J. S., B. F. Hampton, and A. G. Sellars. 1991. "A Continuous UHF Monitor for Gas-insulated Substations". *IEEE Transactions on Electrical Insulation*, vol. 26,no 3, p. 469-478.

Phillips, P. B. and P. Perron. 1988. "Testing for a Unit Root in Time Series Regression". *Biometrika*, vol. 75, No 2, p. 335-346.

Portugués, I., P. I. Moore, and I. A. Glover. 2003. "Characterization of Radio Frequency Interference from High Voltage Electricity Supply Equipment". *ICAP. twelfth International Conference on Antennas and Propagation*, vol. 2, p. p 820-823.

Portugués, I. E. and P. J. Moore. 2006. "Study of Propagation Effects of Wideband Radiated RF Signals from PD Activity". In *IEEE Power Enfineering Society General Meeting*.

Priestley, M. 1967. "Power Spectral AnaLysis of Non-stationary Random Processes". *Journal of Sound and Vibration Elsevier*, vol. 6, issue 1, p. 86-97.

Proakis, J. G. and M. Salehi, 2008. *Digital Communications Fifth Edition*.

Rao, M. M., M. J. thomas, and B. P. Singh. 2007. "Electromagnetic Field Emission from Gas-to-Air Bushing in a GIS During Switching Operations". *IEEE Transactions on Electromagnetic Compatibility*, vol. 49, No 2, p. 313-321.

Rice, S. O. 1944. "Mathematical Analysis of Random Noise". *Bell Syst. Tech. Journal*, vol. 23, p. 282-332.

Rice, S. O. 1945. "Mathematical Analysis of Random Noise : Part III". *Bell Syst. Tech. Journal*, vol. 24, p. 46-156.

Riendeau, S., B. Agba, H. Bertrand, and J. Béland. 2009a. *Création d'un centre d'expérimentation en télégestion dans la cour des postes*. Technical report.

Riendeau, S. and J. Béland. 2009. *Communication dans la cour des postes - étude des besoins*. Technical report.

Riendeau, S., B. Agba, H. Bertrand, and J. Béland. 2009b. *Communication dans la cour des postes : étude des options technologiques*. Technical report.

Sacuto, F., B. L. Agba, F. Gagnon, and F. Labeau. 2012. "Evolution of the RF Characteristics of the Impulsive Noise in High Voltage Environement". In *IEEE SmartGridComm Workshop*.

Sacuto, F., F. Labeau, and B. L. Agba. 2013. "Wideband Time-Correlated Model for Wireless Communications Under Impulsive within Power Substations". *IEEE Transaction on Wireless Communications*, vol. 13 No. 3, p. 1449-1461.

Sadler, B. M. 1996. "Detection in Correlated Impulsive Noise Using Fourth-Order Cumulants". *IEEE Transaction on Signal Processing*, vol. 14 No 11, p. 2793-2800.

Said, S. and D. A. Dickey. 1984. "Testing for Unit Roots in Autoregressive Moving-Average Models of Unknown order". *Biometrika*, vol. 71, p. 599-607.

Samarodnitsky, G. and M. S. Taqqu, 2000. *Stable Non-Gaussian Random Processes : Stochastic Models with Infinite Variance*.

Sarathi, R., A. Reid, and M. Judd. 2008. "Partial Discharge Study in Transformer Oil Due to Particle Movement Under DC Voltage Using the UHF Technique". *Elseiver*, vol. 78 No 11, p. 1819-1825.

Satish, L. and B. Nazneen. 2003. "Wavelet-Based Denoising of Partial Discharge Signals Buried in Excessive noise and Interference". *IEEE tansactions on Dieclectrics and Electrical Insulation*, vol. 10 No 2, p. 354-367.

Schwarz, G. 1978. "Estimating the Dimension of a Model". *The annals of Statistics*, vol. 6, No. 2, p. 461-464.

Shan, Q., I. A. Glover, P. J. Moore, I. E. Portugues, M. Judd, R. Rutherford, and R. J. Watson. 2007. "Performance of Zigbee in Electricity Supply Substations". In *WiCom . International Conference on Wireless Communications, Networking and Mobile Computing*. p. 3871-3874.

Shan, Q., I. Glover, P. J. Moore, I. E. Portugues, M. Judd, R. Rutherford, and R. J. Watson. 2008a. "TEM Horn Antenna for Detection of Impulsive Noise". In *International Symposium on Electromagnetic Compatibility - EMC Europe*. p. 1-6.

Shan, Q., I. Glover, P. J. Moore, I. E. Portugues, R. J. Watson, R. Rutherford, R. Atkinson, and S. Bhatti. 2008b. "Laboratory Assessment of WLAN Performance Degradation in the Presence of Impulsive Noise". In *Wireless Communications and Mobile Computing Conference*. p. 859-863.

Shan, Q., I. Glover, R. C. Atkinson, S. A. Bhatti, I. E. Portugues, P. J. Moore, R. Rutherford, R. J. Watson, M. de Fatima Q. V., A. M. N. Lima, and B. A. Souza. 2011. "Estimation of Impulsive Noise in an Electricity Substation". *IEEE Transaction on Electromagnetic Compatibility*, vol. 53 No 3, p. 653-663.

Shao, M. and C. Nikias. 1993a. *On symmetric stable models for impulsive noise*. Technical report.

Shao, M. and C. Nikias. 1993b. "Signal Processing with Fractional Lower Order Moments: Stable Processes and Their Applications". *Proceedings of the IEEE*, vol. 81, n° 7, p. 986-1010.

Shinde, M. P. and S. N. Gupta. 1974. "A Model of HF Impulsive Atmospheric Noise". *IEEE Transaction on Electromagnetic Compatibility*, vol. EMC-16, No 2, p. 71-75.

Sinaga, H., B. Phung, and T. Blackburn. 2012. "Partial Discharge Localization in Transformers using UHF Detection Method". *IEEE Transaction on Dielectrics and Electrical Insulation*, vol. 19, n° 6, p. 1891-1900.

Snyder, D. L. and M. I. Miller, 1991. *Random Point Processes in Time and Space: Second Edition*.

Spaulding, A. and D. Middleton. 1977. "Optimum Reception in an Impulsive Interference Environment-Part I: Coherent Detection". *IEEE Transactions on Communications*, vol. 25, p. 910 - 923.

Straumann, D., 2005. *Estimation in Conditionally Heteroskedastic Time Series Models*.

Tang, J., W. Li, and Y. Liu. 2009. "Blind Source Separation of Mixed PD Signals Produced by Multiple Insulation Defects in GIS". *IEEE Transaction on Power Delivery*, vol. 25, n° 1, p. 170-176.

Tang, Z., C. Li, X. Cheng, W. Wang, J. Li, and J. Li. 2006. "Partial Discharge Location in Power Transformers Using Wideband RF Detection". *IEEE Transactions on Dielectrics and Electrical Insulation*, vol. 13, n° 6, p. 1193-1199.

Tenbohlen, S., D. Denissov, S. M. Hoek, and S. M. Markalous. 2008. "Partial Discharge Measurement in the Ultra High Frequency (UHF) Range". *IEEE Transactions on Dielectrics and Electrical Insulation*, vol. 15, No 6, p. 1544-1553.

Townsend, S. J., 1910. *The Theory of Ionization of Gases by Collision*.

Trees, H. L. V., 2004. *Optimum Array Processing Part IV : Detection, Estimation and Modulation Theory*.

Trichel, G. W. 1939. "The Mechanism of the Positive Point-to-Plane Corona in Air at Atmospheric Pressure". *Physical Review*, vol. 55 issue 4, p. 382-390.

Trinh, G. N., 2001. *The Electric Power Engineering Handbook*, chapter 5 Corona and Noise. CRC Press.

Tsihrintzis, G. A. and C. L. Nikias. 1995. "Performance of Optimum and Sub-optimum Receivers in the Presence of Impulsive Noise Modeled as an Alpha-stable Process". *IEEE Transactions on Communications*, vol. 43 Issue 234, p. 904-914.

Tsihrintzis, G. A. and C. L. Nikias. 1996. "Fast Estimation of the Parameters of Alpha-stable Impulsive Interference". *IEEE Transactions on Signal Processing*, vol. 44 Issue 6, p. 1492-1503.

US Department of Energy Office. 2007a. *A vision for the modern grid*. Technical report.

US Department of Energy Office. 2007b. *A systems view of the modern grid*. Technical report.

Vaseghi, S. V., 2008. *Advanced Digital Signal Processing and Noise Reduction : Fourth Edition*.

Vasilescu, G., 2005. *Electronic Noise and Interfering Signals: Principles and Applications*.

von Laue, M. 1925. "Comment on K. Zuber's Measurement of the Spark Discharge Delay Time". *Annals of Physics Liepzig*, vol. 76, p. 261-265.

Wang, J., E. E. Kuruoglu, and T. Zhou. 2011. "Alpha-Stable Channel Capacity". *IEEE Communications Letters*, vol. 15 no 10, p. 1107-1109.

Weinstein, E., M. Feder, and A. V. Oppenheim. 1993. "Multi-Channel Signal Separation by Decorrelation". *IEEE Transaction on Speech and Audio Processing*, vol. 1 no 4, p. 405-413.

Weron, A. and R. Weron. 1995. "Computer Simulation of Levy alpha-Stable Variables and Processes". *Lecture Notes in Physics*, vol. 457, p. 379-392.

Wiklundh, K. C., P. F. Stenumgaard, and H. M. Tullberg. 2009. "Channel Capacity of Middleton's Class A Interference Channel". *Electronics Letters*, vol. 45 no 24, p. 1-2.

Wilk, M. B. and R. Gnanadesikan. 1968. "Probability Plotting Methods for the Analysis for the Analysis of Data". *Biometrika*, vol. 55 No. 1, p. 1-17.

Woodward, W. A., H. L. Gray, and A. C. Elliott, 2012. *Applied Time Series Analysis*.

Wu, M., H. Cao, J. Cao, H. L. Nguyen, J. B. Gomes, and S. P. Krishnaswamy. 2015. "An Overview of State-of-the-Art Partial Discharge Analysis Techniques for Condition Monitoring". *IEEE Electrical Insulation Magazine*, vol. 31, n° 6, p. 22-35.

Yan, Y., Y. Qian, H. Sharif, and D. Tipper. 2013. "A Survey on Smart Grid Communication Infractructures: Motivations, Requirements and Challenges". *IEEE Communications Surveys and Tutorials*, vol. 15 no 1, p. 5-20.

Zabin, S. M. and H. V. Poor. 1989. "Parameter Estimation for Middleton Class A Interference Processes". *IEEE Transactions on Communications*, vol. 37 no10, p. 1042-1051.

Zabin, S. M. and H. V. Poor. 1991. "Efficient Estimation of Class A Noise Parameters via the EM [Expectation-Maximization] Algorithms". *IEEE Transaction on Information Theory*, vol. 37 no 1, p. 60-72.

Zimmermann, M. and K. Dostert. 2002. "Analysis and Modelling of Impulsive Noise in Broadband Power-line Communication". *IEEE Transactions on Electromagnetic Compatibility*, vol. 44 No 1, p. 249-258.